University College London

Department of Chemistry

Electrochemical Titrations with Dual Microband Electrodes

by

Hanna Rajantie

Ph.D. 2001

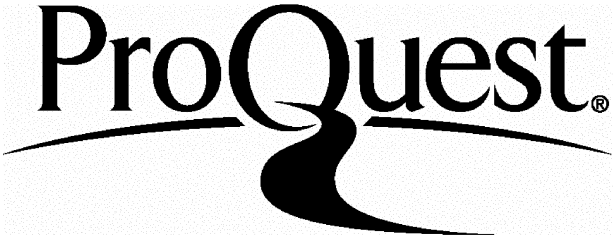

ABSTRACT

The main objective of this thesis is to present a generator-collector mode titration with dual parallel microband electrodes and a miniaturisation of an electroanalytical method. The system is based on manipulation of the mass transport, which is accomplished by using screen-printed microband electrodes, controlling the fluxes of reactive material and vibrating the electrodes in order to stir the solution and to renew the boundary conditions. An analysis method that is easy-to-use, rapid and sensitive is developed.

The titrant is generated electrochemically at the generator electrode by applying a current, and instead of balancing the molar amounts, the fluxes of reactive material are balanced. The end-point is detected either amperometrically or potentiometrically by the appearance of the titrant at the collector electrode: the more analyte is present in the solution the greater the generator current required to reach a certain threshold value of the collector current or the open-circuit potential, and the longer it takes to achieve this value. The method is applied to, *e.g.*, determination of L-ascorbic acid (vitamin C) with ferricyanide and titration of thiosulfate and sulfite with iodine using gold microband electrodes. Silver microband electrodes are employed here for a potentiometric titration where the titrant is electrogenerated by dissolving the generator electrode material and the open-circuit potential of the collector is measured. The use of silver microbands is demonstrated by determination of halides, cyanide and thiosulfate with Ag(I).

The accuracy of these titrations is ± 10 %, and it is mostly limited by the reproducibility of the present fabrication method of the electrodes. The results prove that the method is effective with a simple instrumental set-up, and the actual time needed for common titrations is significantly decreased. A comprehensive basis for further applications and other analytical systems is demonstrated.

PREFACE

This thesis is based on research carried out at University College London during the years 1998-2001. I wish to thank my colleagues and the personnel of the Department of Chemistry for the pleasant atmosphere. I would also like to thank the Engineering and Physical Sciences Research Council (EPSRC) and the Finnish Cultural Foundation for financial support.

I want to express my gratitude to my supervisor Professor David E. Williams for his inspiration, enthusiasm and support. I thank Dr. Daren Caruana and Dr. Jörg Strutwolf for all the guidance and encouragement during this project and Jörg also for inspiring collaboration. I am greatly indebted to them for careful reading of the manuscript and for several useful comments.

I wish to thank the VESSIA project partners Dr. Keith Dawes, Dr. Geoff Garnham, Bruce Grieve, Jim Hambleton, David A. Pearson, Dr. Simon N. Port and Valerie Wheeler for providing an interesting research topic, and Agmet Ltd for manufacturing the microband electrodes.

Many thanks are due to my fellow students Camilla Forssten, Dimitra Georganopoulou, Sean McCormack, Ali Morshed and Dirk Niemeyer, with whom I shared both scientific and personal ups and downs.

Last but not least, I thank my family and friends for their endless support during my studies and my husband Arttu, without whose encouragement and love this thesis would not have been possible.

London, September 2001

Hanna Rajantie

CONTENTS

LIST OF FIGURES

LIST OF TABLES

LIST OF SYMBOLS

a	activity, mol m^{-3}
a_0	integration constant
c	concentration, mol m^{-3}
c^b	concentration in bulk solution, mol m^{-3}
d	distance between microband and reference electrodes, m
e	Neper's constant (≈ 2.7183)
g	dimensionless local gradient
k	second order rate constant, M^{-1} s^{-1}
l	length of microband electrode, m
m	mass transport co-efficient, m s^{-1}
n	order of Bessel function; number of measurements
n_e	number of grid points
r	polar co-ordinate, m
r_o	characteristic dimension of microelectrode, m; radius of cylinder, m
r_1	integration constant
s	argument of Laplace transform; standard deviation
$s_{\bar{x}}$	standard error
t	time, s
v_A	current scan (sweep) rate, A s^{-1}
v_V	potential scan (sweep) rate, V s^{-1}
w	half of microband width, m
x	cartesian co-ordinate, m
$\bar{x}$	arithmetic mean
x_i	individual measured value
y	cartesian co-ordinate, m
z	number of transferring electrons
A	surface area, m^2
C	capacitance, F; dimensionless concentration
D	diffusion co-efficient, m^2 s^{-1}
E	electrode potential, V
F	Faraday's constant, 96485 A s mol^{-1}
FF	feedback factor

G	dimensionless current
$G(x)$	Gaussian distribution
$H(t)$	Heaviside step function
I	current, A
I_C	capacitive current, A
I_F	Faradaic current, A
I_p	peak current, A
$I_n(x)$	modified Bessel function
J_d	flux, mol m^{-2} s^{-1}
$J_n(x)$	Bessel function
K_{sp}	solubility product, *e.g.*, mol^2 m^{-6}
$K_n(x)$	modified Bessel function
$L\{f\}$	Laplace transform of function f
Q	electric charge, C
R	cell resistance, Ω; gas constant, 8.314 J mol^{-1} K^{-1}
SF	shielding factor
T	temperature, K
V	volume, m^3
W	width of microband electrode, m
W_{gap}	gap width between microband electrodes, m
γ	Euler's constant (≈ 0.57722)
γ_A	activity co-efficient
θ	polar co-ordinate, rad
μ	mean
ν	stoichiometric co-efficient
ρ	resistivity, Ω m
σ	deviation
τ	dimensionless time
$\psi(x)$	digamma function
Γ	conformal co-ordinate
$\Gamma(x)$	gamma function
Θ	conformal co-ordinate
Φ	collection efficiency

Subscripts

coll	collector
gen	generator
A	species from which titrant generated
B	titrant
C	analyte

1 Introduction

The main objective of this thesis is to present a generator-collector mode titration with dual microband electrodes. Both amperometric and potentiometric end-point detection methods have been implemented. The system is based on manipulation of the mass transport, which has been accomplished by using microband electrodes, controlling the fluxes of electroactive material and vibrating the electrodes in order to renew the boundary conditions. The capability and the principle of the analytical method are here demonstrated using traditional titrations, which can be further applied to more complicated and demanding systems.

This thesis presents first an introduction to microelectrode theory, the main focus being on microband electrodes. In Chapter 2, different generator-collector systems are discussed as a background to the present titration method, and some theoretical aspects are studied. Chapter 3 contains an introduction to the applications and different analytical systems, and the experimental details are given in Chapter 4. Chapter 5 presents and discusses the results, and the conclusions are drawn in Chapter 6. Discussion on the future work is presented in Chapter 7.

1.1 Introduction to microelectrodes

Microelectrodes are devices where at least one characteristic dimension is in the μ-metre range or smaller, and their properties, *e.g.*, mass transport, are functions of size. [1, 2] Microelectrodes can be used to probe small sample volumes and low concentrations. [3, 4] As the electrode surface areas are small, the currents are low, but, on the other hand, the actual current densities can be extremely high. Due to the low currents the instrumentation can be simpler than with other electrochemical methods: for instance, a two-electrode system can be employed without the problem of high currents passing through the reference electrode. Microelectrodes are economical to fabricate and easy to use. [5, 6]

Mass transport is enhanced due to an increase in the dimensionality of the diffusion problem. Thus, as the size of an electrode is reduced, the diffusion changes from 1-D (planar) to 3-D (spherical or hemi-spherical). [2, 7, 8, 9] The increased mass transport results in high sensitivity in analysis. [5, 10] A time-independent steady state can be reached rapidly, which means that microelectrodes can be used on short time-scales, and it is possible to study rapid kinetics,

i.e., electron transfer reactions. [1, 6] Because of the rapid response fast techniques can be used, which decreases the problem of electrode poisoning. The concentration of electroactive species is perturbed only a small distance from the electrode surface. Therefore, with some electrode geometries, *e.g.* microdisks, the response is independent of convection, and there is no need to control the hydrodynamics of the system. [7]

As the physical size of a microelectrode is small, the double layer capacitance is reduced, [2, 9] and the response to the changes of the applied potential is rapid. Ohmic drop (*IR*-drop), which can be determined by multiplying the cell resistance R by the electrode current I, decreases with a decreasing characteristic dimension on short time-scales and when the total current diminishes.[2, 9] The low ohmic losses allow the use of microelectrodes under highly resistive conditions, even in solid media and in thin adsorbed moisture layers on solid surfaces (so-called 'gas phase' electrochemistry). [5, 11, 12] Since the capacitive effects are diminished and the mass transport is high, the signal-to-noise ratio is excellent. [6]

1.2 Fabrication of microelectrodes

Typical microelectrode geometries are hemi-spheres, disks, rings, bands, wires and cylinders. [1, 6] Fabrication of microelectrodes is relatively cheap but technically demanding. In particular, the production of proper sealing around the electrode, *i.e.* between the active surface and the insulator is difficult. [5] Metal microwires and carbon fibres can be used for fabrication of disk-shaped and cylindrical electrodes. Fine wires, usually platinum or gold but also, *e.g.*, silver, nickel, iridium, mercury and superconducting ceramics, are sealed in a soft glass or epoxy resin.[9] For a ring electrode a film is usually deposited on a ceramic or glass rod, the system is sealed in a concentric glass tube and the cross section is exposed by grinding. [3]

Microband and microarray (closely spaced microband) electrodes are generally fabricated by 'sandwiching' thin metal films, foils or sputtered layers, between insulating layers, *e.g.*, glass and epoxy. [3, 13, 14] The exposed edges are used as electrodes. Typical fabrication methods are also lithographic techniques [15, 16] and screen-printing processes. [4] In a screen-printing method ink is squeezed onto a substrate surface and then fired in a furnace. Screen-printing as a simple and convenient method provides the possibility to mass-produce repeatable electrode geometries, on which the analytical signal is dependent. Mass-production makes it also

possible to use disposable electrodes, whereby the electrode poisoning can be eliminated. [4, 5, 10]

A common problem with microelectrodes is that the exposed surface area is not ideal, *i.e.*, the electrode surface is not absolutely flat or that the sealing between the actual electrode and insulator is improper. This can be caused by several reasons: the electrode surface is not carefully polished but 'cut', the insulating layer is not properly removed or a cracked insulating layer allows the solution to leak between the electrode and the insulator. These non-idealities can distort the diffusion fields at the electrodes. The relative errors are higher than with macroelectrodes. [3, 8, 14, 17, 18, 19]

1.3 Mass transport at microelectrodes

Conventional electrochemical reactions are heterogeneous processes, which take place at the interface between an electrolyte and an electrode. Oxidation occurs at the anode and reduction at the cathode. [20] The rate of reaction, *i.e.*, electron transfer, is determined by a rate constant that is specific to each reaction. If the electron transfer rate is high the reaction is controlled by mass transport. [9] There are three possible contributions for the mass transport to and from the electrode surface: 1) diffusion, which is due to a concentration gradient, 2) migration, which is due to an electrical potential gradient and 3) convection, which is due to a pressure gradient (mechanical stirring) in the solution. [21, 22] In the case of microelectrodes a time-independent steady state may be reached rapidly. [6] The mass transport rate in the steady state is determined by the mass transport co-efficient m [2, 9]

$$(1) \qquad m = \frac{D}{r_o},$$

where D is the diffusion co-efficient of the electroactive species, and r_o is the characteristic dimension of the microelectrode. Particularly, with a characteristic dimension < 10 μm, the resultant high mass transport co-efficient may mean that the contribution of convective transport and migration is negligible. [4] As the diffusion is effective and the *IR*-drop has little influence, an inert electrolyte (supporting electrolyte), which is normally used to diminish the effect of migration, may not be necessary. In the absence of a supporting electrolyte and under highly resistive conditions there can be additional enhancement of the mass transport

limited current due to the effect of electromigration or because the diffusion co-efficient of the electroactive species increases with a decreasing ionic strength. [3, 23, 24, 25]

1.3.1 Diffusion

The diffusion fields for a macroelectrode and a microelectrode are presented in Figure 1.

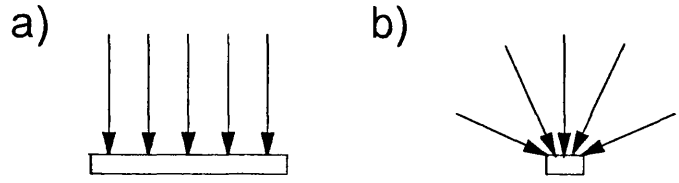

Figure 1. Limiting cases of diffusive mass transport: a) macroelectrode, b) microelectrode.[1, 2]

The diffusive mass transport is linear at macroelectrodes (semi-infinite planar diffusion) and at short times at microelectrodes. That is because the thickness of the diffusion layer is smaller than the electrode radius. [9] At long times, the thickness of the diffusion field exceeds the microelectrode radius and the diffusion changes from planar to three-dimensional (spherical or hemi-spherical). This means that the diffusion field of a microelectrode is non-uniformly distributed, *i.e.*, the rate of diffusion is higher to the edge than to the centre.[1] Usually, the electrode is considered as lying on an infinite insulating plane, and the diffusion current is divided into two components: 1) current due to linear diffusion and 2) current due to radial (edge) diffusion. [4] A spherical microelectrode is an exception due to its uniformly accessible surface. [1, 9] The diffusion field depends on the electrode geometry of a microelectrode, and therefore the experiments to be carried out determine the suitable microelectrode geometry. [3]

In general, diffusion (*i.e.*, flux J_d, mol $m^{-2}s^{-1}$) perpendicular to the electrode surface can be determined by Fick's first law [26]

$$J_d = -D\frac{dc}{dy}, \qquad (2)$$

where c is the concentration of the electroactive species and y is the distance from the electrode surface. The gradient is negative because the flux is in the direction of a lower concentration.

However, because the concentration is initially unknown Fick's first law cannot be used directly to calculate the current. Therefore c must first be determined by Fick's second law [26]

$$\frac{\partial c}{\partial t} = D\nabla^2 c, \tag{3}$$

where t is time and ∇^2 is the Laplacian operator. For instance, for a band electrode $c = c(x, y)$, and Fick's second law is: [2,3]

$$\frac{\partial c}{\partial t} = D\left(\frac{\partial^2 c}{\partial x^2} + \frac{\partial^2 c}{\partial y^2}\right), \tag{4}$$

where the diffusion has been divided into two components: normal and parallel to the electrode surface. In order to determine the current at the electrode, the concentration of the diffusive species is calculated using Fick's second law with relevant initial and boundary conditions. The current is then given by Equation (2).

1.4 Chronoamperometry at microelectrodes

Chronoamperometry, *i.e.*, potential step technique, is a method in which the electrode potential is stepped to a certain value, and the current is measured as a function of time. The initial potential is chosen such that no reaction occurs, and the potential is rapidly changed to a value where the oxidation or reduction takes place. [22] The principle is presented in Figure 2.

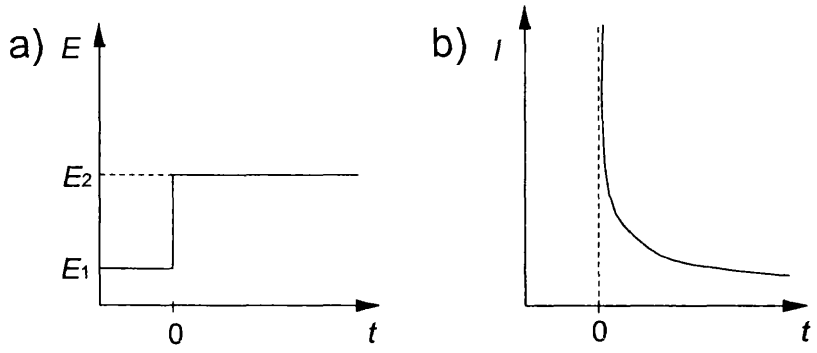

Figure 2. Chronoamperometric measurement: a) initiation, b) response.

The initial and boundary conditions in the chronoamperometric method are:

(5) $c(y,0) = c^b \qquad (y \geq 0),$

(6) $\lim_{y\to\infty} c(y,t) = c^b \qquad (t \geq 0),$

(7) $c(0,t) = 0, \qquad (t > 0),$

where c^b is the concentration of an electroactive species in the bulk solution. With these conditions, Fick's second law (eq.(3)) is solved using co-ordinates that describe each electrode geometry. For instance, after Laplace transforms the results for spherical and disk electrodes consist of a time-dependent and a time-independent part. If planar diffusion is controlling, the current I can be determined by the Cottrell equation [22]

(8) $$I = \frac{zFAD^{1/2}c^b}{\pi^{1/2}t^{1/2}},$$

where z is the number of electrons transferred, F is the Faraday's constant and A is the surface area of the electrode. Equation (8) is valid on short time-scales only. When the duration of the measurement increases the edge effects, *i.e.*, the radial components of diffusion, become more significant. For instance, for a microdisk electrode the current decays to a time-independent steady state where the electrolysis rate is equal to the diffusion rate: [2,9]

(9) $$I = 4zr_{\circ}FDc^{b}.$$

Comparing the time-independent and time-dependent currents the time that is required to reach the steady state can be approximated. Generally, the mass transport can be divided into three categories according to the dimensionless parameter $Dt/r_{\circ}^{2}$. [2, 4, 9, 27] That parameter characterises the type of diffusion. When the time scale is short, *i.e.*, $Dt/r_{\circ}^{2} < 0.01$, mass transport is planar. When the time scale is long a steady state is reached. (The threshold value of the parameter $Dt/r_{\circ}^{2}$ at long times varies in different literature sources, *e.g.*, 1 in Ref. 4, 6 in Ref. 2 and 100 in Ref. 28.) The third category of diffusion consists of intermediate times, and the mass transport is a combination of planar and radial.

The parameter changes according to the electrode geometry. For instance, for a disk electrode the time that is needed to reach the steady state current can be calculated using the ratio of equations (8) and (9): $I_{SteadyState}:I_{Cottrell}= (4/\pi^{1/2})(D^{1/2}t^{1/2}/r_{\circ})$. If the diffusion co-efficient is 10^{-5} cm^2/s, the time when the steady state current is ten times higher than the Cottrell current is 0.49 s for a disk with a radius of 5 μm. Accordingly, the time is 490000 s for a disk with a radius of 5 mm. The time that is needed to reach a steady state is significantly shorter when microelectrodes are used. With microelectrodes the transport rate of the electroactive species increases when the characteristic dimension decreases (eq. (1)).

Microband electrodes are not strictly microelectrodes since the surface area can be relatively large. Only one dimension (*i.e.*, width) has to be in the μ-metre range and thus the active surface area can be larger than the one of microelectrodes with other geometries, whereby higher currents can be used. [29] The current response can be considerably increased by increasing band length. On the other hand, sensitivity to solution convection appears since the diffusion layer can extend far into the solution. [24, 30] A real steady state response is not reached due to two-dimensional diffusion but a so-called quasi steady state is obtained.

Diffusion at a microband electrode can be modelled using a hemi-cylinder of an equivalent area. [13, 27, 31, 32, 33, 34, 35] The cylinder radius $r_{\circ}$ is changed to correspond to the band electrode width W by

(10) $$r_{\circ} = \frac{W}{\pi},$$

which is directly derived from the perimeter of a hemi-cylinder. However, it was observed by Deakin et al. [32] that in practice the corresponding formula was closer to

$$r_e = \frac{W}{4}. \tag{11}$$

The first relation refers to planar diffusion (short times) and the second one is for radial diffusion (long times). Neither of these approximations is accurate if the kinetics is controlling the reaction simultaneously with diffusion. This may happen when the width of the microband is extremely small since the current densities at the edges of the band can reach very large values and the kinetics becomes the limiting factor. [34]

In chronoamperometry, the limiting, quasi steady state current at a microband electrode can be approximated by using the hemi-cylinder assumption as [14, 31, 34]

$$I = \frac{\pi z F D c^b l}{\ln(8\sqrt{Dt}/W)}, \tag{12}$$

where l is the length of the band electrode. Further studies in Ref. 30 resulted in the following equation with a correction term:

$$I = zFDc^b l\left\{\frac{5.553}{\ln(4Dt/W^2)} - \frac{6.791}{\left[\ln(4Dt/W^2)\right]^2}\right\}. \tag{13}$$

A more accurate formula was derived by Szabo et al. [33]

$$I = \pi z F D c^b l\left[\frac{e^{-\left[(\pi Dt)/(W/4)^2\right]^{0.5}/10}}{\sqrt{\frac{\pi Dt}{(W/4)^2}}} + \frac{1}{\ln\left(\sqrt{\frac{4Dt}{(W/4)^2}}e^{-\gamma} + e^{5/3}\right)}\right], \tag{14}$$

where γ is Euler's constant ($\gamma = 0.57722$). Equation (14) can be simplified, if the time scale of the experiment and the microband electrode dimensions are suitable, by leaving out the first term on the right hand side as well as the term $e^{5/3}$. Then, the equation becomes [35]

$$I = \frac{\pi z F D c^b l}{\ln\left(\sqrt{\frac{4Dte^{-\gamma}}{(W/4)^2}}\right)}. \quad (15)$$

The current is not proportional to the surface area but the length of the microband electrode, and the response is relatively insensitive to the band width. The edge effects, *i.e.*, the non-uniform current distribution, are very important in the case of microband electrodes. [36] For instance, comparing the disk and band microelectrodes with the same surface area, the linear diffusion (short time) currents are the same but at long times the currents at the band electrodes are significantly higher (comparing equations (9) and (12)). [14] The mathematical modelling of the flux equations at microband electrodes is complicated, particularly due to the non-uniform current distribution. [30, 32, 37]

1.5 Cyclic voltammetry at microelectrodes

In cyclic voltammetry, the electrode reactions are followed using current-potential curves: the electrode potential is controlled with a triangular waveform, and the current is presented as a function of it. [38] Cyclic voltammetry is a technique that can be used for both preliminary measurements of a new reaction couple and quantitative analysis. [22] With microelectrodes a time-independent steady state can be achieved when the scan rate is reduced (typically for scan rates < 0.020 Vs^{-1}). [7, 31]

At short times, when the planar diffusion is dominating, *i.e.*, with high potential scan rates, the peak current in cyclic voltammetry at a microband electrode for a reversible reaction can be presented as

$$I_p = (2.69\times10^5) z^{\frac{3}{2}} A v_V^{\frac{1}{2}} D^{\frac{1}{2}} c^b, \quad (16)$$

which is the Randles-Sevcik equation, and where v_V is the potential scan rate. [14, 21]

At intermediate times, when diffusion is a combination of planar and radial, an approximate equation for the peak current at a microband, first presented by Aoki, [39] is

$$(17) \qquad I_p = zFc^b Dl\left[0.439p + 0.713p^{0.108} + \frac{0.614p}{1+10.9p^2}\right],$$

where $p = \left(\frac{zFW^2 v_V}{RTD}\right)$ and R is the gas constant.

At long times, *i.e.*, with low potential scan rates, the current approaches a quasi steady state. The voltammogram changes from peak-shaped to sigmoidal (Figure 3). [13]

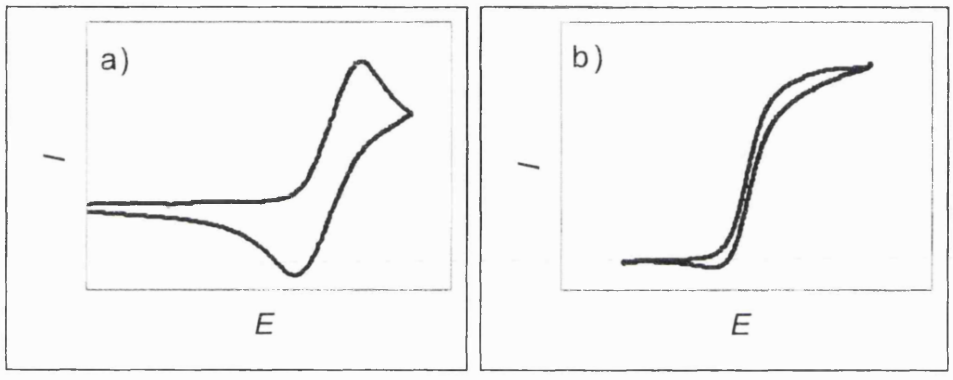

Figure 3. Cyclic voltammograms: a) peak shaped, b) sigmoidal.

For a quasi steady state, Equations (12), (13) and (14) apply to a voltammetric case as well as to a chronoamperometric case. The time t in those equations can be changed to the potential scan (sweep) rate v_V as

$$(18) \qquad t = \frac{E}{v_V} = \frac{RT}{zFv_V},$$

where T is temperature, assuming that the change in potential in a potential sweep corresponds to the time where the quasi steady state is reached. [14]

1.6 Capacitive and ohmic effects at microelectrodes

An electric double layer is formed at the electrode surface because there are excess charges, which are located at the surface and the charges attract ions with opposite charge in the

solution phase. [22, 38] The current that is needed to charge or discharge the double layer is called the capacitive current, and this current flows every time when the electrode potential is changed. [9] In electrochemical experiments the capacitive current distorts the response. The double layer acts as a capacitor. The capacitive current is generally described with the time constant *RC*, which characterises the rate at which the capacitor (double layer) is charged. [40] That comes from the fact that the current to charge the capacitance *C* must flow through the cell resistance *R*. Generally, the resistance of a conductor with the length *l* and the cross section area *A* is determined as

$$R = \frac{\rho l}{A}, \tag{19}$$

where ρ is the resistivity of the material. [41] If *l* is replaced by r_0 (characteristic microelectrode radius) and *A* by the surface area of the microelectrode, it can be concluded that the resistance is inversely proportional to the electrode radius ($R \propto \frac{1}{r_0}$). That means that the resistance of the double layer increases as the electrode radius decreases. Instead, the capacitance of the double layer is proportional to the surface area of the electrode ($C \propto r_0^2$), [9, 40] and as a consequence the product *RC* is proportional to the electrode radius ($RC \propto \frac{1}{r_0} r_0^2 = r_0$). The smaller the radius, the faster the response and the more negligible the distortion. [2, 7, 11]

IR-drop, *i.e.*, ohmic loss, is always present in an electrochemical cell due to resistance in a solution, electrical contacts and in three-dimensional electrodes. [22, 42] When current passes through the cell the resistance causes voltage loss. The total current is the sum of Faradaic I_F (*i.e.*, electric current connected to chemical conversion [21]) and capacitive I_C currents. For instance, the ohmic drop distorts cyclic voltammograms significantly. Since low currents are employed with microelectrodes, the *IR*-drop diminishes. At short times, *I* is proportional to the surface area of the electrode (eq. (8)), *R* is inversely proportional to the electrode radius (eq. (19)), and therefore *IR*-drop is proportional to the electrode radius. At long times, *I* is proportional (eq. (9)) and *R* is inversely proportional (eq. (19)) to the electrode radius. As a consequence, when steady state experiments are carried out, *IR*-drop is independent of the electrode radius and the surface area. [2, 9] Since the effects of *IR*-drop and the double layer

charging current on microelectrodes are diminished, high sweep rates can be used. This leads to a possibility to study rapid chemical reactions. [11]

The currents are usually higher at microband electrodes than at the other microelectrode geometries. Nevertheless, microband electrodes present low ohmic losses. [14, 31] The resistance for a microband electrode can be expressed as [14]

$$R = \frac{\rho}{\pi d} \ln\left(\frac{W + 2d}{W}\right), \tag{20}$$

where d is the distance between the microband and the reference electrode. Equation (20) is derived from the approximation of a resistance of two concentric hemi-cylinders. [14, 31] In the case of microband electrodes, *IR*-drop is the product of the current (eq. (12)) and the resistance (eq. (20)). *IR*-drop is therefore independent of the band length, and thus increasing the length does not increase the ohmic loss. Porat et al. [14] proved that microband electrodes exhibit higher currents than microdisk electrodes when the comparable band width and disk radius were employed, but the *IR*-drop was equal. Therefore microband electrodes are very useful tools in highly resistive media.

1.7 Microelectrodes in analysis

The use of microelectrodes in analysis is based on their properties that have been presented in previous sections. The main features are small electrode dimensions and enhanced mass transport, which lead to high current densities and good sensitivity. Small electrodes can be used to probe small sample volumes and they can be used under demanding physiological conditions, for instance, for analysis in the mammal brain. [43, 44] As a result of reduced capacitive effects the response is fast, and Faradaic-to-capacitive current as well as signal-to-noise ratios are excellent, which again increase sensitivity. [2, 6, 11]

Since the currents and the ohmic drop at microelectrode systems are low, the instrumentation can be simple: the use of a separate reference electrode may be omitted, and the functions of reference and counter electrodes combined by choosing a counter electrode where the potential does not change much when passing the cell current. The use of supporting electrolyte is not necessarily required due to the negligible *IR*-drop and the strong diffusion. For the same reason, stirring of the solution is not necessary. Microelectrodes can be used

outside a laboratory and under extreme conditions, *e.g.*, in highly resistive media as foodstuff [5] and oil [45] or at low temperatures. [6, 9] They are relatively easy and cheap to fabricate and convenient to use due to easy instrumentation and small sample volumes.

Microelectrodes are widely used in traditional analytical methods, like voltammetric methods. [7, 43] The steady state (or quasi steady state) is reached rapidly, and the current is directly proportional to the concentration of electroactive species, *i.e.*, analyte (eq. (9) and (12)). Microelectrodes are very useful in anodic stripping voltammetry, since the response is fast. [46, 47] Very small electrodes also make it possible to study nucleation on the electrode surfaces, since the number of nucleation processes taking place decreases with decreasing surface area. [2, 6, 9] On the other hand, the problem of electrode poisoning is often avoided with microelectrodes, because of the enhanced diffusion both from and to the electrode, and due to fast techniques. [5]

Microelectrodes open up new possibilities for analytical methods: since the three-dimensional mass-transport is strongly enhanced, many reactions that are diffusion controlled at macroelectrodes may become kinetically controlled at microelectrodes. [4, 34] Therefore microelectrodes can be used to study reaction kinetics, and the electroanalytical methods of the future might be based on heterogeneous kinetics of the reactions instead of formal potentials. [9, 48]

1.7.1 Hydrodynamic modulation

Convection is mass transport that is caused by external mechanical force. [21] Convection increases the mass transport of the system leading together with diffusion to convective diffusion problems. Controlled hydrodynamics results in well-defined electrochemical conditions.[20, 22] Hydrodynamic modulation has traditionally been used in analytical chemistry to enhance the sensitivity: the diffusion current is higher than with an electrode of the same size under stationary conditions. Other advantages are that the signals at hydrodynamically modulated electrodes are insensitive to the external movements (noise) and the electrode poisoning can be prevented. [49] Hydrodynamic modulation specifically enhances diffusion-limited processes over kinetic effects. [5, 22]

Traditional ways of changing the hydrodynamics of an analytical cell is the use of vibrating, [49, 50, 51] or rotating [52] electrodes. Also dropping mercury electrodes have been used in order to

enhance the analytical signal. [53] In addition to moving the electrode, the solution itself can be agitated, for instance, by stirring, or the solution flow at the electrode can be controlled. [22] In flow channels, the diffusion-limited currents are dependent on the volume flow rate, [54, 55, 56, 57, 58] and in wall-jet cells the analyte-containing solution is made to impinge on the electrode. [59, 60, 61] Hydrodynamic effects have also been studied using, *e.g.*, laser-activated voltammetry, [62] sonovoltammetry [63, 64] and microwave heating. [65]

Hydrodynamic modulating voltammetry (HMV) is a method where the hydrodynamic mass transport rate to an electrode is varied periodically. [66, 67] HMV has been demonstrated to be a good tool for trace analysis at common solid electrodes, because the method provides a low detection limit. [68] The method reduces interference caused by background effects, *e.g.*, capacitive current, surface reactions and side reactions. [68] Wide amplitude and frequency ranges and time scales can be used. [69] Several methods have been studied, *e.g.*, variation of rotation rate of a rotating disk electrode (RDE), [70] pulsed flow in tubular electrodes [71] as well as vibrating wire, disk and cylinder electrodes. In Ref. 69, Schuette and McCreery employed a combination of HMV and ac voltammetry reducing the background noise and leading to improved detection limit and resolution. HMV can also be combined with ultrasonics resulting in sensitive voltammograms on the micromolar scale. [72]

At microelectrodes, the response becomes independent of convection, particularly when microdisks are employed, because of the extremely effective diffusion. [4] Microband electrodes have exceptional behaviour due to their geometry: the actual surface area may be relatively high although the characteristic dimension is very small. The currents may be relatively high but still the microbands maintain the radial diffusion component. [2, 13] On the other hand, when the currents are increased due to increased microband length the diffusion field can extend into the solution, and the response becomes sensitive to convection. [5, 24, 30] This can be avoided in several ways: 1) using experimental time scales that are short enough, 2) decreasing the band width, which means that the response is close to that of a microring electrode, 3) decreasing the band length, which means that the response is close to that of a microdisk electrode, or 4) using hydrodynamic modulation. [5] In Ref. 73, Williams et al. showed that single microband electrodes can be vibrated in order to enhance the analytical signal modulating the diffusion-limited flux. They also presented that in generator-collector mode titration the collection efficiency fell markedly when continuous vibration was used. Later in this work, the model of continuous pulsed electrode motion and periodically renewed boundary conditions are discussed in relation to generator-collector experiments with dual microband electrodes.

2 Generator-collector systems

2.1 Introduction to generator-collector systems

Generator-collector mode measurements are conventionally made using the ring-disk technique: the products of an electrochemical reaction taking place at the disk electrode are detected at the ring electrode or vice versa. Both amperometric and potentiometric detections have been employed. [74, 75] The electrodes are called generator and collector according to their functions. Collection efficiency Φ in the amperometric case is the collector current I_{coll} divided by the applied generator current I_{gen}: [76]

$$\Phi = \frac{|I_{coll}|}{|I_{gen}|}, \tag{21}$$

but in practice for more precise analysis more complicated equations are employed depending on the geometry of the studied system. [77]

Albery et al. [78, 79, 80, 81] developed a titration method that is based on the ring-disk system and electrogeneration of the titrant at the disk. The titrant reacts with the analyte in the solution and unreacted titrant is detected at the ring. The original work was on titration of proteins with bromine and in Ref. 80 the method was applied to liquid chromatography using a wall-jet arrangement. An early development of a generator-collector mode analytical method, where the electrogeneration of bromine was used to produce the titrant, was the determination of mustard gas. [82] The flux of the electrogenerated titrant was balanced against the flux of the analyte using a flow cell arrangement, and the end-point was detected amperometrically at a platinum indicator electrode. The method was also applied to determination to dihydrogen sulfide and sulfur dioxide.

Generator-collector mode electrode systems have since been applied to other electrode geometries and systems, *e.g.*, dual cylinders, [83] dual disks, [84] dual bands [8, 10, 17, 29, 37, 73] and different interdigitated array (IDA) electrodes, [15, 85, 86, 87, 88, 89, 90, 91, 92, 93] as well as flow channel systems. [94] The main focus has been on collection efficiency determinations, characterisation of the system, both theoretically and experimentally, as well as applications to analytical purposes, *e.g.*, dual band electrode systems as enzyme electrodes. [8]

Dual (micro)band electrodes have the advantage over other electrode geometries that the manufacturing processes that produce reproducible electrode surfaces are easily constructed. Most of the same advantageous features that are common for microelectrodes apply to them as well but the measured currents may be higher and therefore more convenient in experimental arrangements. Bard et al. [17, 86] presented a digital simulation of generator-collector, shielding and feedback phenomena. They used sputtered platinum dual microband electrodes and compared experimental collection efficiencies with the simulated ones. [17] They predicted that the quasi steady state collection efficiency depends on the width of the gap between the electrodes:

$$\Phi = 0.033 + 0.21 \lg \tau - 0.016 (\lg \tau)^2, \quad (22)$$

where τ is dimensionless time:

$$\tau = \frac{4Dt}{W_{gap}^2}, \quad (23)$$

and W_{gap} is the width of the gap between the microband electrodes. Collection efficiency can be increased by decreasing the gap between the electrodes but the problem is the demanding fabrication of very thin and reproducible insulator layers. Another possibility is to increase the width of the collector electrode. [5] Bard et al. [86] reported that the collection efficiency is dependent particularly on the inter-electrode gap and somewhat on the collector electrode width. Increasing the surface area of the generator electrode leads to the situation where more produced species can escape to the bulk and the collection efficiency is not improved. Triple [10, 37] and higher ('multi') [86] band systems have been studied in order to find the optimal collection efficiency.

Important factors in dual electrode systems are shielding and feedback effects. The shielding effect was first studied with ring-disk electrodes: [103] when both electrodes were kept at the same potential the current response at the ring was lower than expected due to the same simultaneous reaction at the disk. The same phenomenon was also detected with closely spaced microband electrodes when they were stepped to the same potential. [17, 86] That is due to the diffusion layers at the adjacent electrodes that overlap each other, and the flux of reactive material to one electrode is less than it would be if the adjacent electrode was

disconnected. The shielding factor *SF*, *i.e.* the decrease in current, for a band electrode system is [17]

$$SF = 1 - \frac{I_{shielded}}{\sum_{j=1}^{n} I_j}, \quad (24)$$

where $I_{shielded}$ is the sum of currents at the shielded electrodes and the sum in the denominator is the sum of the currents if the bands were connected individually without the shielding effect (other bands at open circuit). The effect on individual electrodes may vary due to different diffusion fields: if the band electrode is a so called 'inner' electrode, adjacent to the substrate tile, the diffusion field from behind the substrate does not reach the electrode, whereas with an 'outer' electrode there is no substrate tile on the other side to prevent that diffusion. Therefore the 'inner' electrode is more likely to be affected by the shielding effect. [86]

The feedback effect is closely related to the shielding effect, although a similar phenomenon has not been observed with ring-disk electrode systems. [17, 83, 84, 86] The feedback means that the species produced at the generator electrode diffuses to the collector, undergoes a reaction that produces the original species and diffuses back to the generator reacting there. The feedback factor *FF* can be expressed as

$$FF = 1 - \frac{I_{gen,O}}{I_{gen,C}}, \quad (25)$$

where $I_{gen,O}$ is the generator current without the feedback effect, *i.e.*, when the collector electrode is at open circuit, and $I_{gen,C}$ is the generator current when the collector electrode is connected in generator-collector mode as well. [17] The effect decreases when the inter-electrode gap increases.

2.2 Present application

The titration method using dual parallel microband electrodes is an application of a generator-collector mode experiment. A titrant is electrogenerated by applying a current at one microband electrode and detected at the other microband either as a current flow or a

potential change. The actual titration reaction takes place in the solution, and the presence of the analyte affects the response at the collector electrode. The principle of the titration is presented in Figure 4.

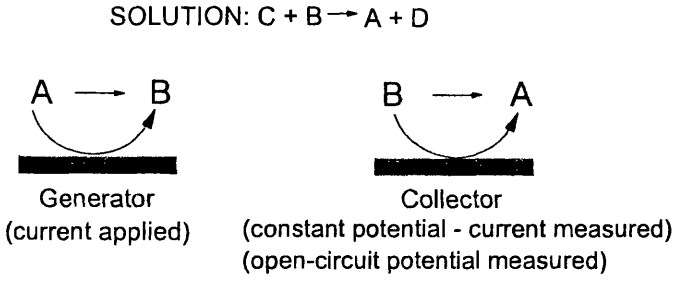

Figure 4. Electrochemical titration using microband electrodes: A, species originally present in the solution; B, titrant; C, analyte. [95] In the amperometric mode the signal is the collector current and in the potentiometric mode the signal is the open-circuit potential.

The presented titration reaction (Figure 4) follows the 'catalytic' mechanism [22, 96] where the species A that reacts at the generator is formed in the actual titration reaction. Another possibility is an EC mechanism (chemical step following electrochemical reaction) [22] where the product of the titration reaction is one compound (not A). The simplest case is when both the analyte C and the formed species D are electrochemically inactive in the potential range in question but the method can also be applied to a case where both C and D are electroactive. [95]

The requirement is that the titration reaction is fast. The required second order rate constant k for the actual titration reaction can be approximated using the time t_D that is needed for produced titrant to diffuse through the inter-electrode gap W_{gap} from the generator to the collector and the half-life of the following titration reaction, t_R: [17]

$$t_D = \frac{W_{gap}^2}{D_{titrant}}, \quad (26)$$

$$t_R = \frac{1}{kc_{analyte}}. \quad (27)$$

Using equations (26) and (27) it can be estimated that, since $t_R < t_D$ is needed in order to detect the change on the collector, therefore

$$k > \frac{D_{titrant}}{W_{gap}^2 c_{analyte}}. \quad (28)$$

The main advantage of this titration method is that it dispenses with a separate titrant solution. There is no need to know the actual sample or titrant volumes or prepare accurate solutions because the fluxes of electroactive species are balanced instead of balancing the molar amounts. The requirement is that the species, from which the titrant is produced, is present in excess. The applied generator current determines the amount of titrant produced according to Faraday's law: [98]

$$Q = It = znF, \quad (29)$$

Equation (29) is valid if the double layer capacitance and charging current are assumed to be negligible.

As a hydrodynamic modulation [95, 99] pulsed motion (vibration) of the microband is used in order to stir the solution, to renew the boundary conditions at the electrode and to improve the reproducibility of the method. After application of the collector potential and when the generator current is still off, the dual microband is vibrated. Then the generator current is applied and the electrochemical measurement is carried out when the electrode is stationary. The motion of the solution dies away on the time scale 1-10 ms, so electrochemical measurement can be treated as being a static solution with the renewed boundary conditions. [73] This leads to reliable mass transport. In this work disposable electrodes are used in order to have a fresh and clean electrode surface for each measurement.

2.2.1 Amperometric end-point detection

Amperometric titration is a traditional indirect electroanalytical method for observing concentration changes of an electroactive species in a solution. [97] It can be employed for common acid-base, redox, precipitation and complexiметric titrations. [98] Amperometric titration is a voltammetric method, since it is based on detection of electrolysis at an indicator electrode and measuring a current-potential curve. [98] The indicator electrode

potential is chosen in order to drive a certain electrode reaction, and it is kept constant during a measurement. The potential is adjusted to be in the diffusion limited current region for the analysed reaction. Conventionally, a titrant is added to the analyte solution in known concentrations and volumes, and the concentration change of the analyte is detected as a change in a current flow. Usually microelectrodes are used as indicator electrodes. The end-point of the titration is solved graphically using a curve where the current is presented as a function of the added titrant volume (Figure 5).[97, 98]

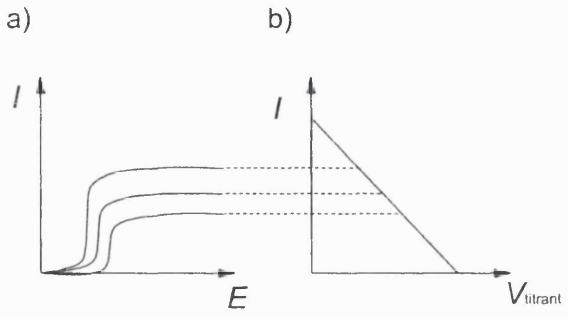

Figure 5. Amperometric titration: a) current-potential curve, b) titration curve. [98] The species that is produced in the presented titration reaction is not electroactive in the potential range of interest (current decreases when titrant added). The end-point is observed when $I = 0$ A.

When two polarising indicator electrodes are employed, the term biamperometric titration is used. The requirement for the current is that a reversible electrode reaction takes place either before the end-point or after it. The potential is applied between the indicator electrodes and the current is measured. The essential feature is that the potential is not determined against any known reference electrode but the actual potential difference between the indicator electrodes is determined by the redox couple in question. [98]

In a generator-collector mode titration (Figure 4), a current is applied at the generator electrode in order to generate the titrant electrochemically. When amperometric end-point detection is used, the collector electrode potential is kept constant. The potential is chosen to drive the reversed reaction to that taking place at the generator. If a compound (or ion) that reacts irreversibly with the produced species is present in the solution this is observed as a decreased collector current and as a lower collection efficiency. The shape of the collector current transient also changes when the analyte is present. The concentration of the analyte can therefore be determined by using both the decrease in the collection efficiency and the change in the shape of the collector current transient that follows the application of the generator current. [95, 99]

2.2.2 Potentiometric end-point detection

Potentiometric titration is a traditional electroanalytical method where the electromotive force of a currentless electrochemical cell is measured. [100] Conventionally, a titrant solution, the accurate concentration of which is known, is added to an analyte solution in known volumes, and the open-circuit potential of an indicator electrode against a reference electrode is measured. The actual titration curve consists of the open-circuit potential of the indicator electrode as a function of added titrant volume (E vs. $V_{titrant}$), and the data analysis is based on derivatives of the curve, the end-point being determined by using the maximum of the first derivative (Figure 6). [60]

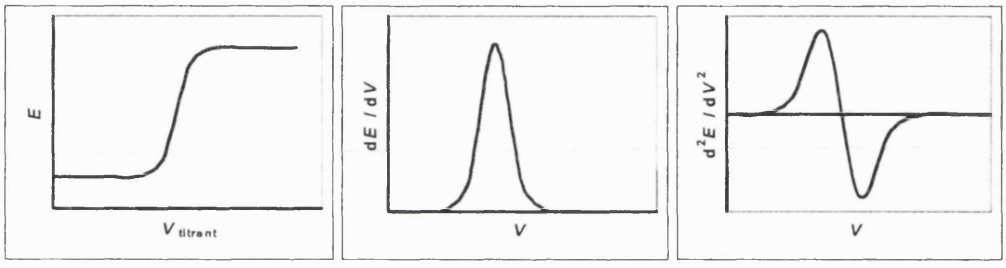

Figure 6. Potentiometric titration curve and its first and second derivatives.

The response of a potentiometric titration can be distorted by the reaction of the actual indicator electrode material and side reactions that affect the electromotive force. When the electrochemical equilibrium of the redox couple in question is reached slowly, a constant current potentiometry may be employed where a low current is applied at the indicator electrode in order to promote the equilibrium. [137]

In the generator-collector mode titration, the titrant is generated electrochemically, as in amperometric titration, by applying a current at the generator (Figure 4):

(30) $\nu_A A \rightarrow \nu_B B \pm e^-$,

where ν_A and ν_B are stoichiometric co-efficients. The open-circuit potential of the collector electrode is determined by the ratio of activities of the ion A in the electrolyte and the titrant B by the Nernst equation [22]

$$E = E^{\circ} \mp \frac{RT}{F} \ln\left(\frac{a_A^{\nu_A}}{a_B^{\nu_B}}\right), \quad (31)$$

where E° is the standard potential of the reaction and a is the activity. In ideal solutions, *i.e.*, at low ionic strengths and low concentrations, activities of the ions can be replaced by their concentrations ($a = \gamma_A c$; activity co-efficient $\gamma_A = 1$). That approximation simplifies the analysis and in many potentiometric titrations describes the system reasonably accurately. [38, 137] When the analyte C is present in the solution the reaction between the titrant and the analyte, presented in Figure 4, takes place. The concentration of A can be assumed to be constant because of a large excess of the electrolyte. On the other hand, if the electrode potential is known the concentration of the titrant B can be determined near the electrode surface using Equation (31), and the more analyte is present in the solution, the more the open-circuit potential of the collector electrode changes. If the analyte is electrochemically active the potential of the indicator (collector) electrode before the end-point depends also on the analyte concentration.

In this work, two different methods of potentiometric experiments are used depending on the way the titrant is generated: a constant current or a ramp current that increases linearly with time. The open-circuit potential of the collector electrode is measured in both cases. When the constant current method is used, a series of measurements with different generator currents is needed in order to produce a traditional titration curve ($E_{\text{open-circuit}}$ vs. I_{gen}). The advantage of the use of a ramp current method is that the whole potentiometric titration curve is obtained during a single scan (Figure 7). The time needed for an analysis decreases significantly, and the data analysis becomes more straightforward. When a current sweep is employed, the double layer charging current, I_C, subtracts from the total current, I, and hence decreases the current for generation of the titrant, I_F. From consideration of a simple parallel equivalent circuit, $I_C/I_F \approx R_F C_{dl} \nu_A / I$, where ν_A = current sweep rate and $R_F C_{dl}$ = time constant. $R_F = dE/dI_F$ is the Faradaic resistance for the generator electrode and C_{dl} is the double layer capacitance. Typically, $R_F C_{dl} \approx 0.01$ s, [22] so the effect is negligible for all except the very first stages of the current ramp for the conditions used in this work.

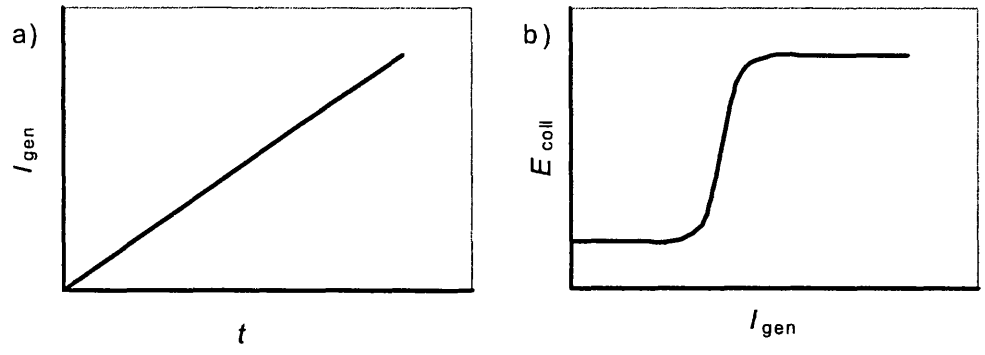

Figure 7. Potentiometric titration with dual microband electrodes using ramp current method: a) initiation, b) response.

2.2.2.1 Precipitation titrations using dissolving silver microbands

A novel application of a generator-collector mode titration is the use of a dissolving generator electrode. [101] Dissolving silver and copper electrodes have been previously employed for determination of diffusion co-efficients of metal cations of interest [102] and for ring-disk electrode studies. [103] In this work, dissolving electrodes are used for a generator-collector mode titration with microband electrodes for the first time. The principle of the titration is analogous to that presented in Figure 4: the titrant is produced by applying a current at the generator electrode, but instead of generating the titrant from a species in the solution the titrant is electrogenerated by dissolving the generator electrode material. The method is here applied to silver microband electrodes and precipitation titrations where the titrant is Ag^+. The open-circuit potential change is detected at the collector electrode (indicator electrode) as the analyte concentration changes.

2.3 System modelling – theoretical discussion

Electrochemical systems are modelled using partial diffusion equations with suitable initial and boundary conditions, as presented in Chapter 1. All mass transport processes, reactions and concentration changes of electroactive species must be taken into account. The purpose of theoretical modelling of the system is to understand the processes taking place, to compare experimental results with calculations and, in many cases, to use the equations with experimental data in order to find out, *e.g.*, kinetic parameters. There are three possibilities of finding the solution to the modelling equation: 1) an analytical solution, 2) a combination

of an analytical and numerical solution, or 3) a computer calculation, *e.g.*, a numerical solution or simulations. In general, the analytical models of electrochemical systems lead to either explicit solutions, *i.e.*, a formula, series or integral, or asymptotic solutions, *i.e.*, formal series accurate at short or long times. [22, 28, 30, 87]

Analytical solutions provide a general quantitative picture of an electrochemical problem, but usually simplifying assumptions have to be made. For instance, when a steady state approximation is used, the solutions of the differential equations may be straightforward. However, many real processes are time-dependent, *i.e.*, non-steady state systems. A typical method for removing the time variable is based on Laplace transforms: [22, 36, 104]

$$L\{f(t)\} = \overline{f}(s) = \int_0^\infty f(t)e^{-st}dt . \qquad (32)$$

The main application of Laplace transforms is in converting derivatives into products, *i.e.*, converting differential equations into algebraic equations. [105]

In addition, in the case of microelectrodes the multi-dimensional diffusion and non-uniform current distribution [106] make the flux equations complicated and therefore numerical methods, which give approximate mathematical solutions, are often employed.

As discussed in sections 1.3 and 1.4, the mass transport at microelectrodes is typically limited to diffusion problems, and diffusion at a microband electrode can be modelled using a hemi-cylinder of equivalent area resulting in approximate equations for a quasi steady state current. For band electrodes, the calculations are often presented in polar co-ordinates, and the basic diffusion equations are Bessel functions. [36, 39, 105, 107] General solutions for double band electrode systems cannot be found in literature but there are several examples of numerical calculations and digital simulations for both microband and other microelectrode systems. [17, 29, 37, 86, 87, 99, 108, 109]

2.3.1 Analytical solution for a double band system

In this section, analytical solutions for the double microband electrode system in the potentiometric mode are presented. Both constant current and ramp current methods for generating the titrant are discussed.

In all of the solutions, let us use the definition I / zFA for the flux J_d in Fick's first law (eq. (2)). [22] We can assume that the surface area of the microband electrode corresponds to a hemi-cylinder with the same perimeter, thus $A = \pi w l$, where $w = W / 2$. Let us model the dual microband system using polar co-ordinates (r, θ) as presented in Figure 8. The microband can be assumed to be infinitely long, if $r << l$ (= electrode length). This means that the diffusion can be approximated to be two-dimensional (x and y directions).

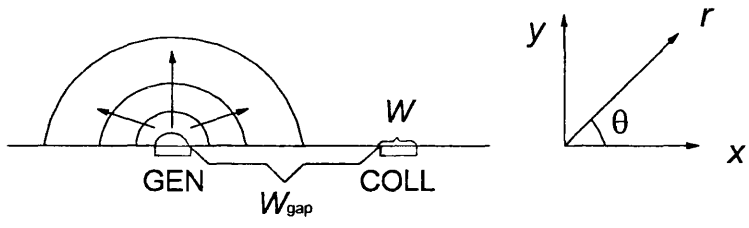

Figure 8. Dual microband system in polar co-ordinates.

In polar co-ordinates

$$r = \sqrt{x^2 + y^2}, \tag{33}$$

$$\theta = \arctan\left(\frac{y}{x}\right), \tag{34}$$

and Fick's second law is [104]

$$\frac{\partial c}{\partial t} = D\left(\frac{\partial^2 c}{\partial r^2} + \frac{1}{r}\frac{\partial c}{\partial r} + \frac{1}{r^2}\frac{\partial^2 c}{\partial \theta^2}\right). \tag{35}$$

In the potentiometric case, the open-circuit potential at the collector electrode is the measured variable. We assume that the collector potential is determined completely by the equilibrium between the species originally present in the solution and the titrant (species A and B, respectively, in Figure 4). The effects of reactions of the indicator electrode material and side reactions are neglected. Our aim is to find out how the titrant concentration changes

as a function of r. At the collector electrode, $r = W_{gap} + W$ (*i.e.*, the distance from the middle of the generator electrode to the middle of the collector electrode).

In the potentiometric case, no reaction takes place at the collector electrode, and the concentration does not change as a function of θ. Therefore, the last term on the right hand side in Equation (35) can be assumed to vanish.

Let us first consider the case where the titrant is generated using the constant current method, and assume that steady state conditions, *i.e.*, $\partial c/\partial t = 0$, prevails for the titrant concentration. The solution of Equation (35) using the steady state assumption is

$$c_B(r) = e^{a_0} \ln\left(\frac{r_1}{r}\right), \tag{36}$$

where a_0 and r_1 are integration constants. The constant r_1 is the distance from the generator electrode to a point where the titrant concentration can be assumed to be 0. We can approximate $r_1 \approx l$ (electrode infinitely long). The integration constant, a_0, can be solved using Fick's first law (eq. (2)):

$$\frac{I_{gen}}{zF\pi rl} = -D_B\left(\frac{\partial c_B}{\partial r}\right) \tag{37}$$

resulting in $a_0 = \ln[I_{gen}/(zF\pi lD_B)]$. Therefore, the concentration of the titrant as a function of r is:

$$c_B(r) = \frac{I_{gen} \ln\left(\frac{r_1}{r}\right)}{zF\pi lD_B}. \tag{38}$$

The concentration of A can be assumed to be constant, and the open-circuit potential of the collector electrode can be calculated using the Nernst equation (eq. (31)).

When the analyte (species C in Figure 4) is present, let us assume that c_C is constant, the value of c_C is high and the diffusion of C is infinitely rapid, leading to the steady state approximation. Then, to the titrant concentration as a function of r applies:

$$(39) \qquad c_B(r) = -\frac{I_{gen}}{zF\pi wl\sqrt{D_B kc_C}K_0'\left(\sqrt{\frac{kc_C}{D_B}}w\right)}K_0\left(\sqrt{\frac{kc_C}{D_B}}r\right)$$

where K_0 is a modified Bessel function, k is the second order rate constant for the reaction between the titrant and the analyte, and c_C is the analyte concentration. A stoichiometric coefficient is included in k in Equation (39). The details of the calculation are presented in Appendix I.

In the second case, the titrant is generated using the ramp current method. The simplest case is when no analyte is present. Let us again use Equation (35) but this time the steady state approximation is not valid. After a Laplace transform, to the titrant concentration as a function of r at long times applies:

$$(40) \qquad c_B(r) = \frac{v_A t}{zF\pi l D_B}\left[\ln(2) - \gamma - \ln\left(\frac{r}{\sqrt{tD_B}}\right) - \frac{\psi(2)}{2}\right],$$

where v_A is the generator current scan rate, γ is Euler's constant ($\gamma = 0.57722$) and ψ is the digamma function. [105] The solution is based on a modified Bessel function. As presented in section 1.4, the response is dependent on the length of the microband electrode rather than the surface area or the electrode width. The details of the calculation are presented in Appendix II.

2.3.2 Combined analytical and numerical solution for a double band system

In this section, some analytical equations, which are difficult to solve without numerical calculations, are presented as examples of a combination of an analytical and numerical solution. The actual analytical forms can be derived as shown in the previous section and Appendices I and II, but for the inverse Laplace transforms of the final equations specific computer programmes have to be employed. The examples are shown for the potentiometric case with the ramp current method as well as for the amperometric case.

As the first example, the potentiometric titration with the ramp current method is discussed. In the previous section, we made an approximation of a long time scale for the system without the analyte. For a more valid solution, the equation for the titrant concentration,

$$\bar{c}_B(r) = -\frac{\nu_A K_0\left(\sqrt{\frac{s}{D_B}}r\right)}{s^{\frac{5}{2}} zF\pi wl\sqrt{D_B}K_0'\left(\sqrt{\frac{s}{D_B}}w\right)}, \tag{41}$$

should be solved using the inverse Laplace transform (see Appendix II). Since the inverse transform for Equation (41) cannot be done analytically, a computer programme that calculates the transforms numerically must be employed. We can use a readily available Fortran77 routine C06LAF, which estimates the value of the inverse Laplace transform of a given function using a Fourier series approximation. We can similarly use a Fortran77 subroutine S18DCF for approximating the values of the modified Bessel functions. [110]

When the analyte is present, the titrant concentration before the inverse Laplace transform is

$$\bar{c}_B(r) = -\frac{\nu_A}{s^2 zF\pi wl\sqrt{D_B(kc_C+s)}K_0'\left(\sqrt{\frac{kc_C+s}{D_B}}w\right)} K_0\left(\sqrt{\frac{kc_C+s}{D_B}}r\right). \tag{42}$$

Here we have again assumed that c_C is constant, the value of c_C is high and the diffusion of C is infinitely rapid. A stoichiometric co-efficient is included in k in Equation (42). The details of the calculation are presented in Appendix III. As in the case with no analyte, the numerical calculation using the computer programme is required in order to approximate the inverse Laplace transform of the equation.

In the potentiometric case, the titrant concentration does not change at the collector electrode, since no reaction takes place. On the contrary, in the amperometric titration the titrant reacts at the collector in the reversed reaction to that taking place at the generator. The measured variable is the collector current.

Let us first consider the case where no analyte is present. The titrant is generated at the generator as in the potentiometric titration with the constant current method. We can assume

that the titrant concentration reaching the collector, reacts there and an equal concentration, but negative, starts to diffuse away from the collector. The approximation leads us to the solution for the collector current

$$\bar{I}_{coll}(s) = -\frac{I_{gen}}{s}\frac{K_0\left(\sqrt{\frac{s}{D_B}}r\right)}{K_0\left(\sqrt{\frac{s}{D_B}}w\right)}, \tag{43}$$

where the inverse Laplace transform has to be carried out numerically. The approximation does not take the feedback effect (eq. (25)) into account. The details of the calculation are presented in Appendix IV.

The second case is when the analyte is present. Let us again assume that c_C is constant, the value of c_C is high and the diffusion of C is infinitely rapid. This leads us to

$$\bar{I}_{coll}(s) = -\frac{I_{gen}}{s}\frac{K_0\left(\sqrt{\frac{kc_C + s}{D_B}}r\right)}{K_0\left(\sqrt{\frac{kc_C + s}{D_B}}w\right)}, \tag{44}$$

where the inverse Laplace transform has to be solved numerically as previously. The details of the calculation are presented in Appendices I-IV.

As presented here, many simplifying approximations have to be made in order to model a dual microband system. For more accurate solutions, the diffusion equation should also be written for both species A and C, which makes the analytical solution even more complicated. Numerical methods and digital simulations provide a tool for progressing with more complicated calculations.

2.3.3 Digital simulation for a double band system

In this section, a digital simulation is presented as an example of a complete numerical solution. In digital simulations a model is set up to describe the electrochemical problem in question, and a computer programme carries out the actual simulation. Typically, the diffusion equations of a certain system are simulated in a dimensionless form. [22] The accuracy of a simulation depends on the choice of parameters. The sources of inaccuracy, in the case of diffusion processes to an electrode, are mainly the calculation of the concentrations, the numerical approximation of the flux at the electrode surface and the integration of the flux over the electrode surface. [111]

The simulations presented in this section describe the present double microband system in the amperometric mode. The procedure employs a finite difference method, and the actual simulations were carried out by J. Strutwolf. [99, 112, 113]

The basic principle of finite difference methods for solving differential equations is to replace derivatives by suitable difference equations that are easier to solve with the applying boundary conditions. A grid is superimposed on the domain of interest and the difference equations are solved for the concentration at each grid point taking the neighbouring grid points into account. The time is also divided into discrete steps. [113]

Both single microbands and generator-collector mode microband systems have been modelled using conformal mapping. [32, 37, 99, 113] The correspondence of the real physical dimensions of a dual microband system in cartesian co-ordinates to the conformal space is shown in Figure 9.

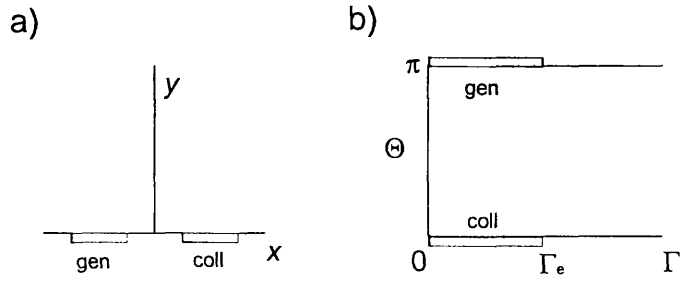

Figure 9. Double band electrode system: a) cartesian, b) conformal co-ordinates.

The gap between the electrodes in the conformal map (Figure 9) is located at the end of the rectangle marked by Θ, the bulk of the solution being towards the open end. The conformal map is defined by [37]

(45) $$x = (W_{gap} / 2)(\cosh \Gamma)(\cos \Theta),$$

(46) $$y = (W_{gap} / 2)(\sinh \Gamma)(\sin \Theta).$$

The electrode width in the conformal space is

(47) $$\Gamma_e = \cosh^{-1}\left(1 + 2W / W_{gap}\right).$$

The grid points in the conformal co-ordinates are equidistant whereas in the cartesian co-ordinates they are not, following approximately the equiconcentration lines at a microelectrode (Figure 10). In cartesian co-ordinates, both x and y directions are infinite, and there are more grid points where the currents are higher. This clarifies the usefulness of the conformal mapping since the non-uniform current distribution at the band electrode in cartesian co-ordinates changes to the uniform current distribution in the conformal space. [113]

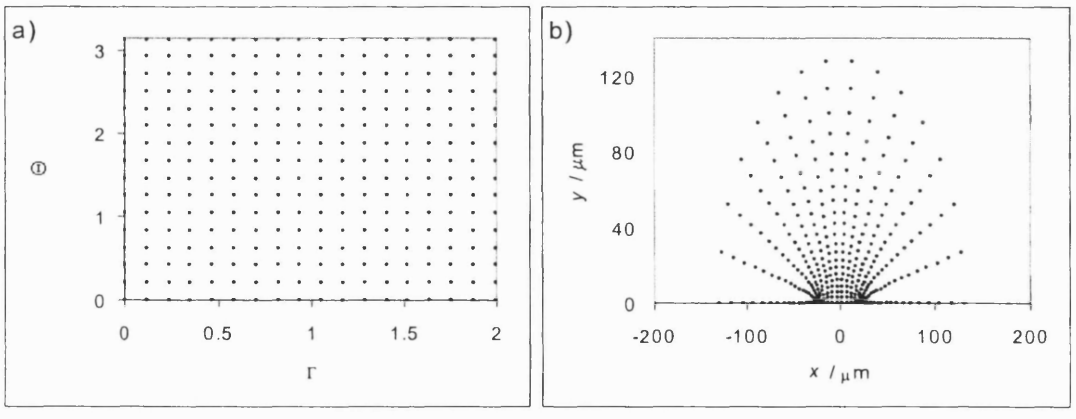

Figure 10. Grid points in a) conformal and b) cartesian co-ordinates.

Fick's second law (eq. (3)) in the conformal space is

(48) $$\frac{\partial C}{\partial \tau} = \frac{1}{(\sinh^2 \Gamma + \sin^2 \Theta)}\left(\frac{\partial^2 C}{\partial \Gamma^2} + \frac{\partial^2 C}{\partial \Theta^2}\right),$$

where C is dimensionless concentration c/c^b, and τ is dimensionless time (equal to eq. (23)) [37, 99, 113]

The boundary conditions for galvanostatic (constant current) conditions at the generator while the collector is held at a potential at which the reversed reaction takes place are (for species A in Figure 4):

(49) $0 \le \Gamma \le \Gamma_{lim};\ 0 \le \Theta \le \pi,\ C_A(\Gamma, \Theta, \tau) = 1,$ $(\tau = 0)$

(50) $0 \le \Gamma \le \Gamma_e;\ \Theta = \pi,\ \partial C_A/\partial\Theta = g(\Gamma)$ (generator). $(\tau > 0)$

(51) $0 \le \Gamma \le \Gamma_e;\ \Theta = 0,\ C_A(\Gamma, \Theta, \tau) = 1$ (collector), $(\tau > 0)$

(52) $\Gamma_e \le \Gamma \le \Gamma_{lim};\ \Theta = \pi,$ and $\Theta = 0,\ \partial C_A/\partial\Theta = 0$ (insulator), $(\tau > 0)$

(53) $\Gamma = 0,\ 0 < \Theta < \pi,\ \partial C_A/\partial\Gamma = 0$ (insulator), $(\tau > 0)$

where $g(\Gamma)$ is the local gradient at the generator electrode. The local gradient at $\Gamma = i\Delta\Gamma$ is g_i and for the first time step [99]

$$g_i = \frac{G_{gen}}{(n_e + 1)\Delta\Gamma}, \qquad (0 \le i \le n_e) \tag{54}$$

where n_e is the number of grid points along the electrode, $\Delta\Gamma$ is the distance between the grid points, and G_{gen} is the dimensionless current at the generator,

$$G_{gen} = \int_0^{\Gamma_e} \left(\frac{\partial C_A}{\partial \Theta} \right)_{\Theta=\pi} d\Gamma. \tag{55}$$

Multiplying Equation (55) by zFc^blD results in the current in Ampére. [99]

For the first time step, Equation (54) is set, and the individual g_i values are then used as boundary conditions. The diffusion equation (Fick's second law, eq. (48)) is solved with the boundary condition $(\partial C_A/\partial\Theta)_{\Theta=\pi} = g(\Gamma)$, resulting in new surface concentrations. The local gradients are then recalculated with the new surface concentrations and the total gradient evaluated. The new local gradients are used as boundary conditions in the next time step. G_{gen} settles rapidly to a constant value. [99]

Simulation of the titration method requires introduction of a second-order homogeneous reaction between analyte and titrant as presented in the previous section. For B (Figure 4) the boundary conditions at the generator (eq. (50)) and collector (eq. (51)) are replaced by

(56) $0 \leq \Gamma \leq \Gamma_e;\ \Theta = \pi,\ \partial C_B/\partial\Theta = -g(\Gamma),$ $(\tau > 0)$

(57) $0 \leq \Gamma \leq \Gamma_e;\ \Theta = 0,\ C_B(\Gamma, \Theta, \tau) = 0,$ $(\tau > 0)$

The dimensionless currents at the collector (G_{coll}) is

(58) $$G_{coll} = \int_0^{\Gamma_e} \left(\frac{\partial C_B}{\partial \Theta} \right)_{\Theta=0} d\Gamma.$$

For the electroinactive species C (Figure 4) the no flux condition $\partial C_C/\partial\Theta = 0$ also prevails at the electrode surfaces. The initial condition is given by $C_C = C_C^b$. [99] Fick's second law (eq. (48)) is then calculated for all species A, B and C. For the actual simulations, 300 × 300 space grid and $\Delta\tau = 0.00112$ were used. [99]

Digital simulations provide a tool for calculating complicated sets of equations the solutions of which would not be possible without the capacity of computers. Successful simulations are in agreement with experimental results and help to analyse the processes taking place.

2.3.4 Reaction layer model

In this section, a reaction layer model is presented in order to approximate an electrochemical titration with dual microband electrodes. [99] Conformal mapping (Figure 9) in the case of an amperometric end-point detection is used in order to present the system. In the conformal space, the electrodes form two sides of a rectangle closed at one end by the insulator and open to the solution at the other end. It can be assumed that, at short times (with a time scale that is longer for lower generator current), the electrogenerated titrant is confined to the space between the electrodes. At longer times and small gap-to-width ratios and sufficiently high generator current, the concentration profile of titrant between generator and collector is approximately linear. A well-defined diffusion layer forms outside the rectangle.

The first case is when no analyte is present. It can be approximated that, within the inter-electrode gap, the concentration of the titrant B (Figure 4) is independent of Γ but varies linearly with Θ. Outside the gap, c_B decreases linearly with Γ as presented in Figure 11.

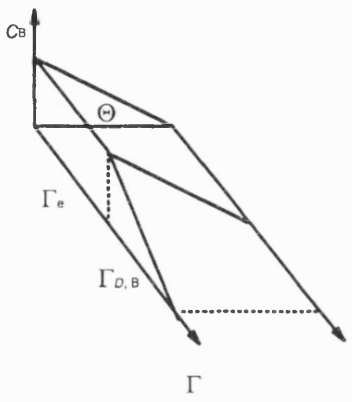

Figure 11. Concentration profile for the titrant in the absence of the analyte in the conformal space. Γ_e is the width of the microband, and $\Gamma_{D,B}$ is the diffusion layer for the titrant.

This approximation does not take into account the amplification of current caused by the feedback effect (eq. (25)). However, with high gap-to-width ratios the effect weakens. [86] If Γ_e is the width of the electrode (Figure 9) and $\Gamma_{D,B}$ is the thickness of the diffusion layer for the titrant, c_B decreases to zero at $\Gamma_e + \Gamma_{D,B}$. The thickness of $\Gamma_{D,B}$ can be estimated by a numerical simulation. [99] If $c_{B,g}$ is the titrant concentration at the generator, the flux across the gap is $c_{B,g}D_B\Gamma_e/\pi$ and the flux into the solution is $c_{B,g}D_B\pi/2\Gamma_{D,B}$. As a consequence, the collection efficiency, Φ, is

$$\Phi = 1 / (1 + \pi^2 / 2\Gamma_e\Gamma_{D,B}). \quad (59)$$

In Ref. 99, simulated and calculated (eq. (59)) collection efficiencies were compared with each other. A good agreement was found when the gap-to-width ratio was smaller than 3 while a deviation was observed for higher ratios due to the invalidity of the linear approximation.

The second case is when the analyte is present, and a fast reaction rate is assumed (eq. (28)). As the generator current is increased a reaction layer forms. Again, it can be approximated that, within the inter-electrode gap, the concentration of the titrant B (Figure 4) is

independent of Γ but varies linearly with Θ. Outside the gap, c_B decreases linearly with Γ as presented in Figure 11. The analyte concentration can be assumed to be zero within the inter-electrode gap. The reaction layer is determined as a layer outside the gap where the analyte concentration = 0 and the titrant concentration decreases linearly. The thickness of the reaction layer, $\Gamma_{D,B}$, is determined by the balance between the fluxes of titrant and analyte. A simplified model is shown in Figure 12.

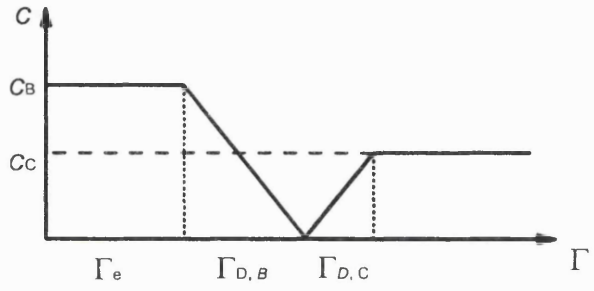

Figure 12. Concentration profiles for the titrant and the analyte as a function of Γ. Γ_e is the width of the microband, $\Gamma_{D,B}$ is the reaction layer, and $\Gamma_{D,C}$ is the diffusion layer for the analyte. An infinitely rapid reaction between titrant and analyte is assumed.

The thickness of the reaction layer is less than the thickness of the diffusion layer for the titrant without the analyte, but approaches that value when the generator current increases.

As for the titrant, a diffusion layer of width $\Gamma_{D,C}$ also forms for the analyte. Similarly, its value may be determined by a numerical simulation. [99] At the inner edge of the analyte diffusion layer, c_C decreases to zero since it is consumed by the reaction with the titrant. It can be assumed that the outer edge of the analyte diffusion layer moves to lower Γ values when the gap width increases. When the analyte concentration increases or the generator current decreases, the inner edge of the analyte diffusion layer moves towards the edge of the gap. At high enough concentration or low enough generator current, the analyte penetrates the gap and has approximately constant concentration within the gap. In Ref. 99, the dimensionless flux of titrant required to balance the flux of analyte to the inner edge of $\Gamma_{D,C}$ was determined to be $\Delta G_B = \nu G_C/\Gamma_{D,C} = \nu C_C/\Gamma_{D,C}$ where ν is the number of moles of titrant required to react with one mole of analyte. That was converted to dimensioned quantities and expressed as an additional, required generator current:

$$\Delta I_{gen} = \frac{z \nu c_C^b F l D_C}{\Gamma_{D,C}}. \quad (60)$$

Hence, the ΔI_{gen} is approximately proportional to the concentration of the analyte.

Experimental data can be presented by plotting the collector current, I_{coll}, as a function of the applied generator current, I_{gen}. ΔI_{gen} is the displacement parallel to the I_{gen} axis between the I_{coll}-I_{gen} curves without the analyte and with the analyte. Thus, ΔI_{gen} is the additional flux from the generator required to balance the flux of analyte (species C in Figure 4) to the edge of the reaction layer. The reaction layer model predicts that when the generator current is sufficiently high, the increase in the collector current lies parallel to the curve where no analyte is present.

Again, in Ref. 99 simulated and calculated (eq. (60)) ΔI_{gen} values were compared with each other. A good agreement was found when the gap-to-width ratio was small (< 3) and the analyte concentration was low (≤ 2.5 mM) but deviations were observed for higher values. If the experimental conditions are fulfilling the assumptions, the analyte concentration can be determined from the displacement of the measured I_{coll}-I_{gen} curve.

3 Applications

3.1 Titration of vitamin C with electrogenerated ferricyanide

L-Ascorbic acid (vitamin C) is an important anti-oxidant for metabolic processes in the human body. [114] It can be found in fresh vegetables and fruits, and it is widely used in the food industry. [115] There is a high demand for a simple, rapid and economical system of analysis, as many of the traditional determination methods are expensive and time-consuming. Conventionally, titrimetry, spectrophotometry and chromatography, as well as enzymatic and electrochemical methods are used for determination of vitamin C. [116, 117] A usual titrant for vitamin C is iodine. [38, 97] There are also many studies reporting an amperometric flow injection analysis for detection of L-ascorbic acid. [117, 118, 119, 120]

The electoanalytical methods for vitamin C determination are based on its irreversible oxidation to dehydroascorbic acid (Figure 13). [5, 10, 121] The electrochemistry has been studied at different electrode materials, and the electrocatalytic oxidation has been investigated at different films, *e.g.*, on Prussian Blue and polypyrrole coated electrodes. [122, 123, 124, 125, 126] In kinetic studies of oxidation of vitamin C, a two-electron transfer in two steps has been reported, but the reaction route may vary. [126, 127] The oxidation of vitamin C is dependent of the pH value and the employed electrode material. [10, 122]

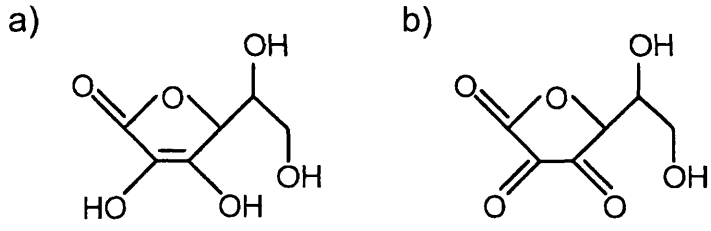

Figure 13. Structures of a) ascorbic acid, b) dehydroascorbic acid.

Ferricyanide, $[Fe(CN)_6]^{3-}$, reacts with vitamin C in a two-step reaction where the first step is rate-determining. The rate of the reaction depends on the pH value of the solution, the rate constant being smaller in acidic solutions. [96, 128, 129, 130, 131, 132] In near neutral pH, the second order rate constant can be estimated to be of order 10^3 $M^{-1}s^{-1}$. [99] In the present method with dual microband electrodes, the titrant, $[Fe(CN)_6]^{3-}$ is electrogenerated at the generator electrode, and the second-order reaction between the titrant and the analyte takes place in the

solution (Figure 4). In the amperometric mode, the reduction of $[Fe(CN)_6]^{3-}$ back to $[Fe(CN)_6]^{4-}$ is detected at the collector, and in the potentiometric mode the open-circuit potential of the collector electrode is mainly determined by the equilibrium of $[Fe(CN)_6]^{4-}$ /$[Fe(CN)_6]^{3-}$. The reactions are: [133]

(61) Generator: $[Fe(CN)_6]^{4-} \rightarrow [Fe(CN)_6]^{3-} + e^-$, $E^o = +0.218$ V vs. SCE

(62) Collector: $[Fe(CN)_6]^{3-} + e^- \rightarrow [Fe(CN)_6]^{4-}$,

(63) Solution: $2[Fe(CN)_6]^{3-} + C_6H_8O_6 \rightarrow 2[Fe(CN)_6]^{4-} + C_6H_6O_6 + 2H^+$.

In the amperometric mode the collector potential is kept at –0.100 V vs. SCE to drive the reduction of $[Fe(CN)_6]^{3-}$ to $[Fe(CN)_6]^{4-}$. Simultaneously, vitamin C is inert at that collector potential which is guaranteed adjusting the experimental conditions (phosphate buffer, pH = 6.8). [121, 125]

3.2 Titrations of thiosulfate and sulfite with electrogenerated iodine

Iodimetry and iodometry are traditional titration methods that are based on the iodide/iodine (I^-/I_2) chemistry. In iodimetry, a reducing analyte is titrated with I_2 to produce I^-, and in iodometry an oxidising analyte is added to I^- solution to produce I_2. The formed I_2 is then titrated with thiosulfate ($S_2O_3^{2-}$) traditionally by using a starch indicator. [38, 137] In the present generator-collector mode titration with dual gold microband electrodes these methods are combined: Firstly, the method is based on electrogeneration of the titrant I_2 from I^-. Secondly, the titration of thiosulfate has been used as an example, which can be applied to back titrations. The determination of sulfite has been demonstrated as another application of a generator-collector mode titration using electrogenerated I_2. In Ref. 134, this type of sulfite titration has been presented in the amperometric mode with platinum macroelectrodes.

Titration of thiosulfate with iodine is a very common titration reaction in analytical chemistry, [135, 136, 137] the stoichiometry of which is well established. Thiosulfate is often used as a reducing agent in redox reactions. [38] It is also used as a fixed salt in photography, and as a detoxicating agent (through thiocyanate formation) in cyanide poisoning. [138] Sodium sulfite is used in the food industry as a preservative and its analysis is important, since it causes allergic reactions to people with asthma. [38, 139] The titration can be applied to sulfur dioxide SO_2 determination. [97, 140, 141] Both sulfur containing compounds are environmentally harmful since under favourable conditions they can form sulfuric acid. [142] The analyses of thiosulfate

and sulfite are mainly based on their electrochemical properties. [38, 137, 138] Both thiosulfate's and sulfite's reactions with iodine have also been applied in a biamperometric mode. [38]

The overall reactions for these titration systems in a generator-collector mode using dual microband electrodes are: [52, 133, 134, 136, 143, 144, 145]

(64) Generator: $2I^- \rightarrow I_2 + 2e^-$, $E^0 = +0.294$ V vs. SCE

(65) Collector: $I_2 + 2e^- \rightarrow 2I^-$,

(66) Solution: $I_2 + 2S_2O_3^{2-} \rightarrow 2I^- + S_4O_6^{2-}$ (thiosulfate),

(67) $I_2 + SO_3^{2-} + H_2O \rightarrow 2I^- + SO_4^{2-} + 2H^+$ (sulfite).

In practice, when an excess of iodide is present in the solution the tri-iodide ion I_3^- is the reactive species instead of iodine I_2, [135, 143, 146] and the generator-collector reactions as well as actual titration reactions change respectively. The pH of the solution in the range of 1...7 has not been observed to affect the redox behaviour of $I^-/I_3^-/I_2$ –systems. [143, 148] The main source of error in an iodide based titration is its oxidation to I_2 due to oxygen, which particularly takes place in acidic solutions and is enhanced by direct sunlight. [137] This can be avoided by using a protective gas (Ar, N_2) and not storing the solutions for a long time.

Margerum et al. [136, 144] studied the reaction mechanisms and kinetics of the reactions (66) and (67) in acidic solutions. They reported very fast ($k > 10^6$ $M^{-1}s^{-1}$) multistep mechanisms for both cases that include short-lived intermediates $I_2S_2O_3^{2-}$ and $IS_2O_3^-$ for thiosulfate titration and ISO_3^- for sulfite titration. The kinetic parameters of $I^-/I_3^-/I_2$ -systems have proven to be dependent on the experimental conditions used. [143]

Both I^- and I_2 adsorb on gold electrodes but the phenomenon is not expected to affect the reversibility of a I^-/I_2 -couple, [143, 147, 148] especially when disposable electrodes are employed. There are also several references [149, 150, 151] reporting the solubility of gold in iodide solutions, but, again this is not expected to cause problems with disposable electrodes. The adsorption phenomenon can be seen in Figure 14 where a cyclic voltammogram of I^- in an acidic solution on a gold microband electrode is presented. The peak at +400 mV vs. SCE is the desorption, 'stripping', peak for I_2, corresponding to the amount deposited during the forward scan. [22, 148]

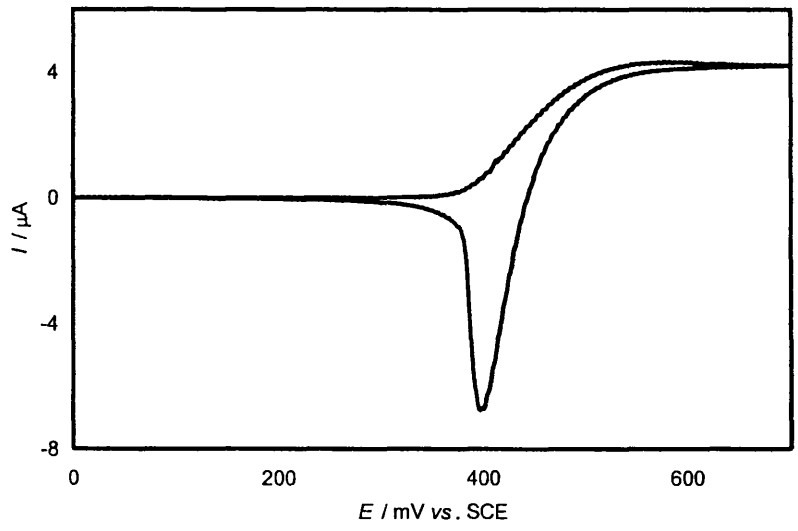

Figure 14. Cyclic voltammogram for iodide at a freshly snapped gold microband electrode. 5 mM KI, supporting electrolyte 0.1 M H_2SO_4, scan rate 25 mV/s.

In the dual microband titration in the amperometric mode, the collector potential of 0.0 V vs. SCE was chosen, a potential that is more negative to the actual desorption peak. The titration was also applied to the potentiometric titration, the end-point being determined by the I^-/I_2 equilibrium.

3.3 Titrations of dichromate and permanganate with electrogenerated iron(II)

Both dichromate ($Cr_2O_7^{2-}$) and permanganate (MnO_4^-) titrations are widely used in analytical chemistry.[137, 141, 152] Both compounds are oxidants commonly used as titrants, and the titrations presented here can be extended to applications where back titrations are needed. An important application where dichromate titration is required is chemical oxygen demand (COD), which is typically used in compliance with industrial regulation. The standard procedure includes oxidising pollutants by dichromate refluxing them for two hours. The excess of dichromate is then analysed, and the actual COD is the O_2 that is chemically equivalent to the $Cr_2O_7^{2-}$ reacted in the oxidation process.[38, 153] Titration of dichromate with Fe^{2+} is analogous to the vitamin C, thiosulfate and sulfite titrations, but determination of permanganate differs from them because the analyte itself is electroactive in the potential range of interest. The reactions are as follows: [133, 152]

(68) Generator: $Fe^{3+} + e^- \rightarrow Fe^{2+}$, $E^0 = +0.437$ V vs. SCE

(69) Collector: $Fe^{2+} \rightarrow Fe^{3+} + e^-$,

(70) Solution: $Cr_2O_7^{2-} + 6Fe^{2+} + 14H^+ \rightarrow 2Cr^{3+} + 6Fe^{3+} + 7H_2O$ (dichromate),

(71) $MnO_4^- + 5Fe^{2+} + 8H^+ \rightarrow Mn^{2+} + 5Fe^{3+} + 4H_2O$ (permanganate).

The experimental conditions are important because both chromium and manganese can be present in several oxidation states. For example, the formation of MnO_2 is prevented by choosing a low pH value. [154]

Sutter and Park [155] studied the kinetics of the reaction between MnO_4^- and Fe(II) in an aqueous acid solution. They reported a very fast reaction ($k \approx 10^5\ M^{-1}s^{-1}$) that progresses via one step in the presence of a low excess of Fe(II) and through two first-order reaction steps when the Fe(II) excess is significant. The rate of reaction in their experiment was not dependent on the proton concentration. The rate of the reaction between dichromate and Fe(II) has been reported to be approximately five times lower than the one between MnO_4^- and Fe(II) [156] but still fast enough for the generator-collector mode titration (eq. (28)).

The cyclic voltammograms of Fe(III), $Cr_2O_7^{2-}$ and MnO_4^- solutions are presented in Figure 15. Permanganate is reduced in the potential range where iron is active as well, and therefore a more complex approach is needed.

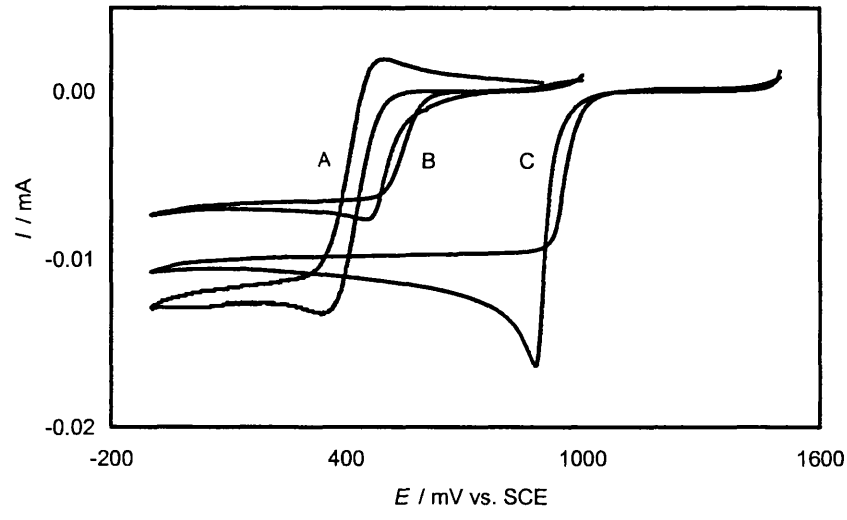

Figure 15. Cyclic voltammograms for iron(III) [A, 50 mM $NH_4Fe(SO_4)_2$], dichromate (B, 2 mM $Na_2Cr_2O_7$) and permanganate (C, 5 mM $KMnO_4$) at freshly snapped gold microband electrodes. Supporting electrolyte 0.1 M H_2SO_4, scan rate 25 mV/s.

When a constant current is applied at the generator both reaction (68) and reduction of permanganate,

(72) $MnO_4^- + 8H^+ + 5e^- \rightarrow Mn^{2+} + 4H_2O$, $E^0 = +1.249$ V, $E_{1/2} = +0.943$ V vs. SCE

take place. [133, 154] Similarly, the current at the collector is the sum of reactions (69) and (72). The reduction potential of dichromate is more negative than that of permanganate (E^0 = +1.088 V vs. SCE, [133] in practice $E_{1/2} \approx +0.500$ V vs. SCE). When a collector potential that is positive enough is chosen an analogous reaction to (72) is not observed. Therefore the dichromate titration can be carried out like the vitamin C, thiosulfate and sulfite titrations. In a generator-collector type titration, the collector potential of +0.850 V vs. SCE in dichromate and +0.600 V vs. SCE in permanganate titration were applied in the amperometric mode. The potentiometric end-point detection was inaccurate due to the electroactivity of the analytes.

3.4 Titrations with dissolving silver microbands

Precipitation titration of halides with $AgNO_3$ is a traditional widely used method in analytical chemistry.[38, 137] Conventionally, the analysis is carried out as a potentiometric titration, in which the potential determining reaction at the silver indicator electrode is [133]

(73) $Ag^+ + e^- \rightarrow Ag$, $E^\circ = +0.558$ V vs. SCE.

The actual potential of the electrode depends on the activity of the Ag^+ ions according to the Nernst equation (eq. (31)). The potential changes when halide ions (*e.g.*, Cl^-, I^-) that react with Ag^+ are present in the solution:

(74) $Ag^+ + X^- \rightarrow AgX$ (s),

where X is the halide in question. If a solid silver halide is present in the solution, the potential of the indicator electrode can be related to the concentrations of the ions using a solubility product of the silver halide, $K_{sp} = [Ag^+][X^-]$. [38] The same principle applies to the titration of other anions, *e.g.*, SCN^-, CN^-, S^{2-}, SO_3^{2-} and $S_2O_3^{2-}$, which form precipitates with Ag^+. [38, 137, 145]

Simultaneous determination of different halides and other anions that precipitate with Ag^+ is an important application. [157, 158] With these combinations the difficulties are the data overlapping each other, side reactions and co-precipitation, which is reduced when a high concentration of nitrate is present. [38] The mathematical procedures of interpreting the data obtained from titration curves have been widely studied. [159, 160, 161] The traditional way of analysis is based on thermodynamic equilibrium and knowledge of solubility products (equilibrium constants). The difficulty is that, *e.g.*, for silver chloride the solubility product is relatively high ($K_{sp} = 10^{-9.5}$) compared to the solubility product of silver iodide ($K_{sp} = 10^{-15.8}$). [135] This means that at the end-point of the chloride titration the AgCl formation is not complete and stoichiometric, and all forms of silver and chloride compounds should be taken into account making the analysis complicated. In general, the simultaneous determination of different compounds in precipitation or complexiметric titration is possible if the ratio of the solubility products or complexation constants is at least 10^6. [98] In addition, important factors are the temperature and the pH value of the solution, since the solubility constants increase significantly with increasing temperature, [38] and the pH value affects the actual reactions taking place.[152, 162, 163] In addition, the ionic strength of the solution has an influence on the solubility products. [137]

In the present method, the titrant (Ag^+) is electrogenerated by dissolving the generator electrode (working electrode) material (silver), instead of generating the titrant from a species in the solution. The potential change is detected at the collector electrode (indicator electrode) the material of which is silver as well. The titration is here applied to the precipitation titration of chloride, iodide, thiosulfate and cyanide with electrogenerated Ag^+. The titration reaction of halides corresponds to eq. (74), assuming a stoichiometric reaction and neglecting other possible silver-halide complexes. The titration reactions for thiosulfate and cyanide are the following:

(75) $Ag^+ + S_2O_3^{2-} \rightarrow Ag_2S_2O_3$ (s) (thiosulfate),

(76) $Ag^+ + CN^- \rightarrow AgCN$ (s) (cyanide).

When the analyte concentration is high the precipitates formed according to equations (75) and (76) dissolve in analyte excess as $[Ag(S_2O_3)_2]^{3-}$ and $[Ag(CN)_2]^-$, respectively. [152, 162, 163] On the other hand, before the end-point when the analyte is present in excess the complexation reaction dominates. [137] Other complexes where the ligand number is higher

may be formed but they can be assumed to be insignificant compared with the mentioned compounds. [137] The thiosulfate-silver complex plays an important role in black-and-white photography. [142] Cyanide is a dangerous poison, and therefore its analysis is crucial. [38]

3.5 Industrial application

PMG (*n*-phosphonomethyl glycine, commercial name glyphosate) is a widely used non-selective herbicide in agriculture, mainly used for weed control. [164, 165, 166, 167] Its active component is an isopropylamine salt. [168] The structures of PMG and related compounds PIDA (*n*-phosphonomethyl iminodiacetic acid) and AMPA (aminomethyl phosphonic acid) are presented in Figure 16.

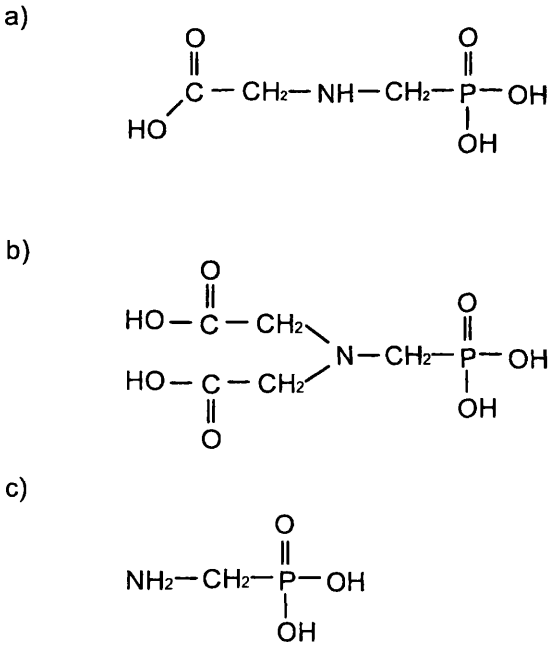

Figure 16. Structures of a) PMG (*n*-phosphonomethyl glycine), b) PIDA (*n*-phosphono-methyl iminodiacetic acid) and c) AMPA (aminomethyl phosphonic acid).

PMG has three functional groups: phosphonate, carboxylate and amino. It exists as a zwitterion with a phosphonate proton delocalised on the amino nitrogen. [169] PMG is an acid with three protonation constants, pK_1: 2.3 (carboxylate oxygen); pK_2: 5.6 (phosphonate oxygen); pK_3: 10.3 (amino nitrogen). [164, 170, 171]

PMG and other phosphoric and amino acid group containing herbicides are typically determined using chromatographic techniques. [172, 173, 174, 176] The objective of this work has been to develop a user-friendly analytical method for detection of PMG that is based on electrochemical titration using dual microband electrodes. The effect of PIDA and AMPA on the response has also been investigated.

The phytotoxicity of PMG is based on an inhibition of a specific plant enzyme (5-enolpyruvate-shikimate-3-phosphate synthase, *i.e.*, EPSP synthase) during the flavonoids synthesis [175, 176] and alterations of other biochemical processes, photosynthesis and respiration properties in plants and microorganisms. [165] It has been reported to be harmless to mammals and other animals, [168, 177] even though some studies suggest that it might cause reproductive disorders. [178, 179, 180, 181] It degrades relatively fast in soils to non-phytotoxic, and partly useful, products CO_2, PO_4^{3-} and NH_3. [166, 170, 182] Much investigation has been focused on the environmental impact of PMG, particularly its influence on groundwater. [166, 174]

Addition of Fe(III) or Al(III) has been observed to reduce the degradation of PMG in soil. [170] These cations bind PMG to clays and organic matter by metal bonds inactivating the biodegradation. [183] Various other metal salts also reduce the effectiveness of the phytotoxic properties of PMG due to complexation. The effect can be compensated by adding citrate or another ligand that complexes the metal ions instead of PMG. [184, 185] In addition, an adsorption of PMG on iron-humic acid [167] and copper-humic acid [183] complexes has been observed to take place in soil. Ammonium salts enhance the phototoxicity of PMG and other herbicides probably by affecting cuticular or membrane adsorption. [184, 186]

PMG has strong chelating properties. [164] It forms complexes, both soluble and insoluble, with several metal ions, *e.g.*, with Fe(III), Al(III), Co(III), La(III), Ca(II), Mg(II), Ba(II), Fe(II), Pb(II), Cu(II), Zn(II), Mn(II), Cd(II), Ni(II), Co(II) and Na(I). [164, 165, 166, 168, 169, 170, 171, 175, 182, 187, 188, 189] Complex formation between PMG and many metal cations has been investigated using, *e.g.*, potentiometric titration, spectrophotometry, polarographic and chromatographic techniques. [165, 168, 175, 164171, 187, 189] Structural studies have been carried out using X-ray diffraction, IR spectroscopy and NMR. [166, 168, 169, 182, 185, 188] Typically, PMG is a tridentate ligand, where the donor sites are two oxygens (phophonate and carboxylate) and one nitrogen (amino). [164, 165, 167, 169] PMG also co-ordinates as a tetradentate ligand if the phosphonate co-ordinates through two oxygens. [165] The pH value affects the reactions of PMG, having an influence on both stoichiometry and actual complexes formed. 1:1

complexes have high stability, but, particularly, at high pH values 2:1 (ligand:metal) complexes become important. [164, 166, 168, 171, 182, 187, 189] In addition, many metal-PMG complexes are polymeric. [169, 182 ,188] At high pH values formation of metal complexes is countered by stability vs. insolubility effects due to formation of competing hydroxide and hydroxo complexes of metal cations. [169, 187] PMG also forms stable complexes with several polyammonium cations. [177] The complexation properties of PIDA and AMPA are very similar to those reported with PMG. [187, 190, 191, 192, 193] As an application, the complexing properties of these ligands may be used for detection of toxic metals. [194]

In addition to the use of PMG as a herbicide, it and other organophosphorous ligands have also been used as corrosion inhibitors particularly for iron and its alloys. This is based on the formation of an inhibiting film on the metal surface. Again, different metal cations have an effect on the inhibiting film formed. [194, 195]

3.5.1 Titration of PMG with electrogenerated iron(III)

In this work, electrogeneration of the titrant, Fe(III), from Fe(II), for the titration of PMG and related compounds (PIDA and AMPA) is used. Iron is stable in both +II and +III oxidation states and its electrochemistry is well known. [38] Fe(III) has been used as a titrant due to its complexing ability with the compounds in question. [165, 166, 171, 187]

Fe(II) forms a complex with PMG as well but the stability constant of that compound is much lower than the one of PMG-Fe(III) complex. [171, 196] In Ref. 166, it was reported that Fe(II) solution was rapidly oxidised to Fe(III) leading to the PMG-Fe(III)complex. The measurements reported here have been carried out at pH 3, since the iron-PMG complex is stable at that pH, and the complexation between Fe(III) and PMG suppresses the hydrolysis of Fe(III). [187] Both soluble and insoluble (K_{sp} less than 10^{-5}) PMG-Fe(III)complexes have been reported, [166, 187] the complexation being highly dependent on experimental conditions. UV-vis spectras of Fe(III) and PMG-Fe(III) complexes have been reported. [165, 187] In Ref. 165, the high absorption values indicate that scattering due to the solid compound is taking place. The dominant PMG- Fe(III) complex has 1:1 ligand to metal ratio ($\log K = 16.1$) [171] and incorporates a tetradentate fully deprotonated PMG^{3-}. [166] Again, if the experimental conditions are changed, *e.g.*, the ligand concentration doubled, a PMG-Fe(III)complex with 2:1 stoichiometry is formed. [171] The actual reactions for the PMG system are presented below. Analogous reactions apply also to PIDA and AMPA.

(77) Generator: $Fe^{2+} \rightarrow Fe^{3+} + e^-$, $E^o = +0.437$ V vs. SCE [133]

(78) Collector: $Fe^{3+} + e^- \rightarrow Fe^{2+}$

(79) Solution: $PMG^{3-} + Fe^{3+} \rightarrow PMG\text{-}Fe$

4 Experimental

4.1 Screen-printed microband electrodes

Disposable microband electrodes were snapped along the scribe line (Figure 17) to expose a fresh surface before a measurement. They were fabricated by a screen-printing method (Agmet Ltd, Reading, UK) using a ceramic alumina substrate, onto which the ink layers of conductor and dielectric materials were printed. The process and materials were chosen based on previous studies presented in Refs. 10 and 73.

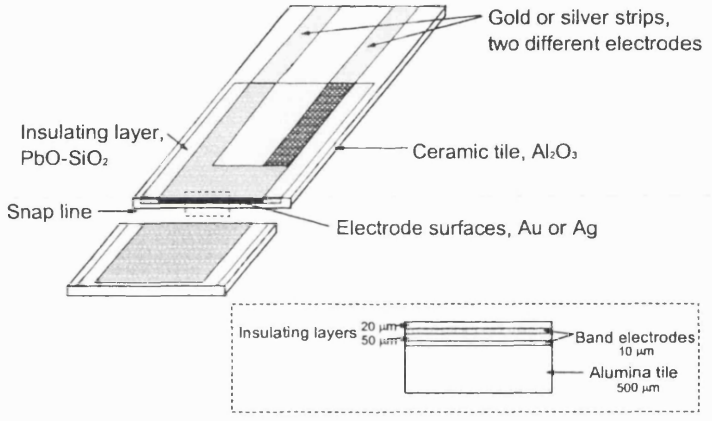

Figure 17. Screen-printed double microband electrode.

After each printed layer the paste was dried in an oven at 125 °C for 10 minutes and then fired in a furnace for 70 minutes. During the first 30 minutes the temperature was raised 28 °C/min to 850 °C, kept at that value for 10 minutes and again decreased 28 °C/min during the last 30 minutes. The substrate was 96 % Al_2O_3 and the dielectric material (commercial name 4905-C) was a $PbO\text{-}SiO_2$ glass with $BaTiO_3$. Two layers of dielectric were printed between the two conductor layers in order to prevent any transfer of metal ions through the insulator. That was also minimised using the same electrode material (the same chemical potential) for both microbands on the same tile in most of the cases. The insulating layer between the electrodes was nominally 50 µm thick, and the thickness of the outermost dielectric layer was 20 µm. The surface area of a microband electrode was nominally 10 µm × 0.5 cm. A scanning electron microscope (SEM) micrograph of a snapped dual microband electrode is presented in Figure 18. The micrograph confirms that the average gap between

the electrodes is 50 μm and the electrode width is 10 μm. The electrodes are parallel and approximately straight but it can also be observed that the snapping procedure leads to a rough surface and a slightly different cross section each time.

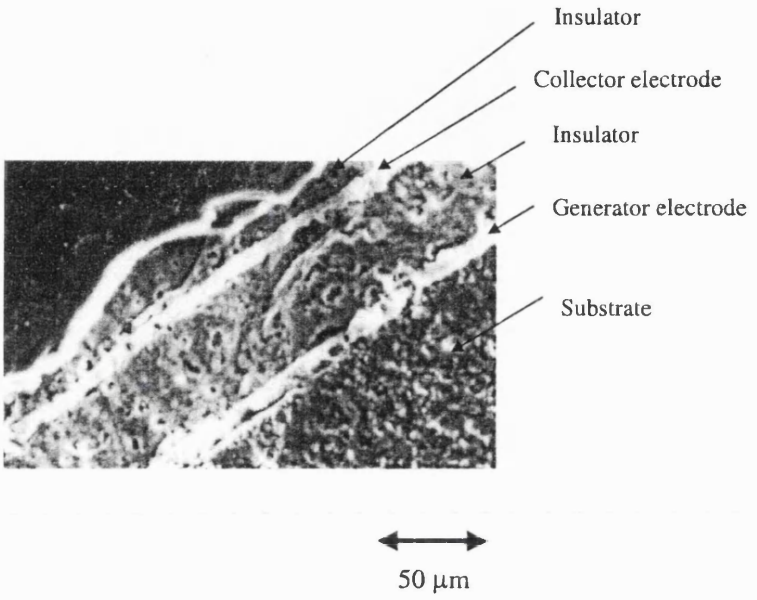

Figure 18. Micrograph of a double microband electrode.

Double gold (commercial name 8880-H) and double silver (commercial name 9912-C) microbands were used in most of the experiments. Some preliminary measurements were also made using platinum (commercial name 5545) and platinum-gold mixture (commercial name 5837) microbands. The used conductor materials contained small amounts of additives in order to secure a proper adhesion of the metal ink to the ceramic substrate or to the insulating material. For instance, the gold ink contained traces of cadmium and CuO. Since the materials were commercial inks they also contained traces of other additives and impurities. In some microband tiles silver strips (9912-C) were printed at the back of the substrate to work as reference and counter electrodes.

4.1.1 Electrode characterisation

The experiments for electrode characterisation were carried out using a reaction couple $[Fe(CN)_6]^{4-}/[Fe(CN)_6]^{3-}$. As a buffer and an inert electrolyte were 0.05 M K_2HPO_4 and 0.05 M KH_2PO_4 (pH 6.8). Gold microband electrodes were employed. The inner (*i.e.*, the one adjacent to the alumina substrate) and outer microband electrodes were studied separately using potential step experiments (chronoamperometry) and cyclic voltammetry in a stationary solution. The collection efficiency experiments were used in order to find out the real geometry of the electrodes (*e.g.*, the gap width between the microbands).

In the generator-collector measurements the generator electrode was the inner microband and the collector was the outer microband. This arrangement was chosen since the geometry of the microband device was not symmetrical: the outermost insulating layer was only 20 μm thick. In Ref. 73, it was reported that the collection efficiency fell significantly if the outer microband was the generator since a similar diffusion field (from behind the outer insulating layer) typical of the outer electrode was not reached at the inner band. In the measurements presented here the gap between the microbands was wider and the effect was not seen very clearly. The procedure of the measurements was standardised using the same geometry, the inner band as the generator, all the time.

4.2 Experimental procedure

The reference electrode was a saturated calomel electrode (SCE) and the counter electrode was platinum with a large surface area. In some measurements, silver strips printed at the back of the alumina substrate worked as reference and counter electrodes. In the electrode characterisation experiments and vitamin C titrations, the microband electrode tile was covered with a hard hydrophobic spray (silicone RS 514-464) before snapping the electrode tile in order to prevent the solution from getting into the electric contacts and to eliminate the crack propagation by the snapping procedure. In other experiments, the silicone spray was omitted due to the low pH value of the solution, without causing difficulty.

The measurements were carried out in an open cell at room temperature. The electrochemical cell was placed in a Faraday cage in order to eliminate external noise but the response was reasonable also without such shielding. All the solutions were prepared using

water purified with Millipore Milli-Q system (18.2 MΩ cm) and all the chemicals were of analytical-reagent grade. The solutions were prepared just immediately prior to the experiments. The solutions were degassed with argon when KI was used as an electrolyte in order to prevent any oxidation due to dissolved oxygen.

4.2.1 Electrochemical measurements

A conventional potentiostat (Autolab: Ecochemie, Utrecht, The Netherlands) or a purpose-built computer-controlled dual potentiostat-galvanostat (Sycopel Scientific, Washington, Tyne & Wear, UK) were used for all electrochemical measurements. The experimental arrangement for the generator-collector measurements is shown in Figure 19.

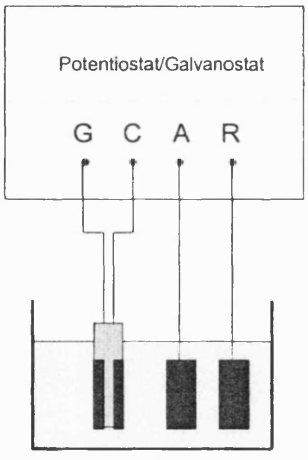

Figure 19. Experimental arrangement. G: generator electrode, C: collector electrode, A: counter (auxiliary) electrode, R: reference electrode.

There were several modes of electrochemical measurements for the generator-collector system, which involved either amperometric or potentiometric end-point detection:

1) In amperometric titration, galvanostatic (constant current) conditions were employed at the generator, and the collector potential was kept constant (potentiostatic), whilst the collector current was measured.

2) In potentiometric titration with a constant current method, galvanostatic conditions were employed at the generator, whilst the open-circuit potential was measured at the collector.

3) In potentiometric titration with a ramp current method, the generator current was increased linearly with time, whilst the open-circuit potential was measured at the collector.

A constant current at the generator electrode was achieved by connecting a battery in series with a resistor and controlling the battery voltage with a potentiometer. This arrangement is shown in Figure 20.

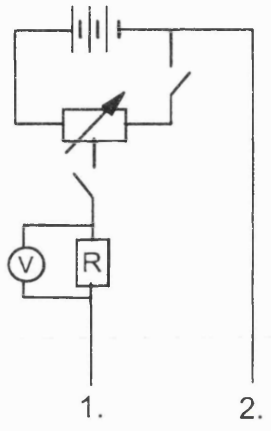

Figure 20. Electric circuit for constant current at the generator electrode. Voltage source: 9 V battery, controlled by a potentiometer. Voltage over the resistor (typically 1 MΩ) was measured in order to calculate the applied generator current, $I = E / R$. 1. generator electrode, 2. counter electrode.

In the amperometric mode, the collector potential was controlled by the potentiostat, and in the potentiometric mode, the open-circuit potential of the collector electrode was measured with an oscilloscope (Tektronix) through a high impedance buffer amplifier (Figure 21). As an alternative route for amperometric titration a purpose-built potentiostat-galvanostat assembly (Sycopel Scientific) was employed: the instrument drove a constant current to the generator while the collector potential was kept constant.

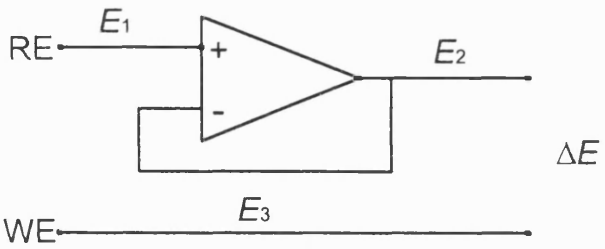

Figure 21. Arrangement for measuring open-circuit potential at the collector electrode via a potentiostat that works as a buffer amplifier. RE: reference electrode, WE: collector (working) electrode. $\Delta E = E_3 - E_2$ = signal at the oscilloscope, $E_1 = E_2$.

The electrochemical measurements with a ramp current were carried out either using a ramp generator (UCL Workshop) through a potentiostat (UCL Workshop) that was converted into a galvanostat by inserting a resistor between the reference and working inputs (Figure 22). [22] The open-circuit signal was recorded with an oscilloscope (Tektronix) through a buffer amplifier as presented in Figure 21. An alternative route of measurement was the use of an Autolab-potentiostat (Ecochemie) that produced the ramp current at the generator electrode and recorded the open-circuit potential at the collector electrode simultaneously.

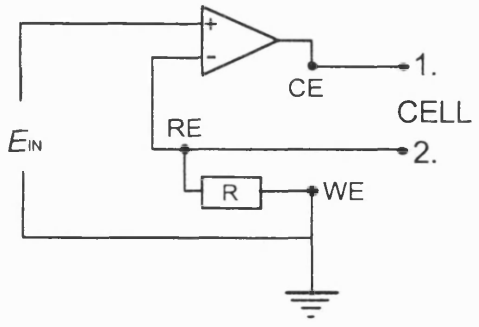

Figure 22. Potentiostat converted into a galvanostat. $I = E_{IN} / R$. RE: reference electrode, WE: working electrode, CE: counter electrode. 1. counter electrode connection, 2. generator electrode connection.

4.2.2 Electrode vibrations

Electrode vibrations were achieved using a toothed wheel fitted to a stepper motor (Figure 23). A push rod between the disc and the electrode holder moved the electrode. The amplitude of the vibration was 2 mm.

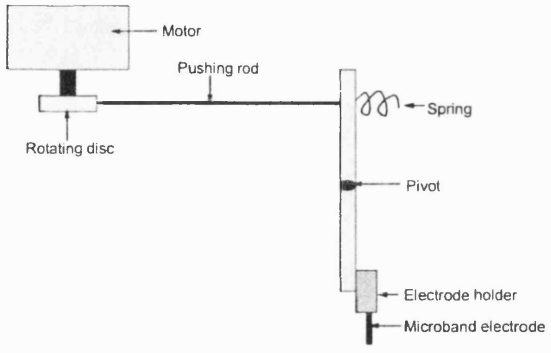

Figure 23. Electrode vibrator set-up.

For the generator-collector experiments, both amperometric and potentiometric, a mode of synchronised electrode motion and electrochemical measurement was explored. The generator current was applied shortly after the movement pulse, and removed shortly before the next movement pulse (Figure 24).

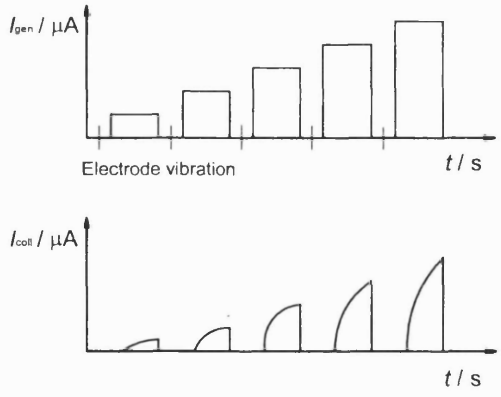

Figure 24. Procedure of a synchronised pulsed motion and an electrochemical (amperometric) measurement. Generator current applied shortly after the movement pulse, and removed shortly before the next movement pulse. The response at the collector measured.

In addition, some experiments were carried out using a fixed generator current and a periodic pulsed motion of the electrode with vibration frequency of 0.5 or 1.0 Hz. The frequency was set by a square-wave generator controlling the stepper motor.

4.2.3 Amperometric titration

In amperometric titration with synchronised pulsed motion, a constant current was applied at the generator and the potential at the collector was kept constant. Gold microband electrodes were used. A new microband was employed and a fresh electrode surface exposed before each set of measurements with a certain analyte concentration. For each analyte concentration nine generator currents $|I_{gen}|$ of 1...9 μA were applied starting from the lowest current. The collector potential was applied just before a movement pulse of the electrode, and the generator current was applied 1 s after the movement. The collector current I_{coll} was measured as a function of time. The experimental conditions and reagents are presented in Table 1.

Table 1. Experimental conditions and reagents for different analytical systems in the amperometric mode. Phosphate buffer, pH 6.8; 0.10 M H_2SO_4, pH 1.5.

Analyte	Titrant	Electrolyte	Supporting Electrolyte	E_{coll} / V vs. SCE
Vitamin C	$[Fe(CN)_6]^{3-}$	0.05 M $K_4Fe(CN)_6$	0.05 M K_2HPO_4, 0.05 M KH_2PO_4	-0.100
Thiosulfate ($S_2O_3^{2-}$)	I_2 (I_3^-)	0.05 M KI	0.10 M H_2SO_4	0.0
Sulfite (SO_3^{2-})	I_2 (I_3^-)	0.05 M KI	0.10 M H_2SO_4	0.0
Dichromate ($Cr_2O_7^{2-}$)	Fe^{2+}	0.05 M $NH_4Fe(SO_4)_2$	0.10 M H_2SO_4	+0.850
Permanganate (MnO_4^-)	Fe^{2+}	0.05 M $NH_4Fe(SO_4)_2$	0.10 M H_2SO_4	+0.600

4.2.4 Potentiometric titration

In potentiometric titration with synchronised pulsed motion, a current was applied at the generator and the collector was kept at open-circuit. A new microband was taken and a clean electrode surface was exposed before each set of measurements with a given analyte

concentration. The microband electrode was vibrated before each measurement, and the generator current was applied 1 s after that movement pulse. For each analyte concentration generator currents of 1, 3, 6 and 9 μA (constant current mode) and scan rates of 0.05; 0.1; 0.2; 0.5 and 1.0 μAs^{-1} (ramp current mode) were used. The open circuit potential of the collector electrode was recorded as a function of time (or generator current).

Titrations of vitamin C, thiosulfate and sulfite using gold microband electrodes, the same applications as presented in Table 1, were also carried out in the potentiometric mode. The experimental conditions in potentiometric titrations with dissolving silver microband electrodes are presented in Table 2. In these titrations, the indicator electrode was a silver microband.

Table 2. Reagents for different analytical systems using dissolving silver microband electrodes, 0.10 M KNO_3, pH 6.0.

Analyte	Titrant	Supporting Electrolyte
Iodide (I^-)	Ag^+	0.10 M KNO_3
Chloride (Cl^-)	Ag^+	0.10 M KNO_3
Thiosulfate ($S_2O_3^{2-}$)	Ag^+	0.10 M KNO_3
Cyanide (CN^-)	Ag^+	0.10 M KNO_3

4.3 Industrial application

Some preliminary cyclic voltammetry measurements with PMG were carried out using either a gold or platinum disk electrode (diameter = 1.6 mm) as a working electrode. The electrodes were polished using alumina powder-water slurry, first with the particle size of 1.0 μm, and then with the particle size of 0.3 μm, rinsed with water and sonicated in order to clean the electrode surface and remove all alumina particles.

Some traditional potentiometric titrations using a burette and magnetic stirrer were carried out in order to find out the actual stoichiometry of the reactions. The indicator electrode in these experiments was either a gold or platinum wire (cleaned electrochemically in an acidic solution), and the reference electrode was SCE.

Amperometric and potentiometric titrations were carried out using the procedure presented in the previous section. The experimental conditions are discussed in the next chapter.

4.4 Error estimation

Experimental errors are generally divided into two categories: systematic (determinate) and random (indeterminate) errors. The first one is a consistent error that distorts the results into the same direction. It can be detected and corrected. The latter one is always present and cannot be eliminated completely. It is due to limitations of the measurement, and it can be both negative and positive. The random error can be investigated by repeating the same measurement under the same conditions and using statistical methods in order to find out the accuracy of the measurement. When the systematic error is small the precision of the result is good, and when the random error is small the accuracy of the result is good. [38, 197]

The average value (arithmetic mean), $\bar{x}$, of the result is the sum of measured values, x_i, divided by the number of measurements, n:

$$\bar{x} = \frac{\sum_i x_i}{n}. \tag{80}$$

Standard deviation, s, tells the area where the result of the next repeated measurement should be in a certain probability, *i.e.*, it tells how close to the mean value the data points are. It determines the error of each individual measurement:

$$s = \sqrt{\frac{\sum \left(x_i - \bar{x}\right)^2}{n-1}}. \tag{81}$$

The error of a series of measurements, *i.e.*, the standard deviation of the mean can be calculated using standard error, $s_{\bar{x}}$:

$$s_{\bar{x}} = \frac{s}{\sqrt{n}}. \tag{82}$$

Standard error tells the area where the mean of a series would be in the probability of 68 %, which follows from the Gaussian distribution: [38]

$$G(x) = \frac{1}{\sigma\sqrt{2\pi}} e^{-\frac{1}{2}\left(\frac{x-\mu}{\sigma}\right)^2}, \tag{83}$$

where the deviation, σ, can be replaced by s and mean, μ, by $\bar{x}$, when the number of measurements is finite. Equation (83) is the Gaussian distribution in its normalised form. Normalisation means that the surface area between the Gaussian curve and x axis is unity:

$$\int_{-\infty}^{\infty} G(x)dx = 1. \tag{84}$$

The random error can be assumed to follow the Gaussian distribution. The Gaussian distribution is a probability density. For instance, the probability that the result is between values a and b can be calculated integrating Equation (83) in the range in question. The more measurements are made the more accurately the average value corresponds to the "real" value. [38, 197]

In this thesis, the primary aim of the data analysis was to find out the accuracy of the analytical method and the reproducibility of the results. Possible sources of systematic errors were eliminated by using chemicals from different sources, preparing the solutions individually for each set of measurements and measuring the same signal with different pieces of equipment.

For each analytical system studied here, the measurements were repeated under the same conditions with different microband electrodes. The arithmetic mean values, standard deviations and standard errors were calculated using Equations (80), (81) and (82) for each case. The error of each individual measurement and the reproducibility of the electrodes were determined using the standard deviation.

5 Results and discussion

5.1 Electrode characterisation

Electrode characterisation was carried out by measuring the electrochemical response on both microbands individually using chronoamperometry and cyclic voltammetry, or using collection efficiency experiments. The experimental results were compared with both values calculated using equations presented in sections 1.4, 1.5, 2.1 and 2.3, and theoretical simulations by J. Strutwolf presented in Ref. 99. The procedure of the simulations has been described in section 2.3.3. The results were further compared with the optical observations.

5.1.1 Individual bands of a double microband electrode

Transients in potential step experiments (chronoamperometry) and cyclic voltammograms in a stationary solution for both microbands (inner and outer) are presented in Figure 25 and Figure 26, respectively.

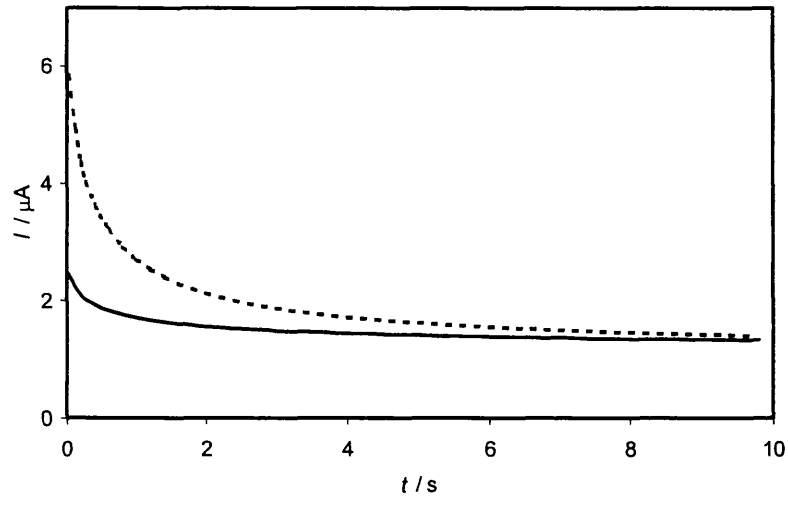

Figure 25. Chronoamperometric transients for inner (dashed line) and outer (solid line) microband in a stationary solution. 5 mM $K_4Fe(CN)_6$, phosphate buffer, potential step: -0.2 V $\rightarrow$ +0.4 V vs. SCE.

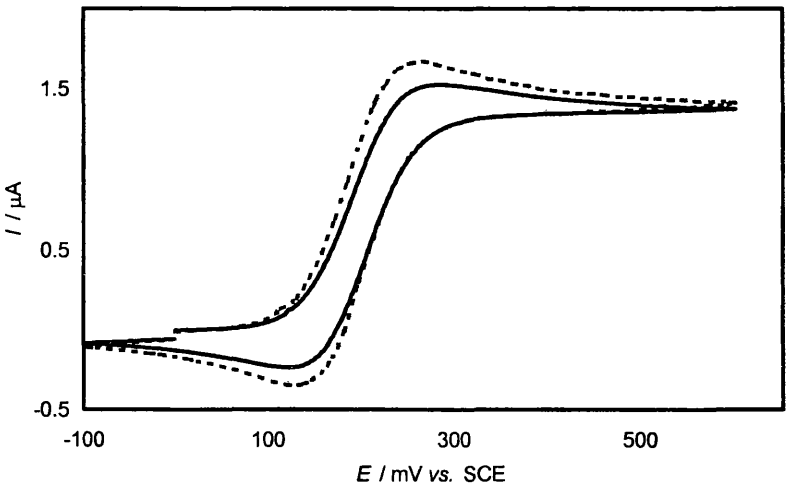

Figure 26. Cyclic voltammograms for inner (dashed line) and outer (solid line) microband in a stationary solution. 5 mM $K_4Fe(CN)_6$, phosphate buffer, scan rate 25 mV/s.

The potential step transients and voltammograms were reproducible when repeating the scans with the same microband electrode. When the measurements were repeated with different microbands, the distortion of the transients and voltammograms was in most cases larger with the inner electrode than with the outer one. The distortion can be assumed to be mainly due to the geometry of the snapping line: as seen in Figure 18, the electrodes are not ideally flat and smooth. The snapping procedure causes defects at the electrode-insulator interface, which changes the diffusion field. In addition, the diffusion at individual microbands is different: the diffusion field at the outer microband may extend over the 20 μm insulating layer, and the diffusion from behind the electrode tile might affect the field.

Calculated theoretical current values for chronoamperometry (potential step) and cyclic voltammetry using different Equations (12), (13), (14) and (17) are presented in Table 3. The different equations give very consistent results. The calculated and experimental (Figure 25 and Figure 26) values are in a good agreement with each other, indicating that despite the snapping procedure the results correspond to the theory reliably.

Table 3. Theoretically calculated quasi steady state currents (Equations (12), (13) and (14)), a peak current in an intermediate time case for the cyclic voltammetry (eq. (17)) and experimental values. Experimental values from four measurements with different microbands at t = 8 s (chronoamperometry) and E = +0.4 V vs. SCE (voltammetry). The time used in chronoamperometric calculations was 8 s, and the potential scan rate in cyclic voltammetry was 0.025 Vs^{-1} (corresponding to time 1.01 s, when T = 293.15 K).

	Limiting current / μA	
Equation	Chronoamperometry	Cyclic voltammetry
(17)	-	1.2 (intermediate time, I_p)
(12)	1.3	1.7
(13)	1.3	1.8
(14)	1.4	1.9
Experimental	1.4 ± 0.1	1.5 ± 0.1

5.1.2 Double microband electrodes

Collector current transients in a generator-collector mode experiment along with the calculated (eq. (43)) and simulated [99] curves are presented in Figure 27. A synchronised single movement pulse of the electrode was applied 1 s before the generator current pulse. In all of the calculations and simulations, the solution was treated as being stationary, and the value $D = 0.7 \times 10^{-9}$ m^2s^{-1} was used for the diffusion co-efficient (in the simulations for all species). [21, 73, 99]

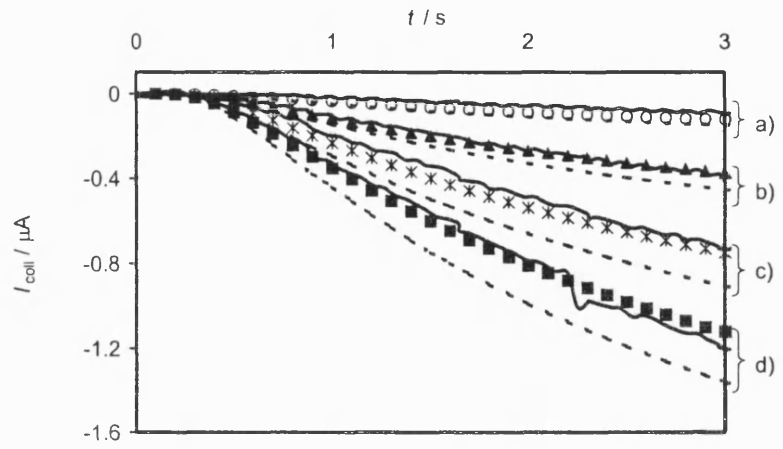

Figure 27. Experimental (solid lines), calculated (eq. (43)) (dashed lines) and simulated (symbols) [99] collector current transients. E_{coll} = -0.1 V vs. SCE, 50 mM $K_4Fe(CN)_6$, phosphate buffer. Applied generator currents at t = 0 s: a) 1, b) 3, c) 6 and d) 9 μA.

There is a delay of approximately 0.5 s after the generator is switched on, until the response is seen at the collector, which is due to the diffusion of the produced electroactive species from the generator to the collector. The experimental and simulated transients are in an excellent agreement with each other, although the relative error is higher when the applied generator current is lower. This is due to the electrode geometry: the imperfections in the electrodes have larger effects when the currents are small. The curves calculated using Equation (43) are also in a good agreement with the experimental values demonstrating that the approximations made deriving Equation (43) are valid for this case. The relative deviation is again higher when the generator current is lower.

Experimental and simulated [99] collector currents as a function of the applied generator current (collection efficiencies) are presented in Figure 28. Each value of the collector current was determined 3 s after the generator current was switched on. The simulations were carried out for different insulating layer thicknesses (gap widths). The experimental values are located close to the simulations for the gap width of 50 μm, which is consistent with the SEM image (Figure 18). Figure 28 also shows that the collection efficiency does not depend significantly on the applied generator current. Particularly, when $t \geq 5$ s, convection and diffusion from behind the electrode were observed to cause discrepancy between the experimental and simulated results. However, in the generator–collector experiments this kind of effect was presumed to be prevented by using the outer electrode as the collector and using short enough time-scale.

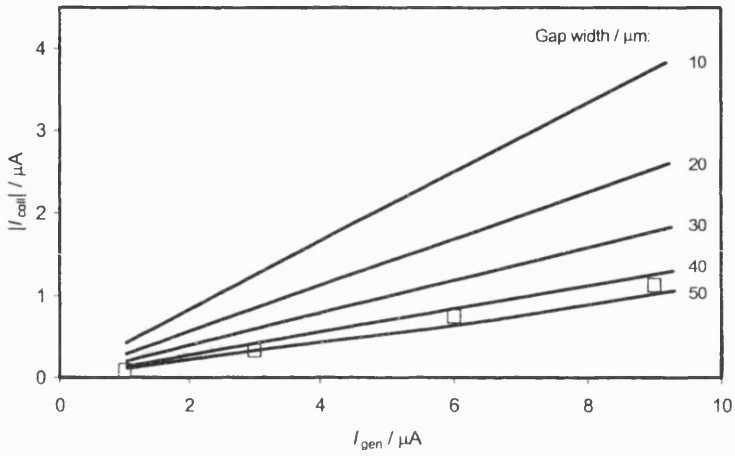

Figure 28. Simulated collector currents as a function of generator current (solid lines) [99] for different gap widths and experimental values (○). E_{coll} = -0.1 V vs. SCE, 50 mM $K_4Fe(CN)_6$, phosphate buffer. Values determined 3 s after the application of the generator current. Experimental results mean values from eight different measurements with different electrodes.

When Equation (22) is used to calculate the collection efficiency for the system with the electrode gap width of 50 µm and t = 3 s, the results is 14.0 %. That is in a good agreement with the experimental values (Figure 27 and Figure 28).

5.1.3 Continuous pulsed electrode motion

Hydrodynamic modulation using vibrating microband and multiple parallel microband electrodes was presented by Williams et al. [73] These systems can be considered with a model, in which the boundary layer is periodically renewed by an instantaneously rapid motion of the electrode. Experimental data of a pulsed electrode under potential step conditions is presented on Figure 29 along with a simulated curve. [99]

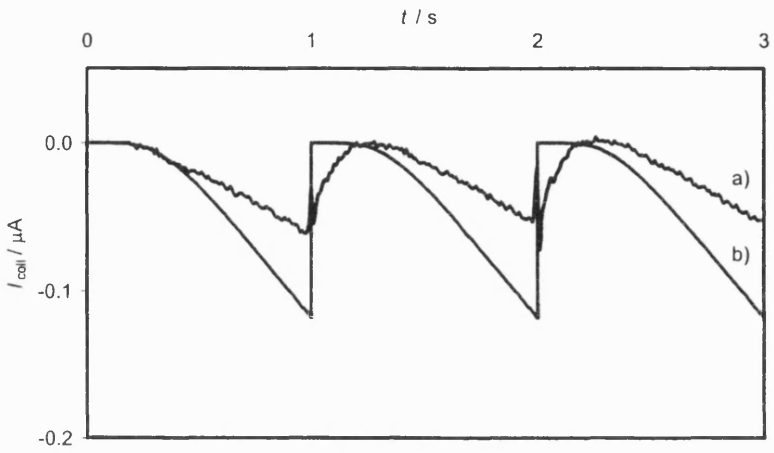

Figure 29. Experimental (a) and simulated [99] (b) collector current transients with a continuous pulsed motion of the microband electrode. Frequency of the movement 1 Hz. E_{coll} = -0.1 V vs. SCE, 5 mM $K_4Fe(CN)_6$, phosphate buffer. Applied generator current 3 μA.

The simulations were performed with periodically renewed boundary conditions. [99] With periodic pulsed motion whilst the generator current is constant, not stepped on and off, the calculated collector currents are significantly higher than the experimental ones. The difference was observed to be dependent on the applied vibration frequency. This behaviour shows that the assumption of renewed boundary conditions is too simple for a continuously pulsed electrode. Due to friction a solution layer moves with the electrode and the boundary layer is not completely renewed, analogous to the diffusion layer at a rotating ring-disk electrode. [22] Interruption of the generator current during the movement of the electrode removes the difficulty, since the motion can then correctly cause the replenishment of the solution within the boundary layer.

5.2 Amperometric titration

Titration of vitamin C with ferricyanide was used as a model system. Other applications of amperometric titration presented in this section are titrations of thiosulfate and sulfite with iodine and determinations of dichromate and permanganate with iron(II). Gold was employed as the microband electrode material.

5.2.1 Titration of vitamin C with electrogenerated ferricyanide

Experimental collector current transients in vitamin C titration are presented in Figure 30. A synchronised single movement pulse of the electrode was applied 1 s before the generator current pulse. Again, a delay of approximately 0.5 s is observed, until the response is seen at the collector. With the same generator current, the collection efficiency (eq. (21)) decreases with increasing analyte concentration, as expected.

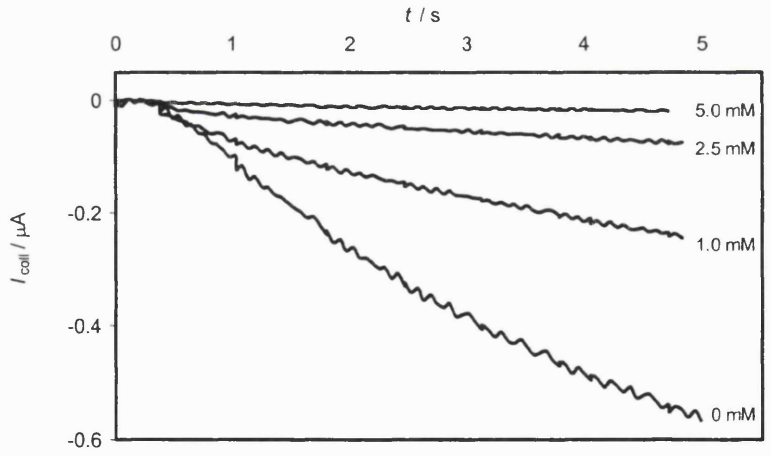

Figure 30. Experimental collector current transients with different vitamin C concentrations. E_{coll} = -0.1 V vs. SCE, 50 mM $K_4Fe(CN)_6$, phosphate buffer. I_{gen} = 3 µA, applied at t = 0 s, *i.e.*, 1 s after the movement pulse of the electrode.

Collector current transients calculated using Equation (44) are shown in Figure 31. The calculated values are significantly lower than the experimental values (Figure 30). This is because the approximations made deriving Equation (44) are too simplified. In reality, the analyte concentration does not stay constant between the electrodes, but decreases significantly due to the actual titration reaction and finite diffusion of the analyte. For a more accurate calculation, a diffusion equation should be written for the analyte as well but that would require more powerful numerical techniques, like digital simulations.

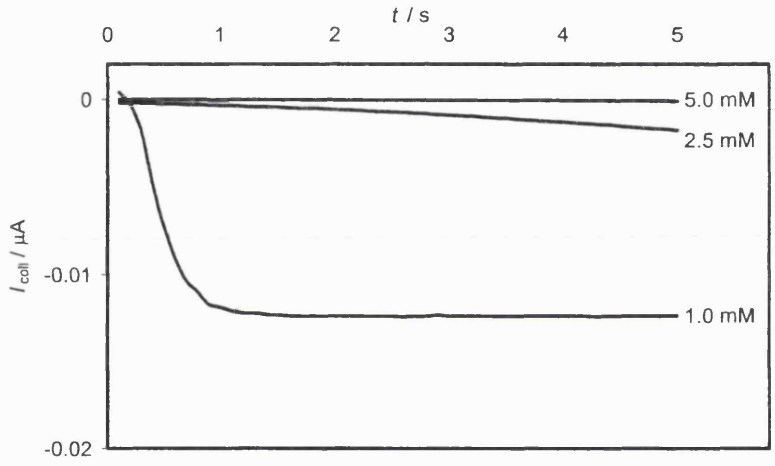

Figure 31. Calculated (eq. (44)) collector current transients with different vitamin C concentrations. I_{gen} = 3 μA, k = 2240 $M^{-1}s^{-1}$ (for the titrant multiplied by the stoichiometric co-efficient 2). [99]

Collector currents against generator current with different analyte concentrations are presented in Figure 32 along with simulated values. [99] The experimental and simulated results are again in an agreement with each other within experimental error. The depletion of the analyte and its finite diffusion are taken into account in the simulation model.

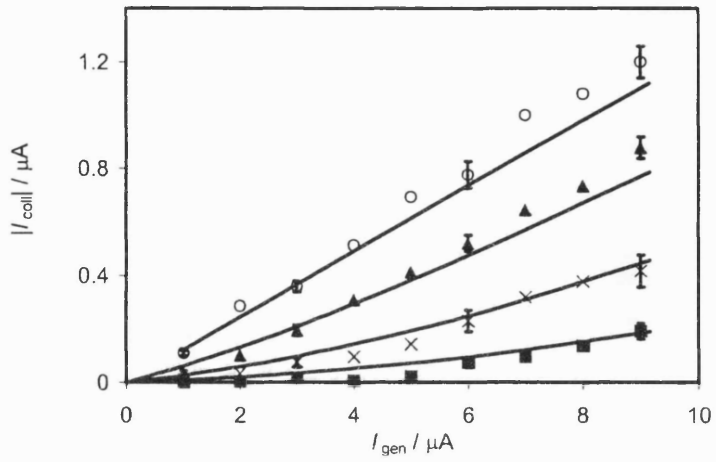

Figure 32. Collector current vs. generator current in vitamin C titration. Experimental values (symbols) and simulated values (solid lines, k = 2240 $M^{-1}s^{-1}$) [99] determined 3 s after generator current was applied. E_{coll} = -0.1 V vs. SCE; 50 mM $K_4Fe(CN)_6$, phosphate buffer; $c_{vitaminC}$ = (o) 0, (▲) 1.0, (×) 2.5 and (■) 5.0 mM. For I_{gen} = 1, 3, 6 and 9 μA mean values from eight measurements with different electrodes; for other I_{gen}, mean values from two measurements.

When the collector current is sufficiently high, then, according to the reaction layer model (eq. (60)), the curve of the collector current as a function of the generator current lies parallel to the curve without the analyte. The phenomenon can be seen in Figure 32. The displacement, ΔI_{gen}, is the additional flux of the titrant from the generator that is required to compensate the flux of the analyte. The displacement of the curve can be used as an analytical signal.

Two ways of implementing the analytical method were used. In the first method, a value of the generator current that is needed to achieve a certain threshold value of the collector current is detected at a fixed time. The second method uses the slope of the initial collector current dependent on $t^{1/2}$.

An example of the first method is presented in Figure 33: the required I_{gen} determines the analyte concentration. One way of implementing the threshold value is to draw a horizontal line in Figure 32 at a certain I_{coll} and determine the required I_{gen}.

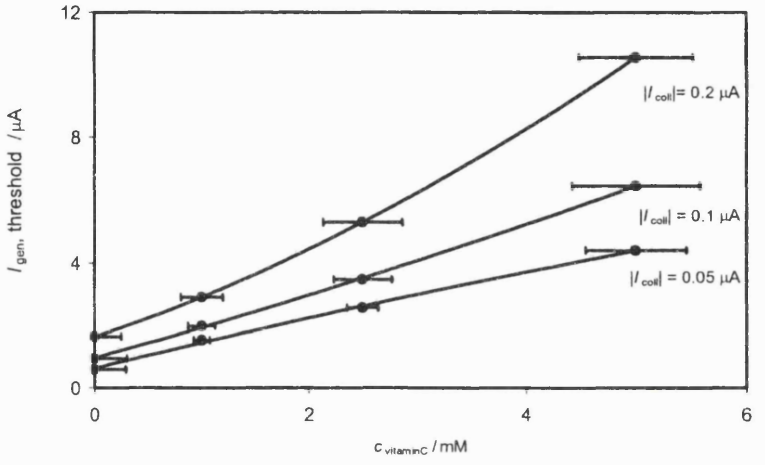

Figure 33. Generator current that is required to produce a certain collector current after a particular time (3 s) in vitamin C titration. E_{coll} = -0.1 V vs. SCE; 50 mM $K_4Fe(CN)_6$, phosphate buffer. Four measurements with different electrodes. Solid lines are fitted trend lines. Errors calculated from standard deviation.

Equation (60) predicts that the results are straight lines, *i.e.*, the required generator current is directly proportional to the analyte concentration. This only applies to low required collector currents in Figure 33 but taking the experimental error into account it is also a valid approximation for higher collector currents. The error bars show the standard deviation of the required I_{gen}, calculated from four measurements with different electrodes for each point. It was approximated that $\Delta I_{gen}/\Delta c_{analyte} = dI_{gen}/dc_{analyte}$. The error bar for each analyte concentration was then calculated using the equation of each trend line.

In the slope method, the collector current transient is plotted as a function of $t^{1/2}$ (Figure 34). Empirically, it was observed that after the time delay in the collector current transient, the transient is linearly dependent on $t^{1/2}$, the slope being dependent on both the analyte concentration and the applied generator current. The slope of the resulting straight line can be further used when modelling the transients.

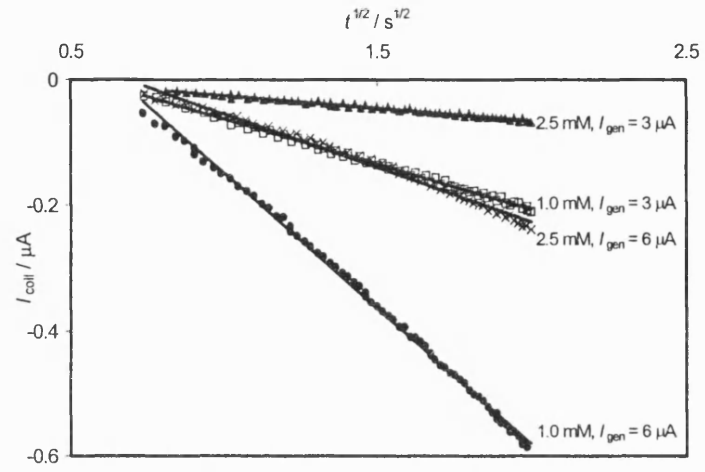

Figure 34. Collector current transients as a function of $t^{1/2}$ ($t = 0$ s when the generator current switched on) with different vitamin C concentrations and generator currents. Symbols: experimental values; solid lines: fitted trend lines. E_{coll} = -0.1 V vs. SCE; 50 mM $K_4Fe(CN)_6$, phosphate buffer.

In Figure 35, experimental transients in vitamin C titration (1.0 mM analyte) together with fitted curves are presented. The slope values used for equation fitting were derived from a different set of experiments in order to demonstrate the general repeatability of the results and reliability of the 'empirical theoretical' representation of the results.

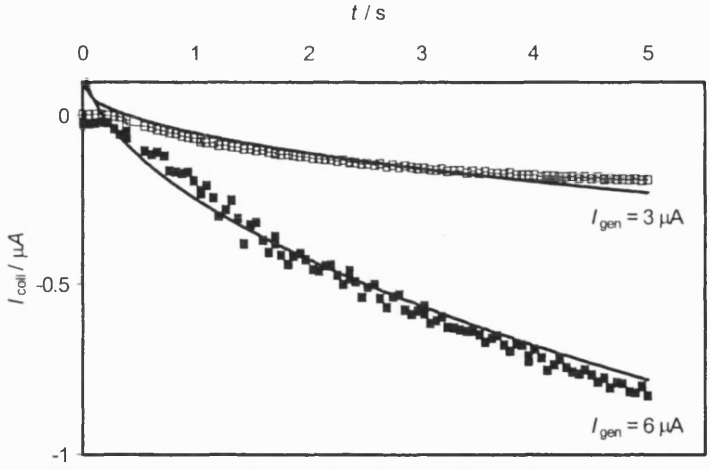

Figure 35. Experimental collector current transients (symbols) and calculated curves (solid lines, calculated using the slopes of I_{coll} vs. $t^{1/2}$ from separate measurements). Generator current applied at t = 0 s. E_{coll} = -0.1 V vs. SCE; 50 mM $K_4Fe(CN)_6$, phosphate buffer, $c_{vitaminC}$ = 1.0 mM.

The agreement is excellent, particularly for times 1.5 s $\leq t \leq$ 4 s. This method creates a reliable basis for data analysis since it uses all of the data in the collector current transient, not only one point measured after a certain time, as is the case with threshold values and collection efficiencies.

A summary of the slopes as a function of vitamin C concentration is presented in Figure 36. The error bars were calculated as in the case of threshold currents.

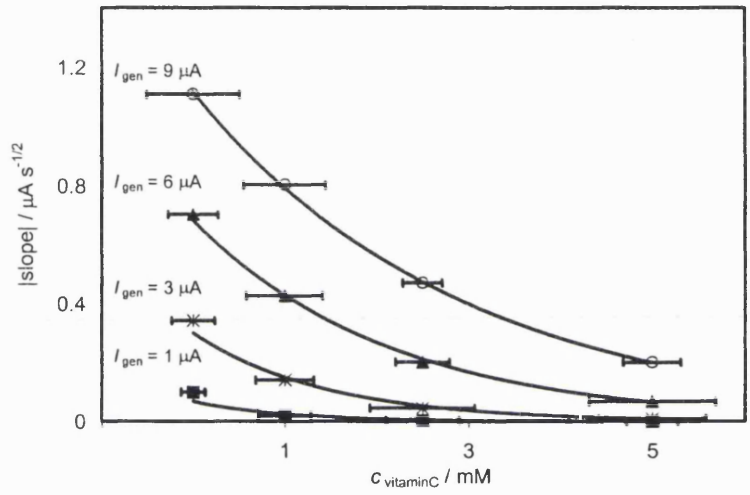

Figure 36. Slope $I_{coll}/t^{1/2}$ (t = 0 s when the generator current switched on) as a function of vitamin C concentration. E_{coll} = -0.1 V vs. SCE; 50 mM $K_4Fe(CN)_6$, phosphate buffer. The diagram gives results for four different electrodes. Solid lines are fitted trend lines. Errors calculated from standard deviation.

At sufficiently short time, the titrant is confined to the space between the electrodes. The increase of collector current as $t^{1/2}$ is a consequence of this, the slope of the curve being dependent on the flux of titrant into the gap. This flux is the difference between the generation rate, at the generator electrode, and the destruction rate, by reaction with the analyte, which is determined by the diffusion rate of analyte into the gap. Thus, the slope depends on both the generator current and the analyte concentration. The value of generator current that is chosen determines the range of analyte concentration that can reliably be determined. The upper limit of analyte concentration that can be measured is determined largely by the time scale accessible before adventitious convection disrupts the concentration profiles.

5.2.2 Titrations of thiosulfate and sulfite with electrogenerated iodine

The principle of the titrations of thiosulfate and sulfite with iodine is analogous to the vitamin C titration. The experimental collector current transients in the thiosulfate titration as a function of t at fixed I_{gen} (Figure 37) are very similar to those presented with vitamin C (Figure 30): The more analyte is present in the solution the lower collector currents (and collection efficiencies).

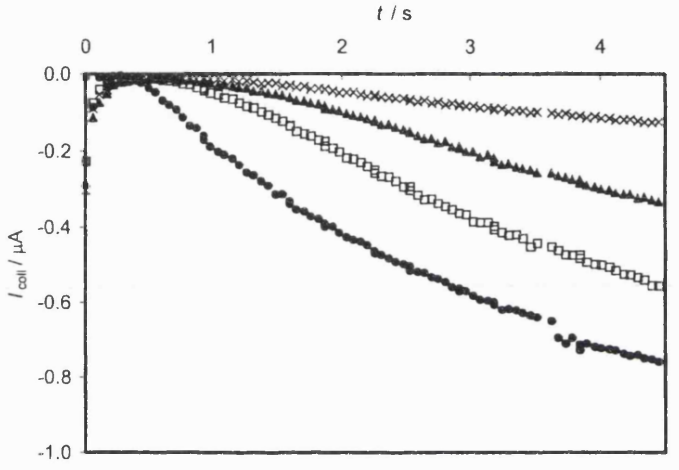

Figure 37. Experimental collector current transients with different thiosulfate concentrations. Generator current applied at t = 0 s, *i.e.* 1 s after the movement pulse of the electrode. I_{gen} = 6 µA, E_{coll} = 0 V vs. SCE, 50 mM KI, 0.1 M H_2SO_4, $c_{thiosulfate}$ = (●): 0; (○): 0.5; (▲): 1.0; (×): 2.0 mM.

Collector currents in both thiosulfate and sulfite titrations as a function of I_{gen} at fixed t are shown in Figure 38 and Figure 39, respectively. The results are in a good agreement with the reaction layer model (eq. (60)): at relatively high generator currents the curve of the collector current as a function of the generator current lies parallel to the curve without the analyte.

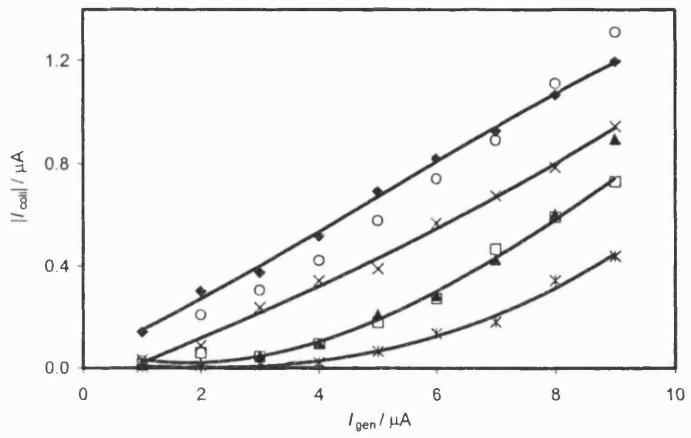

Figure 38. Collector current vs. generator current in thiosulfate titration. Values determined 3 s after generator current was applied. E_{coll} = 0 V vs. SCE; 50 mM KI; 0.1 M H_2SO_4; $c_{thiosulfate}$ = (◆): 0; (o): 0.25; (×): 0.5; (▲): 0.75; (○): 1.0; (✳): 2.0 mM. Mean values from four measurements with different electrodes. Solid lines are fitted trend lines.

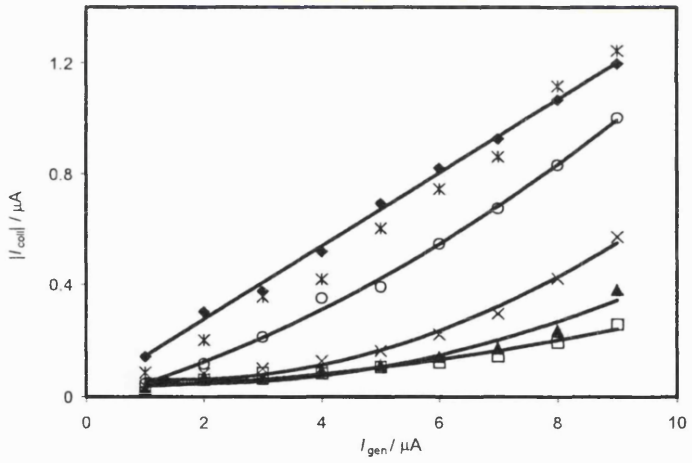

Figure 39. Collector current vs. generator current in sulfite titration. Values determined 3 s after generator current was applied. E_{coll} = 0 V vs. SCE; 50 mM KI; 0.1 M H_2SO_4; $c_{sulfite}$ = (◆): 0; (✳): 0.1; (o): 0.25; (×): 0.5; (▲): 0.75; (○): 1.0 mM. Mean values from four measurements with different electrodes. Solid lines are fitted trend lines.

In Figure 40, the generator current required to reach a particular value of collector current ($|I_{coll}|$ = 0.4 μA) is presented for thiosulfate and sulfite titration. As in the case of vitamin C titration, the results are straight lines since the required generator current is proportional to the analyte concentration.

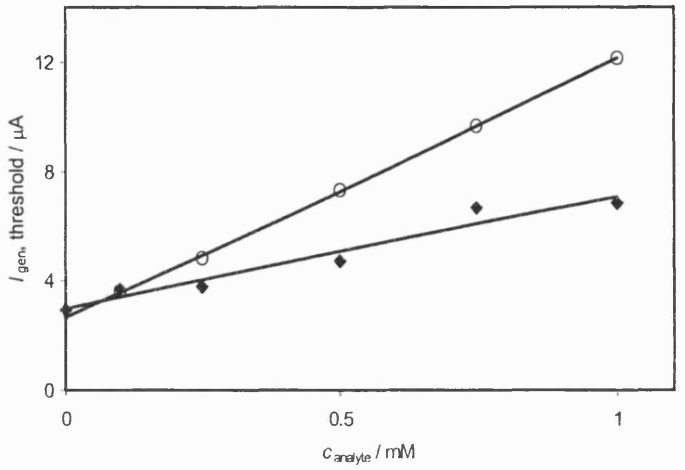

Figure 40. Generator current that is required to produce a collector current, $|I_{coll}|$, of 0.4 μA after a particular time (3 s after the generator current pulse was applied) in thiosulfate (◆) and sulfite (o) titration. E_{coll} = 0 V vs. SCE; 50 mM KI; 0.1 M H_2SO_4. Mean values from four measurements with different electrodes. Solid lines are fitted trend lines.

The difference between the thiosulfate and sulfite titrations is due to different stoichiometries of the reactions (66) and (67): one mole of iodine is reacting with two moles of thiosulfate (66) but one mole of sulfite (67). The reaction layer model (eq. (60)) predicts that the generator current that is required to compensate the flux of the analyte, is proportional to the number of moles of titrant that is needed to react with one mole of analyte. Therefore the displacements of the curves and the required generator currents (Figure 40) in the sulfite titration (slope ≈ 9.5 μA/mM) are approximately twice as high as in the thiosulfate titration (slope ≈ 4.1 μA/mM) with the same analyte concentrations. This leads to a higher possible analyte concentration to be detected in the thiosulfate titration and a lower detection limit in sulfite titration. The rates of both reactions can be assumed to be very fast, and the kinetic differences can be neglected. [136, 144]

In Figure 41, slopes of I_{coll} vs. $t^{1/2}$ against generator current in thiosulfate titration are presented. When all of the data of the *I-t* curve is used, the curves indicating different analyte concentrations are better distinguished than when the collection efficiency is determined using a single point (Figure 38) on the original data curve. It is also observed that when high generator currents are applied, the curves where the analyte is present approach the curve without the analyte: the system starts to reach the behaviour of the reference solution (0 M analyte). The origin of the effect is that the flux of the titrant is greater than the flux of the

analyte, the time variation of the collector current is overwhelmingly determined by the titrant flux.

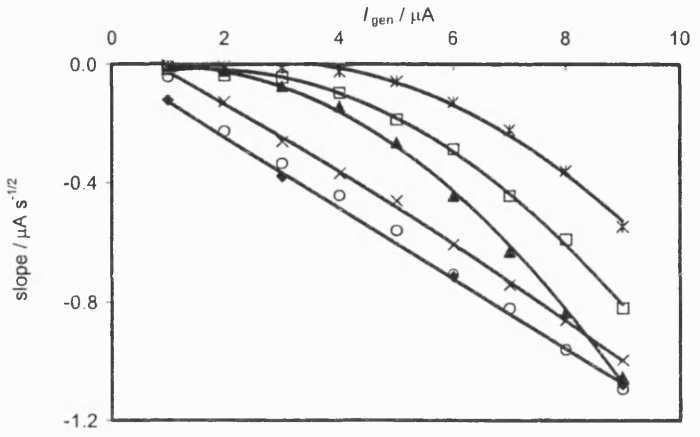

Figure 41. Slope $I_{coll}/t^{1/2}$ (t = 0 s when the generator current switched on) as a function of generator current in thiosulfate titration. E_{coll} = 0 V vs. SCE; 50 mM KI; 0.1 M H_2SO_4; $c_{thiosulfate}$ = (◆): 0; (o): 0.25; (×): 0.5; (▲): 0.75; (○): 1.0; (✶): 2.0 mM. Mean values from four measurements with different electrodes. Solid lines fitted trend lines.

Calibration curves for both thiosulfate and sulfite titrations are shown in Figure 42. Again, the slope values in the sulfite measurements are approximately twice as high as the slope values in the thiosulfate titration due to the stoichiometry.

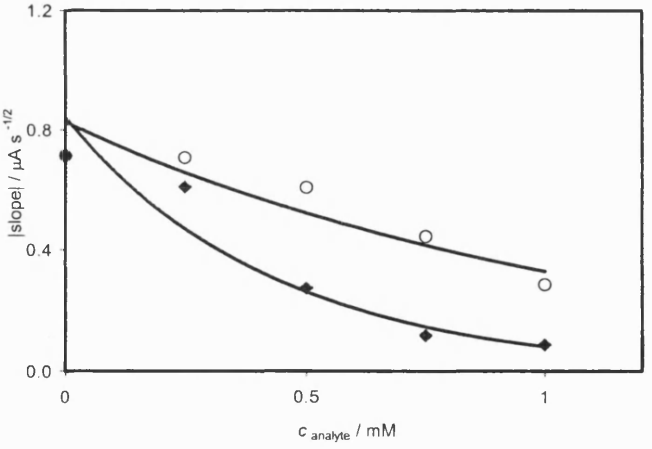

Figure 42. Slope $I_{coll}/t^{1/2}$ (t = 0 s when the generator current switched on) as a function of analyte concentration in thiosulfate (◆) and sulfite (o) titration. E_{coll} = 0 V vs. SCE; I_{gen} = 6.0 μA; 50 mM KI; 0.1 M H_2SO_4. Mean values from four measurements with different electrodes for each point. Solid lines are fitted trend lines.

5.2.2.1 Electrode poisoning

Deviation in the results can be caused by electrode poisoning. The same microband electrode was used for the entire set of measurements with a given analyte concentration (9 scans, currents from 1 to 9 μA). The actual effect of poisoning was studied by doing sets of measurements where the same solution (iodine present), the same generator current and the same microband electrode were used for nine scans in a row. An example of the results is shown in Figure 43.

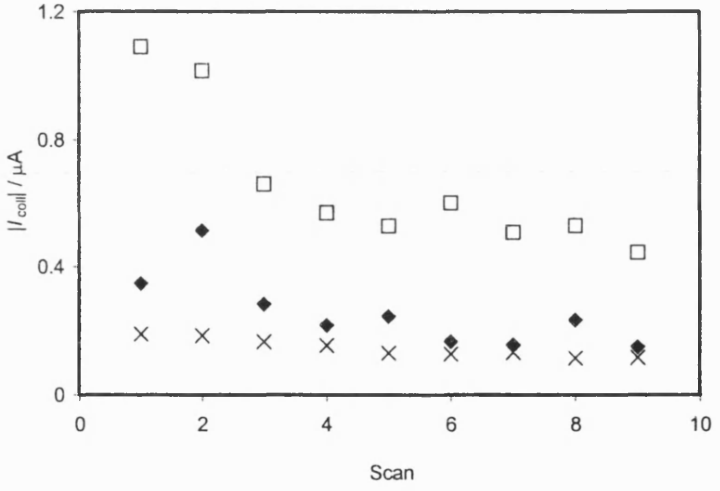

Figure 43. Effect of electrode poisoning on the measured collector current (at t = 3 s) when the scan was repeated with the same microband electrode. E_{coll} = 0 V vs. SCE; I_{gen} = 6 μA; 50 mM KI; 0.1 M H_2SO_4. (○): 0 mM analyte; (◆): 1.0 mM thiosulfate; (×): 1.0 mM sulfite.

The currents become smaller when the scans are repeated with the same microband, particularly when no analyte is present. Variation in the currents occurs also due to other effects (*e.g.*, convective effects, noise). The electrode poisoning is most probably because of adsorbed species, especially I_2, [146] at the electrode surface, since the effect is strongest when there is no analyte to react with I_2 in the system. In addition, the surface structure of a just snapped (fractured) electrode differs from a used or polished one.[18] Reliable results are achieved when disposable electrodes are used immediately after snapping to expose the gold, for a single measurement only, and the results from the same scans are compared with each other. The reactivity of the insulating material and its effect on the behaviour of the gold

electrodes could also be investigated. After repeated measurements on a given electrode, darkening of the electrode or a dark precipitate at the electrode surface was observed by an optical microscope. The effect originated particularly at the boundary of the electrode material and insulator and may have been due to an electro-oxidation of lead leached out from the insulator (Figure 17; dielectric: $PbO\text{-}SiO_2$ glass containing barium titanate).

5.2.3 Titrations of dichromate and permanganate with electrogenerated iron(II)

5.2.3.1 Dichromate titration

Titration of dichromate with Fe(II) is analogous to the vitamin C, thiosulfate and sulfite titrations presented in previous sections. Collector currents in dichromate titration as a function of I_{gen} at fixed t are shown in Figure 44. The reaction layer behaviour can be seen as parallel curves when the generator current is relatively high.

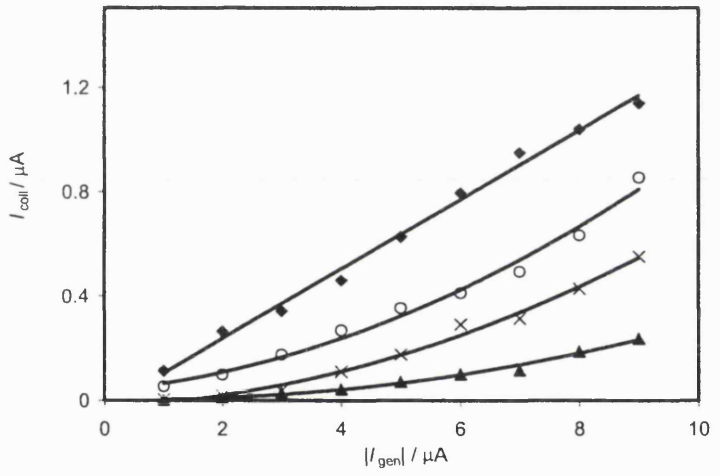

Figure 44. Collector current vs. generator current in dichromate titration. Values determined 3 s after generator current was applied. E_{coll} = +0.850 V vs. SCE; 50 mM $NH_4Fe(SO_4)_2$; 0.1 M H_2SO_4; $c_{dichromate}$ = (◆): 0; (o): 0.1; (×): 0.25; (▲): 0.5 mM. Mean values from four measurements with different electrodes. Solid lines are fitted trend lines.

Calibration curves, *i.e.,* absolute values of the generator current required to reach a particular value of the collector current, for the dichromate titration are presented in Figure 45. The threshold values are relatively high because of the stoichiometry of the reaction (70): one mole of dichromate reacts with six moles of Fe(II).

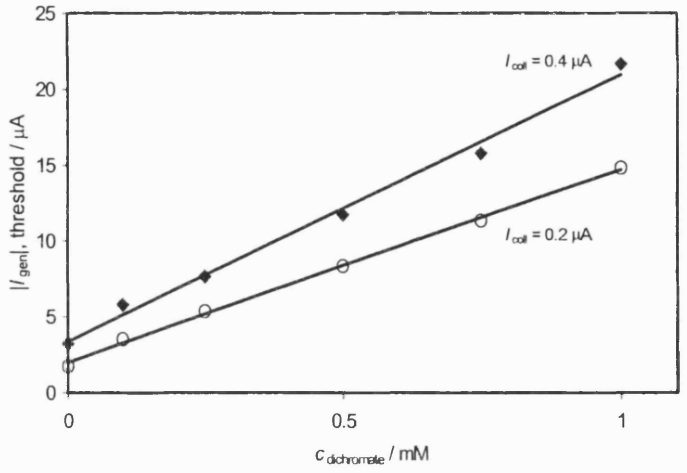

Figure 45. Generator current that is required to produce a certain collector current after a particular time (3 s) in dichromate titration. E_{coll} = +0.850 V vs. SCE; 50 mM $NH_4Fe(SO_4)_2$, 0.1 M H_2SO_4, 50 mM KH_2PO_4. For higher analyte concentrations, I_{gen} was in the range –10 to –20 μA. Four measurements with different electrodes. Solid lines are fitted trend lines.

The effect of stoichiometry was also seen as a delay of the collector current after the generator was switched on, and the delay increased with an increasing analyte concentration. As a comparison, experimental collector current transients in dichromate and sulfite titrations are shown in Figure 46.

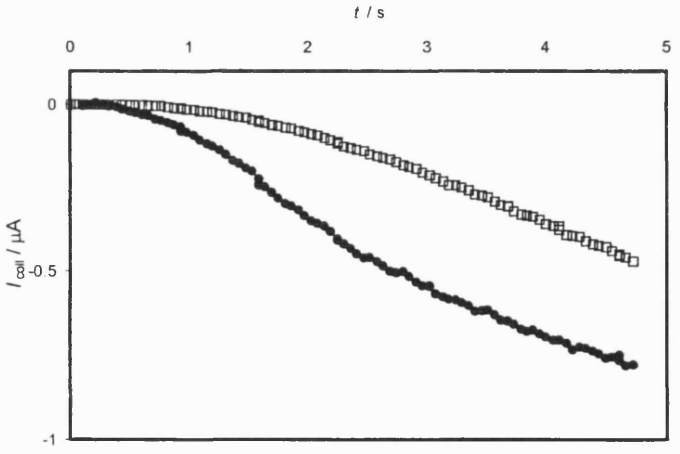

Figure 46. Experimental collector current transients with 1.0 mM dichromate (○) and sulfite (●). Generator current applied at t = 0 s, *i.e.*, 1 s after the movement pulse of the electrode. $|I_{gen}|$ = 6 μA (for dichromate, the current multiplied by –1), E_{coll} = +0.850 V (dichromate) and 0 V (sulfite) vs. SCE, 50 mM and $NH_4Fe(SO_4)_2$ (dichromate) and KI (sulfite), 0.1 M H_2SO_4.

5.2.3.2 Permanganate titration

Titration of permanganate with Fe(II) differs from the previously presented titrations since the analyte itself is electroactive. Experimental collector current transients and the collector currents with different analyte concentrations are given in Figure 47 and Figure 48, respectively. Two different detection methods are compared with each other. In a direct detection method, no iron is present in the solution and the generator electrode is completely disconnected. The collector potential is stepped to a value on the diffusion limit for reaction (72) at $t = 0$, and only one value (diffusion limited current) is detected for each concentration. In an indirect method, the Fe(III) concentration is 50 mM, *i.e.*, the same as in $Cr_2O_7^{2-}$ titration, and Fe(II) (titrant) is generated electrochemically at the generator electrode. The total current detected at the collector presents a sum of the oxidation of Fe(II) back to Fe(III) as well as reaction (72). In the experimental data, the transients (Figure 47) at times $0 \le t \le 1$, *i.e.*, before the generator is switched on, are consistent with the transients of the direct detection method (reaction (72)).

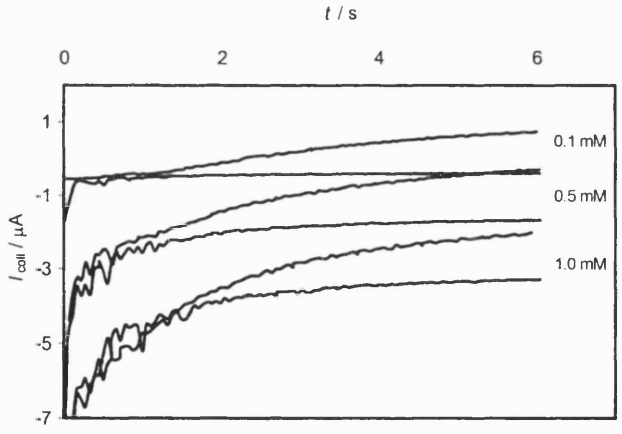

Figure 47. Collector current transients with different permanganate concentrations. E_{coll} = +0.6 V vs. SCE; 0.1 M H_2SO_4. Lower transients for a direct method: no iron present, generator disconnected. Upper transients for an indirect method: Fe(II) electrogenerated, 50 mM $NH_4Fe(SO_4)_2$; I_{gen} = -6 µA.

In Figure 48, the collector current value for the indirect method is the difference between the current at the point when I_{gen} is switched on (t = 1 s) and 3 s after that. Analogous values are recorded for the direct method as well. The dual microband system has the advantage over a

simple determination of permanganate concentration through the limiting current for reaction (72) by providing an additional, complementary route to check the measurement. The permanganate system demonstrates the capability of the dual microband system to be used to measure concentrations of electroactive species accurately and reproducibly.

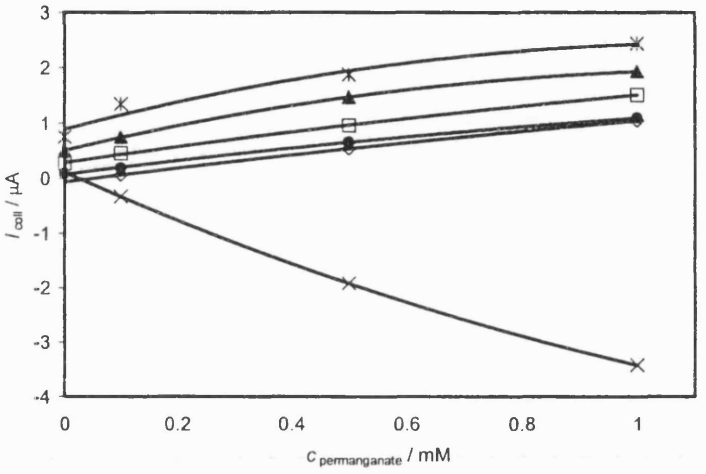

Figure 48. Calibration curves for permanganate titration. Direct detection method (×), *i.e.*, no iron present in the solution and the generator disconnected. The value recorded 4 s after the movement pulse of the electrode. Indirect method where Fe(II) electrogenerated: I_{gen} = (●): -1 μA; (○): -3 μA; (▲): -6 μA; (✶): -9 μA. The current value is the difference between the current at t = 1 s (when the generator current switched on) and t = 4 s. The current difference in direct detection, $I(t = 4\ s) - I(t = 1\ s)$ for $I_{gen} = 0$: (◇). E_{coll} = +0.6 V vs. SCE. Mean values from four measurements with different electrodes. Solid lines fitted trend lines.

5.2.4 Amperometric titration: conclusions

The error bars presented in Figure 33 and Figure 36 show the standard deviation (eq. (81)) and therefore the repeatability between different electrodes. Typically, the accuracy was ± 10 %. That was the case in all amperometric titrations presented here, although the error bars have been left out in order to ensure the clarity of the figure presentation. The detection limit depends on the analyte to be measured and the stoichiometry of the actual titration reaction. At present, the method is capable of measuring millimolar (parts per million, ppm) levels.

The experimental errors were mainly due to the irreproducibility of the surfaces of the microband electrodes, inaccuracy of the solution preparation and external factors, *e.g.*, electrical noise. The reliability of the experimental arrangement was tested by using different pieces of equipment (*e.g.*, different potentiostats, reference electrodes) to measure analogous signals. It was observed that the results were very consistent with each other, and the error due to experimental set-up was negligible.

The snapping procedure may lead to deviations from the ideal geometry and distortion of the diffusion field. When different microband electrodes were employed to measure an analogous signal with the same solution the error of a single measurement (standard deviation, eq. (81)) was approximately the same as observed with different solutions and different microbands. Therefore it was concluded that the main source of error was the irreproducibility of the electrode geometry.

The repeatability of the measurements might be improved by improving the manufacturing process of the microband electrodes. Different substrate materials may change the snapping procedure and decrease the distortion. Both the conductor and dielectric inks may also affect the fracturing properties but the best possible compromise between various electric and breaking properties should be found. The accuracy could also be improved by establishing more reproducible experimental conditions, *i.e.*, identical chemical environments and careful temperature control, but that would affect the user-friendliness of the method.

5.3 Potentiometric titration

Titrations of vitamin C, thiosulfate and sulfite, the same applications demonstrated in the amperometric mode, are here presented in the potentiometric mode. Gold was employed as the electrode material. In addition, potentiometric titrations of chloride, iodide, thiosulfate and cyanide using silver microband electrodes are presented.

5.3.1 Constant current method using gold microbands

Open-circuit potentials of the collector electrode against time in vitamin C titration with the constant current method are presented in Figure 49. The measured collector potentials become more negative when the analyte concentration increases, which is consistent with the Nernst equation (eq. (31)): the $[Fe(CN)_6]^{3-}$ concentration at the collector electrode decreases with an increasing analyte concentration if the experimental conditions (T and $c_{ferrocyanide}$) are the same. For a full titration curve (E_{coll} vs. I_{gen}), several scans with different generator currents must be carried out and the accuracy of the system is limited unless the number of scans is very high. Results of thiosulfate and sulfite titrations with iodine using the constant current method were analogous to the vitamin C results.

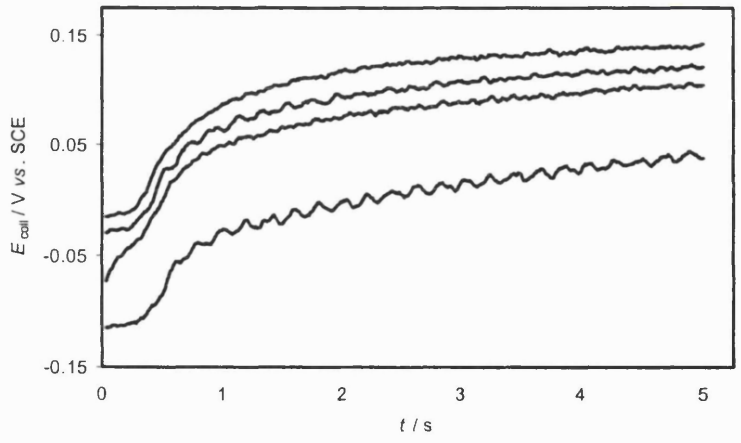

Figure 49. Open-circuit potentials of the collector electrode in potentiometric vitamin C titration with constant current method. Au microbands. I_{gen} = 6 μA, applied at t = 0 s. 50 mM $K_4Fe(CN)_6$, phosphate buffer. Vitamin C concentrations: 0; 1.0; 2.5; 5.0 mM (transients from top to bottom).

In Table 4, experimental open-circuit potentials are compared with values calculated using Equations (38), (39) for the titrant concentration and the Nernst equation (eq.(31)) for the open-circuit potential assuming that the concentration of A (Figure 4) is constant (50 mM). Both Equations (38) and (39) give the same value for the solution without analyte (if 0.1 μM analyte concentration is assumed in eq. (39)). The calculated potential values differ from the experimental ones. The deviation in the case without the analyte may be due to the hemi-cylinder approximation where the assumed electrode surface area is approximately 1.5 times larger than the real area. This is consistent with the results by Deakin et al. [32] (eq. (11)). The approximation $r_1 \approx l$ is sufficient: ten times smaller or larger r_1 values do not change the potential significantly. The results where the analyte is present are consistent with the amperometric results presented in section 5.2.1; the theoretical model does not take the depletion or diffusion of the analyte into account.

Table 4. Calculated (eq. (38), (39) and (31)) and experimental open-circuit potentials in potentiometric vitamin C titration with the constant current method (I_{gen} = 6 μA). The experimental values determined at t = 4 s, mean values from three different measurements with different microband electrodes. T = 293.15 K, k = 2240 $M^{-1}s^{-1}$ (for the titrant multiplied by the stoichiometric co-efficient 2). [99]

	E / V vs. SCE	
$c_{Vitamin\ C}$ / mM	Calculated	Experimental / ± 0.020
0	+0.200	+0.140
1.0	+0.040	+0.120
2.5	-0.030	+0.100
5.0	-0.110	+0.030

5.3.2 Ramp current method using gold microbands

Open-circuit potentials of the collector electrode against the applied generator current in thiosulfate titration with the ramp current method are shown in Figure 50. The end-point of the titration can be determined as a point where the first derivative (dE/dI) of the curve reaches its maximum. The end-points shift to higher currents when the analyte concentration

increases. A higher flux of the titrant from the generator electrode is needed in order to reach the end-point because it is consumed in the inter-electrode gap by the analyte.

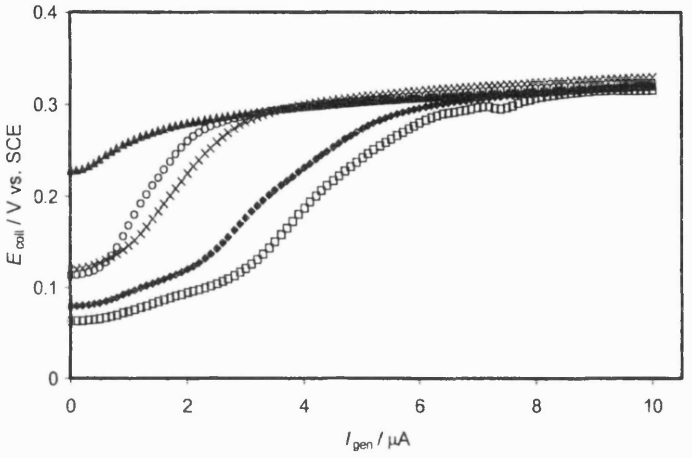

Figure 50. Open-circuit potentials of the collector electrode in potentiometric thiosulfate titration with ramp current method. Au microbands. Generator current scan started at $t = 0$ s, *i.e.*, 1 s after the movement pulse of the electrode. I_{gen} scanned from 0 to 10 μA at 0.2 μA/s. 50 mM KI; 0.1 M H_2SO_4; $c_{thiosulfate} = 0$ (▲); 0.5 (o); 1.0 (×); 2.0 (◆); 3.0 (□) mM.

Both experimental and calculated open-circuit potentials of the collector electrode against the applied generator current in vitamin C titration with the ramp current method are shown in Figure 51. Equations (40), (41) and (42) were used for the calculations of the titrant concentrations and the calculated values were substituted into the Nernst equation (eq.(31)) that gave the open-circuit potential. Equation (40) gives the analytical solution for the case where no analyte is present and it is valid at long times. It can be seen in Figure 51 that the approximation is valid, and the calculated curve is in a good agreement with the experimental one at long times. Equation (41) provides a more accurate solution when no analyte is present but requires a numerical calculation for the Laplace transform. Now the agreement between the calculated and experimental curves is excellent even at short times. Equation (42) gives the solution for the case where the analyte is present. This time deviations from the experimental curves are obvious. This is because the approximations made deriving Equation (42) are too simplified. As in the case of amperometric titration, the analyte concentration does not stay constant between the electrodes, but decreases significantly due to the actual titration reaction. In the very first part of the curves the deviation is not that significant, since the approximation can be assumed to be valid at short

times. For a more accurate calculation, a diffusion equation should also be written for the analyte but that would require more powerful numerical techniques.

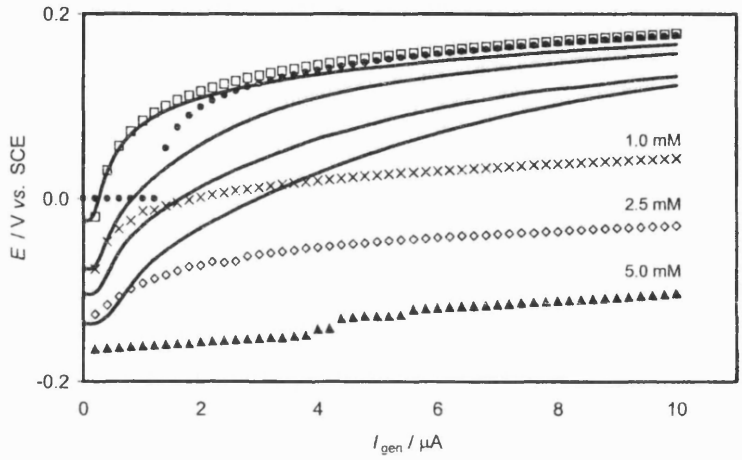

Figure 51. Experimental (solid lines) and calculated (symbols) open-circuit potentials of the collector electrode in potentiometric vitamin C titration with ramp current method. Au microbands. Generator current scan started at $t = 0$ s, *i.e.*, 1 s after the movement pulse of the electrode. I_{gen} scanned from 0 to 10 μA at 0.2 μA/s. 50 mM $K_4Fe(CN)_6$; phosphate buffer; $c_{vitaminC} = 0$; 1.0; 2.5; 5.0 mM (experimental curves from top to bottom), 0 mM: (●, eq. (40)), (□ eq. (41)). Other calculated values using Equation (42). $T = 293.15$ K, $k = 2240$ $M^{-1}s^{-1}$ (for the titrant multiplied by the stoichiometric co-efficient 2). [99]

The potential of the gold electrode at the start of the current ramp would be a mixed potential, determined by the concentrations of all redox active species in the solution, including dissolved oxygen. [137] Other elements contributing to the mixed potential would be redox reactions of the gold itself and of the metal oxide additives (chiefly CuO) present to secure adhesion of the Au to the substrate. The latter fact was evidenced by different open-circuit potentials for the generator and collector electrodes, which end up with different additive concentrations because they are bounded by different materials (substrate and insulator).

The potential of the gold microbands on the same electrode tile differed from each other by approximately 60 mV, the potential of the inner electrode being more positive independent of the electrolyte solution. This may also be due to the difference in the manufacturing process: the inner electrode material layer goes through the furnace more often than the outer

layer, and the impurities in the commercial ink may change the properties of the conductor. The same phenomenon was not seen when silver or platinum-gold mixture was the electrode material.

The mixed potential could change with time. The question is whether such drifts might affect the measured end-point. Drifts were indeed observed (for instance, the first part of the titration curves shown in Figure 50). However, the drifts were slow enough that the end-point was not affected. More redox active electrode materials (platinum and platinum-gold mixture) improved somewhat the stability of the initial potential but gave the same result for the end-point.

The dependence of the end-point on the analyte concentration in vitamin C, thiosulfate and sulfite titration is presented in Figure 52. The difference between the end-points in the thiosulfate and sulfite titrations is due to the different stoichiometry as presented previously with the amperometric titration. One mole of sulfite consumes one mole of titrant whereas in thiosulfate titration one mole of analyte reacts with 0.5 mole of titrant. The generator currents at which the titration end-points are detected are approximately twice as high in the sulfite titration (slope ≈ 2.6 μA/mM) than in the thiosulfate titration (slope ≈ 1.0 μA/mM). This is in a good agreement with the reaction layer model (eq. (60)).

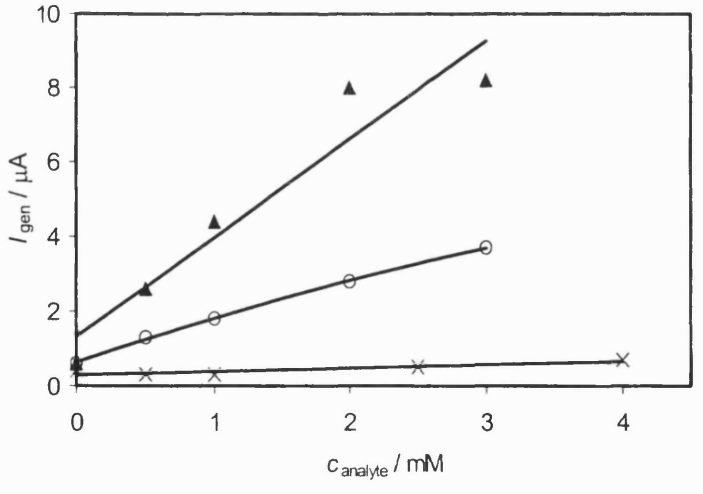

Figure 52. Generator currents where end-point (maximum value of the 1st derivative) reached in potentiometric titrations of vitamin C (×), thiosulfate (o) and sulfite (▲) with ramp current method. Au microbands. Generator current scan rate 0.2 μA/s. Solid lines are fitted trend lines.

It can be seen that the generator current where the maximum of the first derivative of the vitamin C titration is achieved does not change with the analyte concentration as expected. This is due to finite rate of the titration reaction. As Equation (28) presents, important parameters are the diffusion co-efficient of the titrant and the analyte concentration. If the reaction time is not significantly less than the time to cross the gap then the system is limited by the finite rate of the reaction. In thiosulfate and sulfite titrations the reaction rates are significant ($>10^6$ $M^{-1}s^{-1}$), [136, 144] but in vitamin C titration the rate constant (10^3 $M^{-1}s^{-1}$) [99] becomes important. The difference in the measured collector potential between different vitamin C concentrations was indeed seen, not in the location of the maximum of the first derivative but as a change of the collector potential that was achieved at the end of a generator current ramp (Figure 51). The finite rate of the reaction does not affect the amperometric response: the measured collector current is directly proportional to the titrant concentration and when a small amount of the titrant is at the collector, the response is not observed. Instead, in the potentiometric mode the collector potential depends on the logarithm of the titrant concentration and the response is much more sensitive to low concentrations of the titrant at the collector.

Amperometric titration with dual microband electrodes provides an analytical method for systems where the rate of the titration reaction is finite, *e.g.*, titration of vitamin C with ferricyanide. For fast titration reactions, *e.g.*, thiosulfate with iodine, both amperometric and potentiometric measurements give reliable results. The disadvantage of the potentiometric method is the drift of the potential. On the other hand, the potentiometric mode opens up completely new possibilities due to the very sensitive response to the concentration of the electroactive species.

5.3.3 Precipitation titrations using dissolving silver microbands

Transients in chloride and iodide titrations with dissolving silver electrodes are presented in Figure 53 and Figure 54, respectively. The potentials detected at the silver collector microband are very stable, and the end-points can be determined very accurately with both analytes. The open-circuit potential before the end-point becomes more negative when a halide (particularly iodide) is present, probably due to adsorption of the halide on the indicator electrode. For 1.0 mM chloride solution two curves are shown: a transient where a

microband was used for the first time, and a transient where a microband was used for a repeated scan.

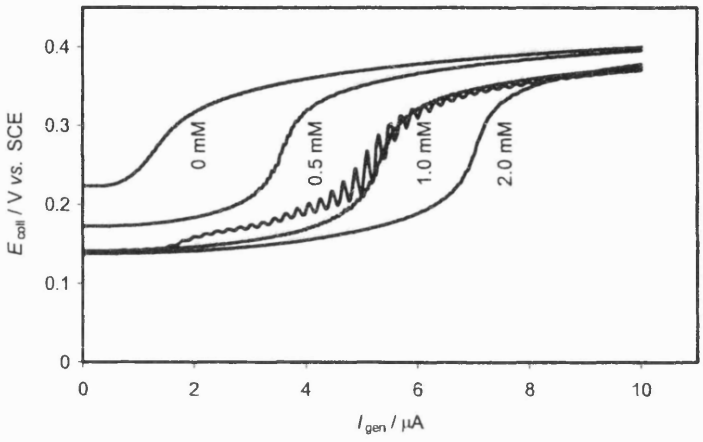

Figure 53. Open-circuit potentials of the collector electrode in potentiometric chloride titration with ramp current method. Ag microbands. Each microband electrode was used for four scans at lower sweep rates before these scans. For 1.0 mM analyte the transients with a new electrode (oscillations) and an old one compared with each other. Generator current scan started at $t = 0$ s, *i.e.*, 1 s after the movement pulse of the electrode. I_{gen} scanned from 0 to 10 μA at 1.0 μA/s. 0.1 M KNO_3.

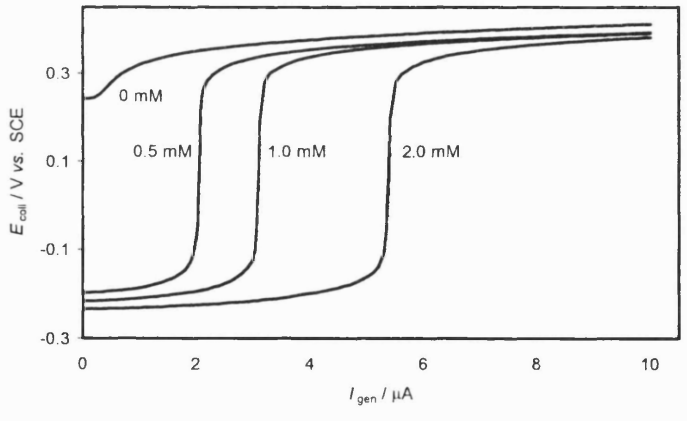

Figure 54. Open-circuit potentials of the collector electrode in potentiometric iodide titration with ramp current method. Ag microbands. Each microband electrode was used for two scans (0.05 and 0.1 μA/s) before these scans. Generator current scan started at $t = 0$ s, *i.e.*, 1 s after the movement pulse of the electrode. I_{gen} scanned from 0 to 10 μA at 0.2 μA/s. 0.1 M KNO_3.

In chloride titration, a small nucleation peak was seen in the titration curve just before the end-point when the silver microband was employed for the first time but disappeared when the electrode was used repeatedly. In addition, with clean ('new') electrodes oscillations in the titration curve were seen at high scan rates. This effect also disappeared when the electrode was used for a following scan. Similar phenomena were not observed with iodide. This is most probably due to different solubility products and equilibrium constants of the systems: in chloride titration, supersaturation, *i.e.*, a situation where the concentration of the solute at the indicator electrode is higher than expected at equilibrium, takes place before the nucleation. During the second scan a small amount of the AgCl precipitate is already present at the indicator electrode and similar nucleation does not occur. The solubility product of AgI ($K_{sp} = 10^{-15.8}$) is significantly lower than that of AgCl ($K_{sp} = 10^{-9.5}$) [133] and therefore an excess of I^-, which would lead to supersaturation, cannot be detected at the indicator electrode. An increase in temperature and ionic strength can be expected to increase the solubility products. [38, 137]

When a dissolving microband electrode is used repeatedly for current scans the recess of the electrode material is obvious. This leads to a changed diffusion field and a longer diffusion path for the titrant, and therefore the end-point is at a higher generator current than with an electrode that is used for the first time. However, if two scans with 'new' and 'old' (not used for more than 4 scans previously) microbands were compared with each other (Figure 53; 1.0 mM Cl^-) the variation in the end-point currents was not more than the variation between two individual ('new') microbands. As an advantage, the dissolution process can be assumed to flatten the roughness of the electrode surface that is as a consequence of the snapping procedure.

The dependence of the end-point on the analyte concentration and scan rate for iodide titration is presented in Figure 55. The end-points in the chloride titration were similar to the ones in the iodide titration (Figure 55). It can be seen that with an increase of the current scan rate, a higher current is needed for the end-point. This is because of the delay in response caused by the transit time for the titrant across the gap, clearly seen in measurements at constant generator current.

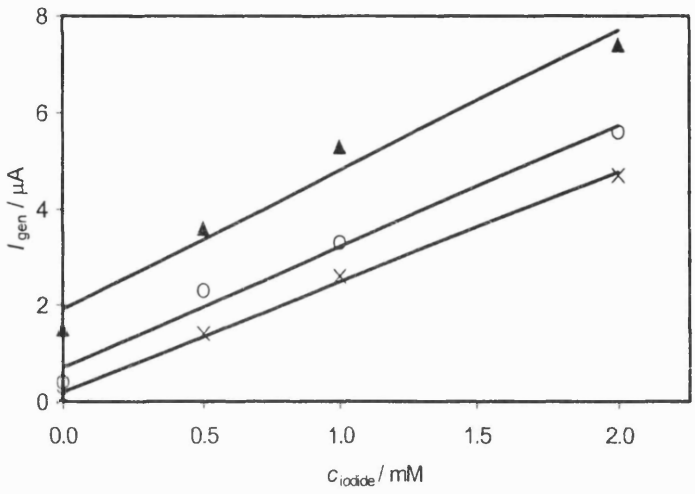

Figure 55. Generator currents where end-point (maximum value of the 1st derivative) reached in potentiometric iodide titration. Ag microbands. Generator current scan rate 0.05 (×), 0.2 (o) and 1.0 (▲) µA/s. Solid lines are fitted trend lines.

Transients in titrations of iodide and chloride combinations are presented in Figure 56. Two steps in the titration curves can be clearly seen when the chloride concentration is relatively high (1 mM). The first step is for the formation of AgI and the second one is for the formation of AgCl due to different solubility products of the compounds. When the scan rate of the generator current increases the accuracy becomes limited. When the chloride concentration is significantly lower than iodide concentration the second step cannot be clearly seen most probably due to co-precipitation, but the location of the second step is the same when the total concentration of the halides is the same (1.5 mM). This is an interesting phenomenon the interpretation of which is not straightforward. Above all, this system is a flux balance rather than a mass balance method which may lead to specific reaction/diffusion layers (analogous to the model presented in section 2.3.4) for each halide. In addition to the effect of solubility products and co-precipitation, the reaction rates and the actual formation processes of the precipitates may become important.

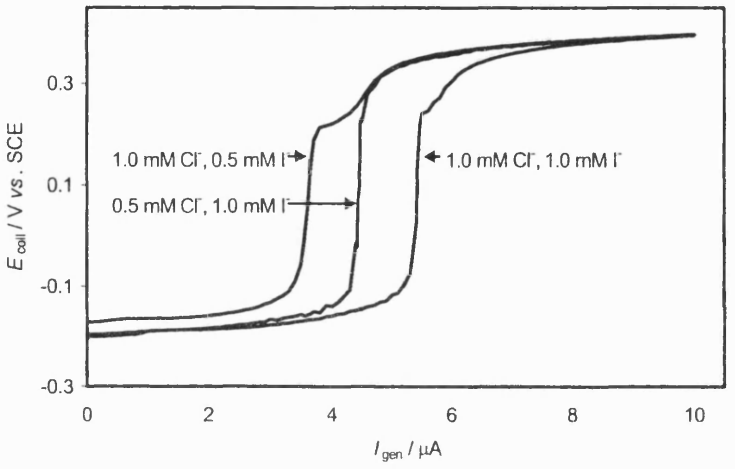

Figure 56. Open-circuit potentials of the collector electrode in potentiometric titration of combination of chloride and iodide with ramp current method. Ag microbands. Generator current scan started at $t = 0$ s, *i.e.*, 1 s after the movement pulse of the electrode. I_{gen} scanned from 0 to 10 μA at 0.2 μA/s. 0.1 M KNO_3.

Transients in cyanide titration are presented in Figure 57. With relatively high analyte concentration (1 mM) a second titration step can be observed due to formation of a soluble complex, $[Ag(CN)_2]^-$.

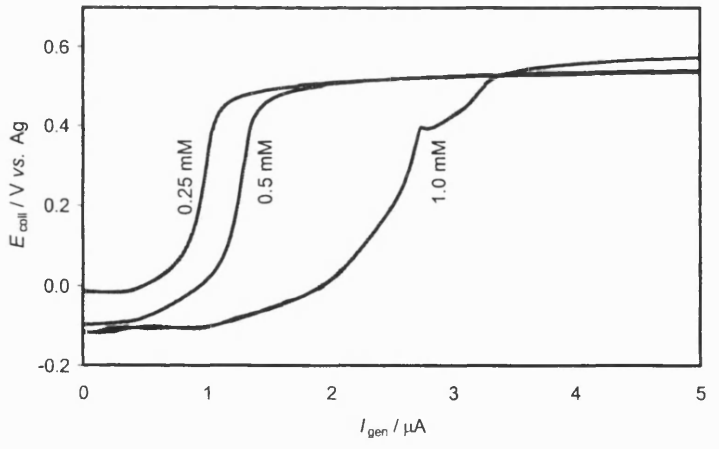

Figure 57. Open-circuit potentials of the collector electrode in potentiometric cyanide titration with ramp current method. Ag microbands. Generator current scan started at $t = 0$ s, *i.e.*, 1 s after the movement pulse of the electrode. I_{gen} scanned from 0 to 10 μA at 0.2 μA/s. 0.1 M KNO_3.

In thiosulfate titration, an analogous second step, indicating the formation of $[Ag(S_2O_3)_2]^{3-}$, was only seen when the scan rate was low (0.05 μA/s) and the analyte concentration was high (2.0 mM). In addition, in thiosulfate titration curves a similar nucleation peak to that seen in chloride titrations was detected, signalling a relatively slow precipitation or formation of $[Ag(S_2O_3)]^-$. [162]

The dependence of the end-point on the analyte concentration for thiosulfate and cyanide titrations is presented in Figure 58. The response is approximately linear. When the scan rate was increased the response changed as presented in Figure 55.

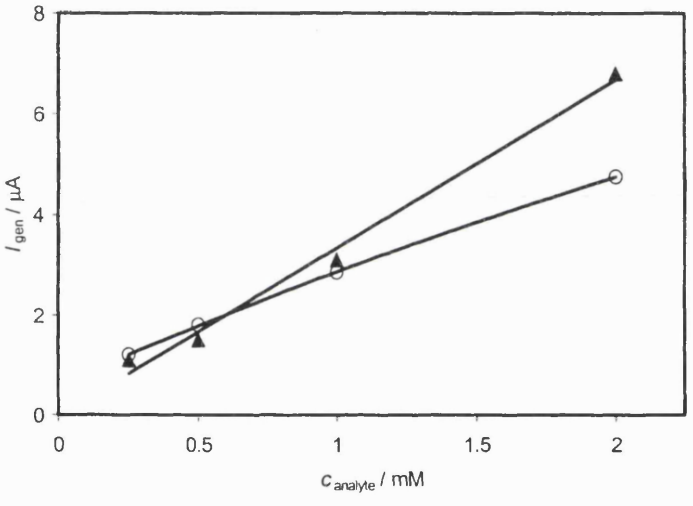

Figure 58. Generator currents where end-point (maximum value of the 1st derivative) reached in potentiometric titrations of thiosulfate (o) and cyanide (▲) with ramp current method. Ag microbands. Generator current scan rate 0.2 μA/s. Mean values from two different measurements with different electrodes. Solid lines are fitted trend lines.

Since soluble cyanide and thiosulfate complexes are formed in the presence of a relatively high analyte concentration there is a possibility of an error: the highest step of the actual titration curve might signal the formation of a soluble complex instead of a precipitate. An analysis of the shape of the curve or a setting of a 'threshold value' for the collector potential could improve the reliability of the method. The pH value of the solution has an influence on the reactions. In silver thiosulfate systems, a catalytic reaction that forms sulfuric acid has been reported. [162] In the time scale of these measurements, the pH change should not cause a major problem. The effect of pH value was not studied here, but, in preliminary cyanide experiments at high pH (11-12) the formation of Ag_2O was observed to cause interference.

Conventionally, determination of cyanide with $AgNO_3$ is carried out as a potentiometric titration where the indicator electrode material is silver and the pH value is kept highly alkaline (11-12). [137, 152] The interference caused in the microband system is most probably due to the generation process of the titrant: the generator electrode is polarised as a consequence of the application of the current. Therefore the formation of Ag_2O takes place. A similar effect was seen in Ref. 163 where a silver disk electrode was polarised using anodic stripping voltammetry and the reduction peak of the Ag_2O overlapped the AgCN peak.

In some measurements, the microband devices using silver strips printed on the tile as counter and reference electrodes gave the same transient form and end-point current as were obtained using SCE reference. An example is presented in Figure 59. In the time scale of the experiments, these simple disposable strips are stable and provide all electrodes that are needed for a potentiometric titration which is fast and reasonably accurate.

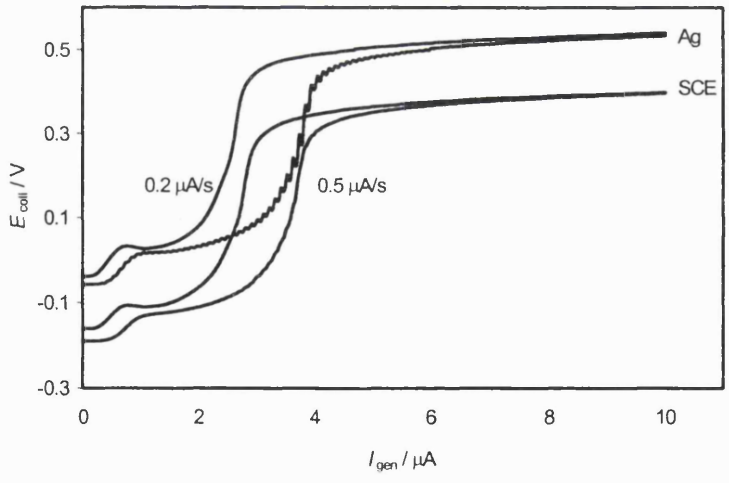

Figure 59. Open-circuit potentials of the collector electrode in potentiometric thiosulfate titration ($c_{analyte}$ = 1.0 mM) with ramp current method. Ag microbands. Reference electrode: either Ag printed on the electrode tile or SCE. Generator current scan started at t = 0 s, *i.e.*, 1 s after the movement pulse of the electrode. I_{gen} scanned from 0 to 10 μA. 0.1 M KNO_3.

5.3.4 Potentiometric titration: conclusions

A typical standard deviation in all cases was 10 % (three to four measurements with different electrodes), mainly due to the non-ideality of the electrode geometry. This is consistent with the amperometric results.

The data analysis of the potentiometric titration curve based on the first derivative is limited if the reaction rate is finite. For further studies on the system, a combination of the data that consists of the derivative, the shape of the titration curve, the start potential and the potential reached after the end-point (mainly determined by the Nernstian equilibrium between the titrant and the species originally in the solution) could lead to a more accurate analysis. Simultaneous detection of different components would require more investigation particularly on the dynamics of the system.

In addition, a generator current sequence mode where the current is stepped between two different values, increasing incrementally with time, would be an interesting application. The measurement of the collector potential would be made as a difference between the potentials just prior to the generator step to the higher value and just prior to the step back to the lower value. That kind of method, analogous to square wave voltammetry [22] might make the analysis more accurate.

When choosing an analytical method several aspects have to be taken into account. The flux of the titrant from the generator electrode is balanced against the flux of the analyte from the solution. This is done by adjusting the generator current scale or scan rate. The stoichiometry of the actual titration reaction is an important factor as well as the diffusion of reactive materials. On one hand, if the analyte concentration is too high no signal is recorded at the collector since all of the generated titrant is removed by the titration reaction. On the other hand, if the analyte concentration is very low the collector signal cannot be distinguished from the signal without the analyte. The lowest concentration that can be distinguished determines the detection limit. As presented in previous sections, the finite reaction rate becomes significant particularly in the potentiometric titration. Important factors are also electrode material and possible adsorption of solution species.

5.4 Industrial application

In this section, the industrial application is presented. The system was first explored using some conventional experimental techniques. Both amperometric and potentiometric titrations using gold microband electrodes were used for the analysis of PMG, and the potentiometric end-point detection was further applied to the determination of PIDA and AMPA.

5.4.1 Preliminary experiments and characterisation of the system

Various Fe(III) compounds as possible titrants were tested. PMG forms an insoluble complex with Fe(III) from $Fe_2(SO_4)_3$, $NH_4Fe(SO_4)_2$ and $FeCl_3$, but it does not react with Fe(III) from $K_3Fe(CN)_6$. Therefore $FeSO_4$ and $(NH_4)_2Fe(SO_4)_2$ were mainly used in the experiments as a source of the titrant. In addition, the electrochemical properties of those two compounds are very similar. $FeCl_3$ cannot be used due to a limited solubility of $FeCl_2$.

The experiments were carried out at pH 3, and that value was adjusted with different inert electrolytes and buffers. Phosphate buffers cannot be used because iron and phosphate form a complex, which adsorbs on the electrode surface. [198] Citrate and acetate form complexes with iron, and particularly, citrate-Fe(III) complex has a high stability constant. [199, 200] These reactions would compete with the actual titration reaction of PMG. [184] The same is also true for OH^-, which reacts with Fe(III) and PMG. [169, 198] In most of the experiments, a combination of sodium sulfate (Na_2SO_4) and sulfuric acid (H_2SO_4) was used as an inert electrolyte in mole ratio 24:1, respectively (typically 96 mM : 4 mM). The anion of the inert electrolyte is the same as the anion of the reacting compound, $FeSO_4$, and therefore, it is not interfering. Na^+ has been reported to form a complex with PMG [177] but that interaction is much weaker than the actual reaction between Fe(III) and PMG.

Cyclic voltammetry was used for the preliminary experiments. Cyclic voltammograms of Fe(II) on gold and platinum disk electrodes with and without PMG are presented in Figure 60. The response is very similar for both electrode materials. When PMG is present in the solution a solid PMG-Fe(III) compound passivates the electrode. The same phenomenon was also seen when microband electrodes were employed.

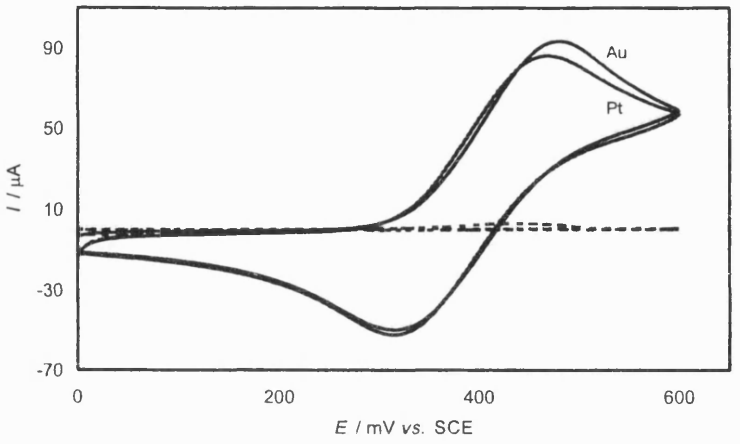

Figure 60. Cyclic voltammograms of Fe(II) at gold and platinum disk electrodes. 50 mM $NH_4Fe(SO_4)_2$, 48 mM Na_2SO_4, 2 mM H_2SO_4, pH 3. Dashed lines: 2.5 mM PMG, Au and Pt disks. Scan rate 25 mV/s.

Cyclic voltammograms on a gold microband electrode in an acetic acid - acetate buffer (no iron present) with and without PMG are presented in Figure 61. The oxidation peak at approximately +1.1 V vs. SCE, which refers to the formation of Au_2O, is significantly higher when PMG is present in the solution. The reduction peaks in both cases are approximately the same size. This may indicate that PMG tends to adsorb and become oxidised in presence of gold(I)oxide. A similar effect has been reported with other organic molecules. [201, 202]

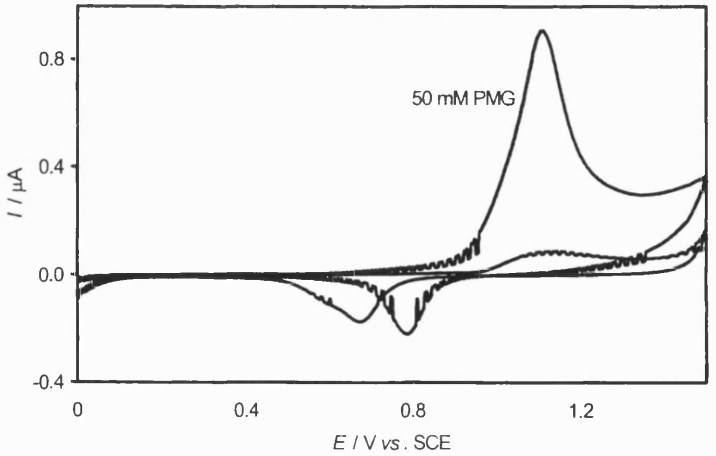

Figure 61. Cyclic voltammograms at a gold microband electrode. Acetic acid - acetate buffer, pH 3, no iron present. Scan rate 25 mV/s.

5.4.2 Conventional potentiometric titration

Traditional potentiometric titration curves for PMG, PIDA and AMPA with Fe(III) at pH 3 using a gold wire as an indicator electrode are presented in Figure 62. The graph confirms the 1:1 stoichiometry for all of the reactions (due to inaccuracy of the method, ratio ≈ 1:1.4, ligand:Fe(III)). The titrations worked similarly when platinum was used as an indicator electrode material. None of the compounds is electrochemically active, *i.e.*, none changes the potential of the indicator electrode when added to the inert electrolyte. In addition, it was observed that the pH value of the solution does not affect the Fe(II)/Fe(III) equilibrium potential or the actual titration reactions in the pH range of approximately 2.5...7.0. It was observed that at lower pH values the titration reactions do not progress.

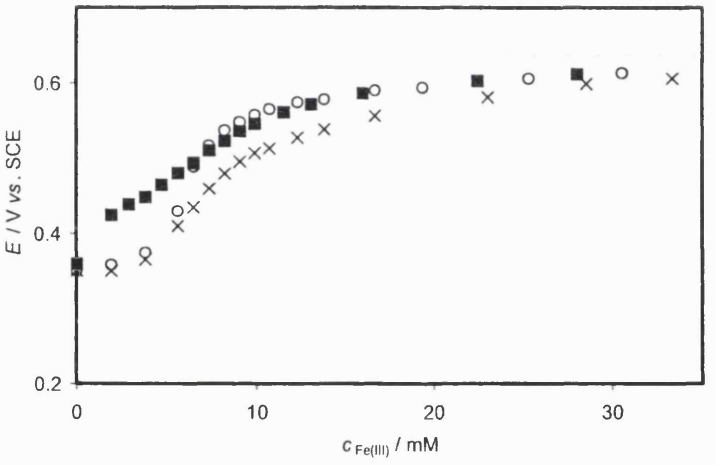

Figure 62. Potentiometric titration of PMG (×), PIDA (o) and AMPA (■) with Fe(III). Au wire as an indicator electrode. The concentration of each compound was 5.0 mM. 96 mM Na_2SO_4, 4 mM H_2SO_4, pH 3.

A conventional potentiometric titration curve for a combination of PMG, PIDA and AMPA (concentration of each 1.0 mM) with Fe(III) at pH 3 is presented in Figure 63. It is obvious that separate titration steps for each compound cannot be seen, and the titration end-point signals that the total stoichiometry changes to 3:1 (ligand:metal) when all of the compounds are present in the solution. The contribution of each individual compound cannot be detected, and therefore a conventional quantitative titration of the compounds in the same solution is not possible.

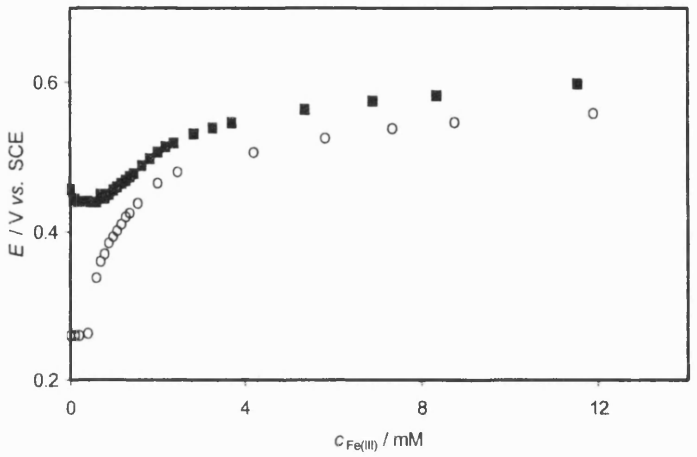

Figure 63. Potentiometric titration of a combination of PMG (1.0 mM), PIDA (1.0 mM) and AMPA (1.0 mM) with Fe(III). Au (o) and Pt (■) wire as an indicator electrode. 96 mM Na_2SO_4, 4 mM H_2SO_4, pH 3.

5.4.3 Amperometric titration

Collector current transients in the amperometric mode for 0 mM and 1.0 mM PMG solutions are presented in Figure 64. A clean microelectrode surface was employed for each measurement. The collection efficiency (eq. (21)) becomes smaller when PMG is present in the solution, as expected.

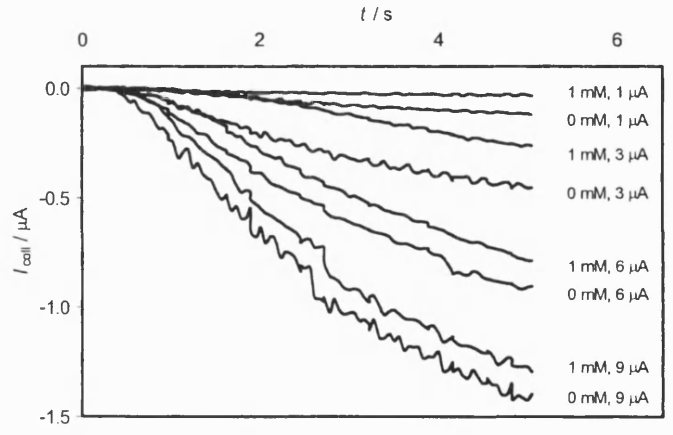

Figure 64. Amperometric titration of PMG (1.0 mM) with electrogenerated Fe(III). Generator current applied at t = 0 s, *i.e.*, 1 s after the movement pulse of the electrode. E_{coll} = -0.1 V vs. SCE. 50 mM $FeSO_4$, 96 mM Na_2SO_4, 4 mM H_2SO_4, pH 3. A clean microband electrode for each scan.

Collector current transients for a 1.0 mM PMG solution are shown in Figure 65. The same electrode was used for several similar (the same generator current) scans in a row. The transients change when the measurement is repeated, and the collection efficiencies become smaller. That is most probably due to the PMG-iron(III) precipitate at the collector electrode ('electrode poisoning'). This demonstrates that a clean electrode surface is necessary for the experimental reliability.

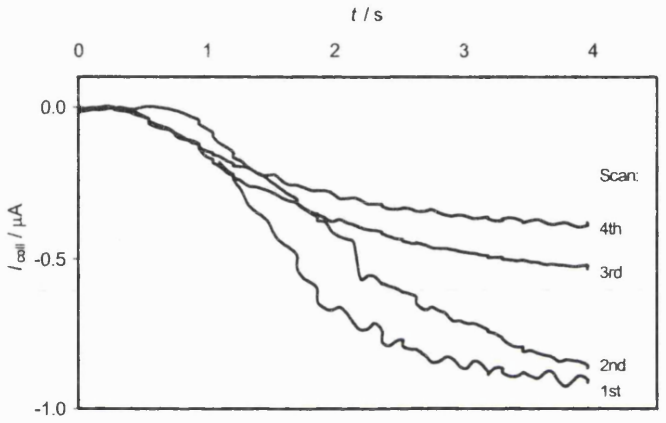

Figure 65. Amperometric titration of PMG (1 mM) with electrogenerated Fe(III). Generator current applied at t = 0 s, *i.e.*, 1 s after the movement pulse of the electrode. I_{gen} = 6 µA, E_{coll} = -0.1 V vs. SCE. 50 mM $FeSO_4$, 96 mM Na_2SO_4, 4 mM H_2SO_4, pH 3. The same microband for all scans.

In Figure 66, amperometric transients for 1.0 mM PMG solutions are shown. Different electrolytes (either $FeSO_4$ or $(NH_4)_2Fe(SO_4)_2$) were used. It can be seen that the transients are similar with both electrolytes when the measurements are made immediately after solution preparation. When the solutions are left in an open cell for approximately 30 minutes, the transients change. When $FeSO_4$ is the electrolyte, the shape of the curve is the same in both cases. The shift in current is caused by oxidation of Fe(II) to Fe(III) due to dissolved oxygen. When $(NH_4)_2Fe(SO_4)_2$ is the electrolyte, the shape of the curve changes in addition to the shift. This leads to an error if the collection efficiency is determined at only one point of the curve. For instance, at t = 3 s, the collection efficiencies with both electrolytes are approximately the same but before and after that point the collector currents are clearly different. In the case of $(NH_4)_2Fe(SO_4)_2$, the collector current starts to change very soon

after the generator current is switched on. That might indicate that H^+ ions that have high mobility [38] move to the collector electrode instead of Fe(III) ions. That may signal a pH change near the electrode, which may be caused by interaction between NH_4^+ and PMG. There are several references [184, 186, 203, 204] reporting changes in phytotoxic properties of PMG in the presence of ammonium but the actual mechanism in not clear. In this particular system, the $FeSO_4$ electrolyte gives more reliable response but the change seen in the case of $(NH_4)_2Fe(SO_4)_2$ opens up speculation, whether the method could be used for pH detection in very specific systems.

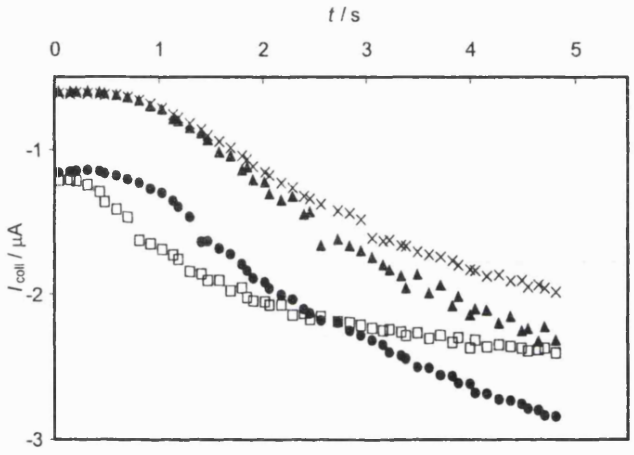

Figure 66. Amperometric titration of PMG (1 mM) with electrogenerated Fe(III). Generator current applied at t = 0 s, *i.e.*, 1 s after the movement pulse of the electrode. E_{coll} = -0.1 V vs. SCE. 96 mM Na_2SO_4, 4 mM H_2SO_4, pH 3. 50 mM $FeSO_4$: (▲) fresh solution, (●) solution left in an open cell for 30 min. 50 mM $(NH_4)_2Fe(SO_4)_2$: (×) fresh solution, (○) solution left in an open cell for 30 min.

5.4.4 Potentiometric titration

5.4.4.1 Constant current method

Open-circuit potentials of the collector electrode against time in PMG titration with the constant current method are presented in Figure 67. Again, the curves follow the Nernst equation (eq. (31)): the Fe(III) concentration at the collector electrode decreases with an increasing analyte concentration, and the achieved open-circuit potential becomes more

negative. As in the case of potentiometric vitamin C titration with the constant current mode, for a full titration curve (E_{coll} vs. I_{gen}) several scans with different generator currents must be carried out and the accuracy of the system is limited unless the number of scans is very high.

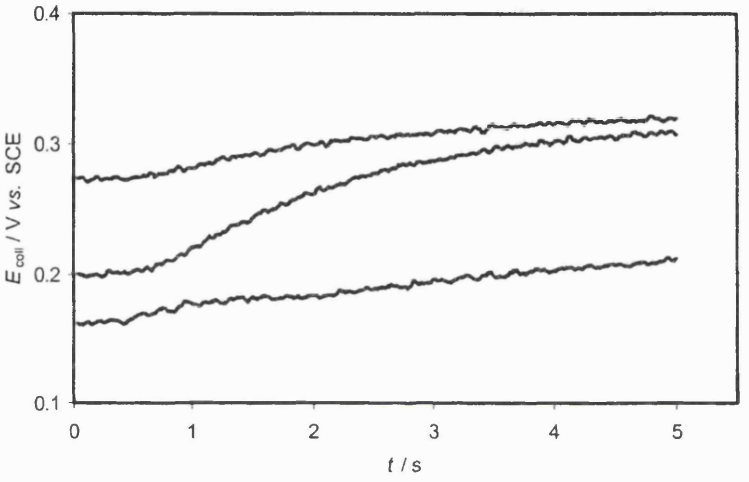

Figure 67. Open-circuit potentials in PMG titration with constant current method. Au micro-bands. 50 mM $FeSO_4$, 96 mM Na_2SO_4, 4 mM H_2SO_4, pH 3. PMG concentration 0; 1.0; 5.0 mM (transients from top to bottom).

5.4.4.2 Ramp current method

Open-circuit potentials of the collector electrode against the applied generator current in PMG, PIDA and AMPA titrations with the ramp current method are shown in Figure 68, Figure 69 and Figure 70, respectively.

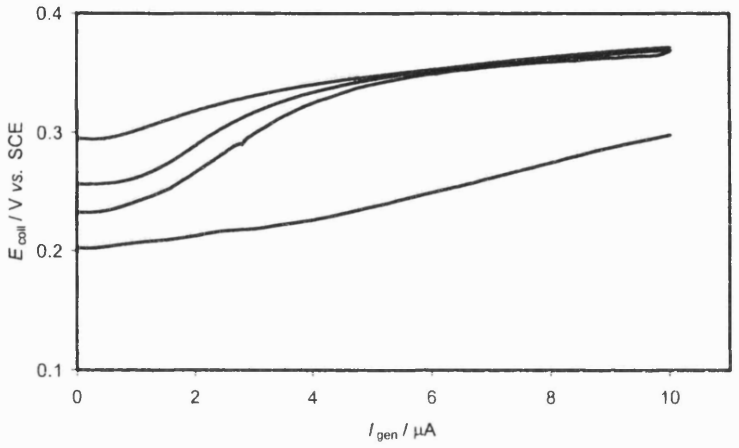

Figure 68. Open-circuit potentials in PMG titration with ramp current method. Au microbands. Generator current applied at t = 0 s, *i.e.*, 1 s after the movement pulse of the electrode. I_{gen} scanned from 0 to 10 μA at 0.2 μA/s. 50 mM $FeSO_4$, 96 mM Na_2SO_4, 4 mM H_2SO_4, pH 3. Analyte concentrations: 0; 0.5; 1.0; 2.0 mM (transients from top to bottom).

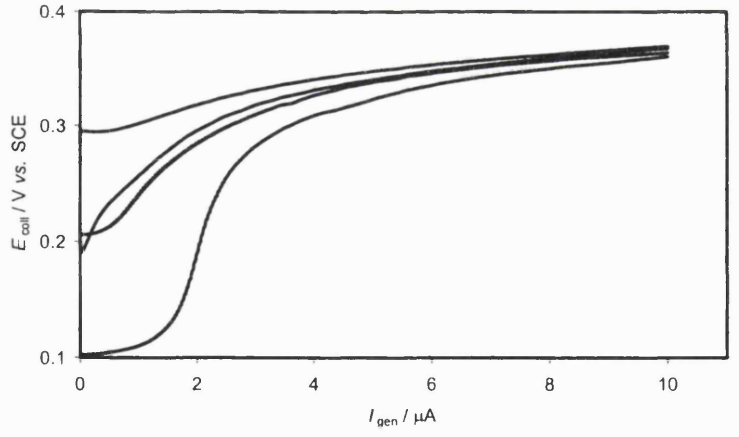

Figure 69. Open-circuit potentials in PIDA titration with ramp current method. Au microbands. Generator current applied at t = 0 s, *i.e.*, 1 s after the movement pulse of the electrode. I_{gen} scanned from 0 to 10 μA at 0.2 μA/s. 50 mM $FeSO_4$, 96 mM Na_2SO_4, 4 mM H_2SO_4, pH 3. Analyte concentrations: 0; 0.5; 1.0; 2.0 mM (transients from top to bottom).

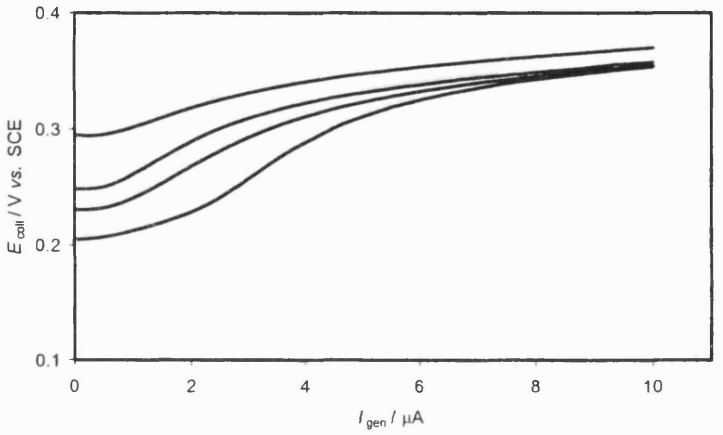

Figure 70. Open-circuit potentials in AMPA titration with ramp current method. Au microbands. Generator current applied at t = 0 s, *i.e.*, 1 s after the movement pulse of the electrode. I_{gen} scanned from 0 to 10 μA at 0.2 μA/s. 50 mM $FeSO_4$, 96 mM Na_2SO_4, 4 mM H_2SO_4, pH 3. Analyte concentrations: 0; 0.5; 1.0; 2.0 mM (transients from top to bottom).

As presented in previous chapters, the end-point of the titration can be determined as a point where the first derivative (dE/dI) of the curve reaches its maximum. The end-points shift to higher currents when the analyte concentration increases, since a higher flux of the titrant is needed in order to reach the end-point. As presented previously, the potential of the gold electrode at the start of the current ramp would be a mixed potential, determined by the concentrations of all redox active species in the solution, including dissolved oxygen. The mixed potential would also be affected by redox reactions of the gold itself and of the metal oxide additives of the ink. The drifts of the potentials in the first part of the titration curves are caused by changes in the mixed potential.

The dependence of the end-point on the generator current scan rate in PMG, PIDA and AMPA titrations is presented in Figure 71. The end-points (maximum of the first derivative) of PMG and AMPA differ clearly from the reference curve (no analyte present). However, the end-points of PIDA are very close to the reference. This can be assumed to be due to differences in kinetic parameters, since the stoichiometries of the reactions are the same. Unfortunately, there are no literature reference pointing the actual kinetic values. Again, the data analysis method that only takes into account the first derivative of the titration curve might be limited, and for a more accurate data analysis, a method that takes more parameters into account would be required.

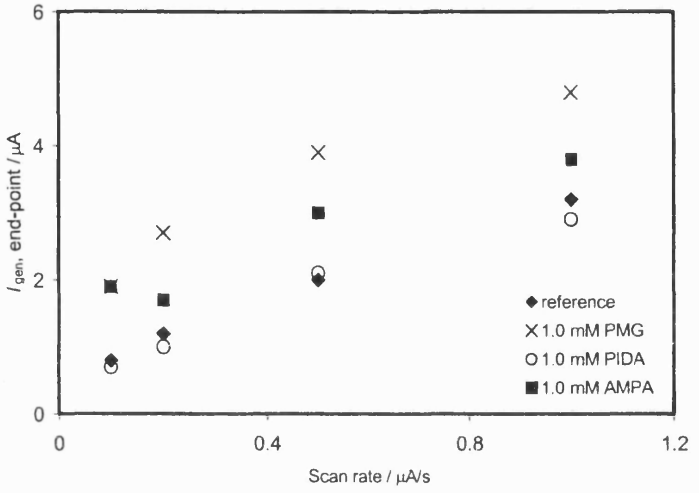

Figure 71. Dependence of the end-point (maximum of the first derivative) on the current scan rate in potentiometric PMG, PIDA and AMPA titrations. Generator current applied at t = 0 s, *i.e.*, 1 s after the movement pulse of the electrode. I_{gen} scanned from 0 to 10 μA. 50 mM $FeSO_4$, 96 mM Na_2SO_4, 4 mM H_2SO_4, pH 3.

The transients in potentiometric titrations of combinations of PMG, PIDA and AMPA are presented in Figure 72. The compounds cannot be distinguished with this method since the curves with different concentration combinations overlap each other. This is in an agreement with the results of the conventional titration. However, Figure 68, Figure 69, Figure 70 and Figure 72 clearly show that it can be qualitatively analysed whether one or more of the compounds is present in the solution, since both the start potentials and the potentials achieved at the end of the generator ramp differ from the reference curve (no analyte present).

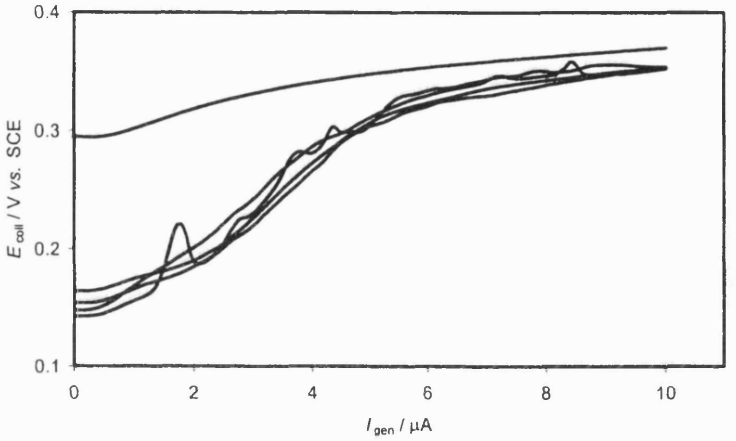

Figure 72. Open-circuit potentials in titration of combinations of PMG, PIDA and AMPA with electrogenerated Fe(III) with ramp current method. Au microbands. Generator current applied at $t = 0$ s, *i.e.*, 1 s after the movement pulse of the electrode. I_{gen} scanned from 0 to 10 μA at 0.2 μA/s. 50 mM $FeSO_4$, 96 mM Na_2SO_4, 4 mM H_2SO_4, pH 3. Analyte concentration combinations: (1+1+1) mM, (1+1+0.5) mM, (1+0.5+1) mM and (0.5+1+1) mM. The uppermost transient without any analyte.

5.4.5 Industrial application: conclusions

A typical standard deviation was 10 % (calculated using three to four measurements with different electrodes). This is consistent with the results presented in the previous sections. The electrode poisoning has an important role in all PMG measurements, and a clean electrode surface is necessary for reliable results. The quantitative analysis of PMG is possible if no interfering compound, PIDA or AMPA, is present. It can be qualitatively analysed whether one or more of those compounds is in the sample but the compounds cannot be distinguished with the present method.

In References 169 and 205, Sagatys et al. reported a silver complex of PMG. The potentiometric titration of PMG and its derivatives using dissolving silver microband electrodes would provide an interesting topic for further studies.

6 Conclusions

This thesis presents an electrochemical titration using disposable dual microband electrodes in generator-collector mode. The principle of both amperometric and potentiometric end-point detection has been demonstrated with several applications. A good agreement between experiments and theory has been observed in voltammetric and potential step experiments. Analytical and semi-analytical equations for a dual microband system have been proved to provide consistent results with the experiments without the analyte, but for the electrochemical titration numerical solutions are required. A good agreement has been observed between experimental results and digital simulations in the amperometric titration of vitamin C.

The method presented here does not need calibration if the electrode geometry is reproducible, which decreases the time and effort needed for many common conventional titrations. However, the snapping procedure used in order to expose a clean electrode surface may lead to deviations from the ideal geometry and distortion of the diffusion field. The accuracy of the analysis is ± 10 %, and the error is mainly caused by the non-ideality of the electrode surfaces.

The titration of vitamin C with ferricyanide, the titration of thiosulfate and sulfite with iodine and the determination of dichromate and permanganate with iron(II) have been proved to work reliably in the amperometric mode. The results have shown the usability of the method in various titration systems, including determination of an electroactive analyte. The titration can further be extended to several applications, *e.g.*, back titrations. The determination of dichromate has the potential to be applied to chemical oxygen demand (COD). The detection limit depends on the analyte to be measured and the stoichiometry of the actual reaction. At present, the method is capable of measuring mM (ppm) levels.

The basis for the potentiometric titration using dual microband electrodes with a ramp current method has been established. The potentiometric titration of vitamin C with ferricyanide as well as the determination of thiosulfate and sulfite with iodine, the same applications that have been presented in the amperometric mode, have been demonstrated with gold microband electrodes. The importance of the rate of the titration reaction has been presented in relation to the choice between the amperometric and potentiometric modes. If the reaction rate is finite, the amperometric titration provides a reliable way of analysis. In

the potentiometric mode, the system becomes limited by the finite reaction rate but, on the other hand, the potentiometric method provides a sensitive method for detecting low concentrations of electroactive species.

A new application that uses a dissolving silver microband as a generator electrode and silver as an indicator electrode have been proven to work reliably for the determination of chloride, iodide, thiosulfate and cyanide. The potentiometric method presented here can be applied to several precipitation and complexiметric titrations, probably even to applications using other dissolving electrode materials, *e.g.*, Cu or Co.

The principle of a generator-collector mode titration for analysing PMG, PIDA and AMPA, industrial applications, has been demonstrated, although the chemistry of those compounds has been proved to be complicated. Potentiometric titration works reliably for all of the mentioned compounds when they are separately present in the solution. Qualitative analysis of combinations of the compounds is also possible but the quantitative analysis does not work most probably due to interactions between the compounds and changes in stoichiometry.

7 Future work

The future of this kind of analytical method is promising and encouraging since the results are reliable even with a simple and straightforward experimental arrangement. The accuracy of the measurements might be improved by improving the electrode fabrication process, which would further allow measurements with lower detection limits.

More work is needed in order to improve the data analysis and for optimising the system in order to measure different compounds simultaneously. Further studies on effects of reaction rate, formation of reaction layers and flux balance would be required in order to understand the actual processes taking place in the inter-electrode gap.

In addition, different microband electrode materials as potentiometric indicator electrodes and various generator current sequences could be studied. Particularly, more investigation would be required in order to find out the suitability and stability of different electrode materials for each analytical system.

The actual complexation chemistry related to the industrial application could be studied using different experimental conditions and their effects on stoichiometry and titration response. More work is required on the surface effects of the organophosphorous ligands. For instance, the film forming properties of different compounds might be used as an analytical signal. Other electrode materials, particularly dissolving electrodes, need further investigation.

APPENDIX I

When the analyte is present in the solution, Fick's second law (eq. (35)) for the titrant is:

$$\text{(I)} \qquad \frac{\partial c_B}{\partial t} = D_B\left(\frac{\partial^2 c_B}{\partial r^2} + \frac{1}{r}\frac{\partial c_B}{\partial r}\right) - kc_C c_B .$$

It is assumed that the analyte concentration is constant and high, and the diffusion of the analyte is infinitely rapid. For a more accurate solution an analogous diffusion equation should also be written for both species A and C.

Let us assume the steady state:

$$\text{(II)} \qquad D_B\frac{\partial^2 c_B}{\partial r^2} + \frac{D_B}{r}\frac{\partial c_B}{\partial r} - kc_C c_B = 0 .$$

Equation (II) is a linear, second-order homogenous differential equation.

The differential equation

$$\text{(III)} \qquad x^2 y'' + xy' + (x^2 - n^2)y = 0$$

is the Bessel equation of order n. [105] Its general solution is

$$\text{(IV)} \qquad y(x) = aJ_n(x) + bJ_{-n}(x),$$

where $J_n(x)$ is the Bessel function of order n.

A modified form of the Bessel equation is [105]

$$\text{(V)} \qquad x^2 y'' + xy' + (-x^2 - n^2)y = 0,$$

the general solution of which is

(VI) $$y(x) = aK_n(x) + bI_n(x).$$

When we transform Equation (II) into the Bessel equation [104] we get a form of a modified Bessel equation where $n = 0$ and $x = \sqrt{\frac{kc_C}{D_B}}r$. We choose a modified Bessel function, the value of which decreases as x (or r) increases, which applies to the dual microband system. This kind of modified Bessel function is $K_0(x)$, and with the applying argument the function becomes $K_0\left(\sqrt{\frac{kc_C}{D_B}}r\right)$. By using Equation (VI), we can write for the titrant concentration:

(VII) $$c_B(r) = a_0 K_0\left(\sqrt{\frac{kc_C}{D_B}}r\right).$$

The constant a_0 can be solved using Fick's first law (eq. (2)) and assuming the hemi-cylinder geometry at $r = w$ ($w = W/2$) and a steady state:

(VIII) $$\frac{I_{gen}}{zF\pi wl} = -D_B\left(\frac{\partial c_B}{\partial r}\right)_{r=w}.$$

After solving a_0 and substituting into Equation (VII) we have for the titrant concentration as a function of r:

(IX) $$c_B(r) = -\frac{I_{gen}K_0\left(\sqrt{\frac{kc_C}{D_B}}r\right)}{zF\pi wl\sqrt{D_B kc_C}K_0'\left(\sqrt{\frac{kc_C}{D_B}}w\right)},$$

which is Equation (39).

APPENDIX II

The potentiometric titration system with the ramp current method is time-dependent. In the first case, no analyte is present. Fick's second law (eq. (35)) after a Laplace transform can be written as

$$\text{(X)} \quad D_B \frac{\partial^2 \bar{c}_B}{\partial r^2} + \frac{D_B}{r}\frac{\partial \bar{c}_B}{\partial r} - s\bar{c}_B = 0.$$

The solution of Equation (X) follows the route presented in Appendix I, resulting in the following equation for the titrant concentration:

$$\text{(XI)} \quad \bar{c}_B(r) = a_0 K_0\left(\sqrt{\frac{s}{D_B}}r\right).$$

The constant a_0 can be solved in an analogous way using Fick's first law (eq. (2)), but this time the generator current depends on time as $I_{gen} = v_A t$, where v_A is the current scan rate:

$$\text{(XII)} \quad L\left\{\frac{v_A t}{F\pi w l}\right\} = -D_B\left(\frac{\partial \bar{c}_B}{\partial r}\right)_{r=w}$$

By using a Laplace transform $L\{t\} = 1 / s^2$, [206] after solving a_0 and substituting into Equation (XI) we have for the titrant concentration as a function of r:

$$\text{(XIII)} \quad \bar{c}_B(r) = -\frac{v_A K_0\left(\sqrt{\frac{s}{D_B}}r\right)}{s^{\frac{5}{2}} zF\pi w l\sqrt{D_B}K_0'\left(\sqrt{\frac{s}{D_B}}w\right)}.$$

The modified Bessel function $K_0(x)$ can be expressed as a series expansion: [105]

$$\text{(XIV)} \quad K_0(x) = -\ln x - \gamma + \ln 2 + \ldots,$$

where γ is Euler's constant (γ = 0.57722). If we assume $\sqrt{\frac{s}{D_B}}r << 1$, *i.e.*, long times, we can write after differentiating Equation (XIV) and substituting into Equation (XIII):

$$\text{(XV)} \qquad \bar{c}_B(r) = \frac{\nu_A}{s^2 zF\pi d D_B}\left[\ln(2) - \gamma - \ln\left(\sqrt{\frac{s}{D_B}}r\right)\right].$$

By using inverse Laplace transforms $L^{-1}\{1/s^2\} = t$ and $L^{-1}\left\{\frac{1}{s^d}\ln s\right\} = \frac{t^{d-1}}{\Gamma(d)}[\psi(d) - \ln t]$, $(d > 0)$,[206] we have

$$\text{(XVI)} \qquad c_B(r) = \frac{\nu_A t}{zF\pi d D_B}\left[\ln(2) - \gamma - \ln\left(\frac{r}{t^{\frac{1}{2\Gamma(2)}}\sqrt{D_B}}\right) - \frac{\psi(2)}{2\Gamma(2)}\right],$$

which is Equation (40), and where we can use $\Gamma(2) = 1$ and $\psi(2) \approx 0.42278$.

APPENDIX III

As mentioned in Appendix II, the potentiometric titration system with the ramp current method is time-dependent. The second case is when the analyte is present. Fick's second law (eq. (35)) after a Laplace transform can be written as

(XVII) $$D_B \frac{\partial^2 \bar{c}_B}{\partial r^2} + \frac{D_B}{r}\frac{\partial \bar{c}_B}{\partial r} - (kc_C + s)\bar{c}_B = 0 .$$

It is assumed that the c_C is constant, the value of c_C is high and the diffusion of C is infinitely rapid. For a more accurate solution an analogous diffusion equation should also be written for both species A and C.

The solution of Equation (XVII) follows the route presented in Appendices I and II, resulting in the following equation for the titrant concentration:

(XVIII) $$\bar{c}_B(r) = -\frac{v_A K_0\left(\sqrt{\frac{kc_C + s}{D_B}}\, r\right)}{s^2 zF\pi w l \sqrt{D_B(kc_C + s)}\, K_0'\left(\sqrt{\frac{kc_C + s}{D_B}}\, w\right)} .$$

Now we can use a readily available Fortran77 routine C06LAF that estimates the value of the inverse Laplace transform of a given function using a Fourier series approximation. We can similarly use a Fortran77 subroutine S18DCF for approximating the values of the modified Bessel functions. [110]

APPENDIX IV

The amperometric case is time-dependent, since the opposite reaction to that at the generator takes place at the collector. Let us first ignore the collector and focus on the case with no analyte. We can write for the titrant concentration

$$\text{(XIX)} \qquad \bar{c}_B(r) = a_0 K_0\left(\sqrt{\frac{s}{D_B}}r\right),$$

which is analogous to Equation (XI). The constant a_0 can be solved, as previously, using Fick's first law (eq. (2))

$$\text{(XX)} \qquad L\left\{\frac{I_{gen}(t)}{F\pi wl}\right\} = -D_B\left(\frac{\partial \bar{c}_B}{\partial r}\right)_{r=w},$$

and we get for the titrant concentration as a function of r

$$\text{(XXI)} \qquad \bar{c}_B(r) = -\bar{I}_{gen}(s)\frac{K_0\left(\sqrt{\frac{s}{D_B}}r\right)}{zF\pi wl\sqrt{D_B s}K_0'\left(\sqrt{\frac{s}{D_B}}w\right)}.$$

Let us approximate that the total concentration consists of the concentration of the titrant generated at the generator, $c_{B,gen}$, and the 'assumed' negative concentration of the titrant reacted at the collector, $-c_{B,coll}$. The total concentration at the surface of the collector is 0. Thus, the concentration of titrant from the generator to the collector is equal to the concentration of reacted titrant that is diffusing away from the collector. We can write

$$\text{(XXII)} \qquad \bar{c}_{B,gen}(s,r) = -\bar{c}_{B,coll}(s,w),$$

where the left hand side refers to the concentration of the species generated at the generator (*i.e.*, titrant) and the right hand side refers to the species generated at the collector. Now r =

$W_{gap} + W / 2$, which is analogous to the distance w from the collector electrode. By using Equations (XXI) and (XXII) we can now write for the collector current

$$\text{(XXIII)} \qquad \bar{I}_{coll}(s) = -\bar{I}_{gen}(s)\frac{K_0\left(\sqrt{\frac{s}{D_B}}r\right)}{K_0\left(\sqrt{\frac{s}{D_B}}w\right)},$$

where the generator current follows a step function, *i.e.*, its value is 0 until it is stepped to a constant value. By using the Laplace transform for the step function, $L^{-1}\{H(t)\} = 1 / s$, [206] we get

$$\text{(XXIV)} \qquad \bar{I}_{coll}(s) = -\frac{I_{gen}}{s}\frac{K_0\left(\sqrt{\frac{s}{D_B}}r\right)}{K_0\left(\sqrt{\frac{s}{D_B}}w\right)}.$$

When the analyte is present in the solution, let us assume that the amperometric system changes as presented in Appendix III. We can write for the collector current

$$\text{(XXV)} \qquad \bar{I}_{coll}(s) = -\frac{I_{gen}}{s}\frac{K_0\left(\sqrt{\frac{kc_C + s}{D_B}}r\right)}{K_0\left(\sqrt{\frac{kc_C + s}{D_B}}w\right)}.$$

We can again use the Fortran77 routines C06LAF in order to estimate the value of the inverse Laplace transform and the Fortran77 subroutine S18DCF for approximating the values of the modified Bessel functions. [110]

References

1. D. Pletcher, in M.I. Montenegro, M.A. Queiros, J.L. Daschbach (Eds.), *Microelectrodes: Theory and Applications*, Kluwer, Dordrecht, 1991, pp. 3-16.
2. J. Heinze, *Angew. Chem. Int. Ed. Engl.*, 1993, **32**, 1268.
3. A. C. Michael and R. M. Wightman, in P.T. Kissinger, W.R. Heineman (Eds.), *Laboratory Techniques in Electroanalytical Chemistry*, 2nd edn., Marcel Dekker Inc., New York, 1996, pp. 367-402.
4. J. Wang, *Analytical Electrochemistry*, 1st edn., VCH Publishers Inc., New York, 1994, p. 95.
5. D.E. Williams, in M.I. Montenegro, M.A. Queiros, J.L. Daschbach (Eds.), *Microelectrodes: Theory and Applications*, Kluwer, Dordrecht, 1991, pp. 415-427.
6. S. Pons, M. Fleischmann, *Anal. Chem.*, 1987, **59**, 1391A.
7. R. M. Wightman, *Anal. Chem.*, 1981, **53**, 1125A.
8. H.A.O. Hill, N.A. Klein, I.S.M. Psalti, N.J.Walton, *Anal. Chem.*, 1989, **61**, 2200.
9. R. J. Forster, *Chem Soc. Rev.*, 1994, **23**, 289.
10. D.H. Craston, N. El-Murr, C.P. Jones, D.E. Williams, *Talanta,* 1991, **38**, 17.
11. J. O. Howell, R. M. Wightman, *Anal. Chem.*, 1984, **56**, 524.
12. J. Ghoroghchian, F. Sarfarazi, T. Dibble, J. Cassidy, J. J. Smith, A. Russell, G. Dunmore, M. Fleischmann, S. Pons, *Anal. Chem.*, 1986, **58**, 2278.
13. K. R. Wehmeyer, M. R. Deakin, R. M., Wightman, *Anal. Chem.*, 1985, **57**, 1913.
14. Z. Porat, J. C. Crooker, Y. Zhang, Y. Le Mest, R. W. Murray, *Anal. Chem.*, 1997, **69**, 5073.
15. D. G. Sanderson, L. B. Anderson, *Anal. Chem.*, 1985, **57**, 2388.
16. W. Thormann, P. van der Bosch, A. M. Bond, *Anal. Chem.*, 1985, **57**, 2764.
17. T. Varco Shea, A. J. Bard, *Anal. Chem.*, 1987, **59**, 2101.
18. D. J. Caruana, J. V. Bannister, *J. Electroanal. Chem.*, 1997, **424**, 197.
19. J. A. Alden, J. Booth, R. G. Compton, R. A. W. Dryfe, G. H. W. Sanders, *J. Electroanal. Chem.*, 1995, **389**, 45.
20. G. Sundholm, *Sähkökemia*, 1st edn., Otatieto, Hämeenlinna, 1987, 240 p.
21. J. Koryta, J. Dvořák, L. Kavan, *Principles of Electrochemistry*, 2nd edn., John Wiley & Sons Ltd., Guildford, 1993, 486 p.
22. R. Greef, R. Peat, L.M. Peter, D. Pletcher, J. Robinson (Eds.), *Instrumental Methods in Electrochemistry*, 2nd edn., Ellis Horwood Ltd., Bodmin, 1990, 443 p.
23. C. Amatore, M. R. Deakin, R. M. Wightman, *J. Electroanal. Chem.*, 1987, **225**, 49.

24. J. E. Bartelt, M. R. Deakin, C. Amatore, R. M. Wightman, *Anal. Chem.*, 1988, **60**, 2167.
25. J. D. Norton, W. E. Benson, H. S. White, B. D. Pendley, H. D. Abruna, *Anal. Chem.*, 1991, **63**, 1909.
26. A. Fick, *Ann. Phys. Chem.* (Leipzig), 1855, **94**, 59.
27. C. A. Amatore, M. R. Deakin, R. M. Wightman, *J. Electroanal. Chem.*, 1986, **206**, 23.
28. D. K. Cope, D. E. Tallman, *J. Electroanal. Chem.*, 1995, **396**, 265.
29. K. Nakatani, N. Terui, N. Kitamura, *Bull. Chem. Soc. Jpn.*, 1996, **69**, 997.
30. S. Coen, D. K. Cope, D. E. Tallman, *J. Electroanal. Chem.*, 1986, **215**, 29.
31. P. M. Kovach, W. L. Caudill, D. G. Peters, R. M. Wightman, *J. Electroanal. Chem.*, 1985, **185**, 285.
32. M. R. Deakin, R. M. Wightman, C. A. Amatore, *J. Electroanal. Chem.*, 1986, **215**, 49.
33. A. Szabo, D. K. Cope, D. E. Tallman, P. M. Kovach, R. M. Wightman, *J. Electroanal. Chem.*, 1987, **217**, 417.
34. C. A. Amatore, B. Fosset, M. R. Deakin, R. M. Wightman, *J. Electroanal. Chem.*, 1987, **225**, 33.
35. M. Samuelsson, M. Armgarth, C. Nylander, *Anal. Chem.*, 1991, **63**, 931.
36. K. B. Oldham, *J. Electroanal. Chem.*, 1981, **122**, 1
37. B. Fosset, C. A. Amatore, J. E. Bartelt, A. C. Michael, R. M. Wightman, *Anal. Chem.*, 1991, **63**, 306.
38. D. C. Harris, *Quantitative Chemical Analysis*, W. H Freeman & Co, New York, 4th edn., 1996, 837 p.
39. K. Aoki, *Electroanalysis*, 1993, **5**, 627.
40. W. E. Gettys, F. J. Keller, M. J. Skove, *Physics: Classical and Modern*, 1st int. edn., McGraw-Hill Company, Inc., 1989, pp. 578-581.
41. G. W. Castellan, *Physical Chemistry*, 3rd edn., The Benjamin/Cummings Publishing Company, Inc., Menlo Park CA, 1983, pp. 765-767.
42. K. Vuorilehto, PhD Thesis, Helsinki University of Technology, 1997.
43. A. G. Ewing, M. A. Dayton, R. M. Wightman, *Anal. Chem.*, 1981, **53**, 1842.
44. R. M. Wightman, L. J. May, A. C. Michael, *Anal. Chem.*, 1988, **60**, 769A.
45. A. M. Farrington, J. M. Slater, *Analyst*, 1997, **122**, 593.
46. A. S. Baranski, *Anal. Chem.*, 1987, **59**, 662.
47. D. K. Y. Wong, A. G. Ewing, *Anal. Chem.*, 1990, **62**, 2697.
48. A. Russell, K. Repka, T. Dibble, J. Ghoroghcian. J. J. Smith, M. Fleischmann, C. H. Pitt, S. Pons, *Anal. Chem.*, 1986, **58**, 2961.

49. E. D. Harris, A. J. Lindsey, *Analyst*, 1951, **76**, 647.
50. E. D. Harris, A. J. Lindsey, *Analyst*, 1951, **76**, 650.
51. K. W. Pratt, Jr., D. C. Johnson, *Electrochim. Acta*, 1982, **27**, 1013.
52. I. M. Kolthoff , J. Jordan, *J. Am Chem Soc.* 1953, **75**, 1571.
53. H. A. Laitinen, *Anal. Chem.*, 1949, **21**, 66.
54. T. Matsue, A. Aoki, E. Ando, I. Uchida, *Anal. Chem.*, 1990, **62**, 409.
55. R. G. Compton, R. G. Wellington, P. J. Dobson, P.A. Leigh, *J. Electroanal. Chem.*, 1994, **370**, 129.
56. M. J. Bidwell, J. A. Alden, R. G. Compton, *J. Electroanal. Chem.*, 1996, **414**, 247.
57. A. C. Fisher, C. W. Davies, Q. Fulian, M. Walters, *Electroanalysis*, 1997, **9**, 849.
58. J. A. Alden, M. A. Feldman, E. Hill, F. Prieto, M. Oyama, B. A. Coles, R. G. Compton, P. J. Dobson, P. A. Leigh, *Anal. Chem.*, 1998, **70**, 1707.
59. W. J. Albery, *J. Electroanal. Chem.*, 1985, **191**, 1.
60. D. R. Crow, *Principles and Applications of Electrochemistry*, T. J. Press Ltd., Padstow, 4th edn., 1994, pp. 189-195.
61. A. Lindgren, F.-D. Munteanu, I. G. Gazaryan, T. Ruzgas, L. Gorton, *J. Electroanal. Chem.*, 1998, **458**, 113.
62. R. P. Akkermans, M. F. Suarez, S. L. Roberts, Q. Fulian, R. G. Compton, *Electroanalysis*, 1999, **11**, 1191.
63. R. P. Akkermans, M. Wu, R. G. Compton, *Electroanalysis*, 1998, **12**, 814.
64. F. Marken, R. P. Akkermans, R. G. Compton, *J. Electroanal. Chem.*, 1996, **415**, 55.
65. F. Qiu, R. G. Compton, B. A. Coles, F. Marken, *J. Electroanal. Chem.*, 2000, **492**, 150.
66. J. Wang, *Talanta*, 1981, **28**, 369.
67. S.A. Schuette, R.L. McCreery, *Anal. Chem.*, 1986, **58**, 1778.
68. J. Wang, B.A. Freiha, *Anal. Chem.*, 1982, **54**, 1231.
69. S.A. Schuette, R.L. McCreery, *Anal. Chem.*, 1987, **59**, 2692.
70. A. J. Bard, L. R. Faulkner, *Electrochemical Methods – Fundamentals and Applications*, 1st edn., John Wiley & Sons, Inc., Singapore, 1980, pp. 309-312.
71. W. J. Blaedel, Z. Yim, *Anal. Chem.*, 1980, **52**, 564.
72. H. D. Dewald, B. A. Peterson, *Anal. Chem.*, 1990, **62**, 779.
73. D. E. Williams, K. Ellis, A Colville, S. J. Dennison, G. Laguillo, J. Larsen,

J. Electroanal. Chem. 1997, **432**, 159.

74. W. J. Albery, *Trans. Faraday Soc.*, 1966, **62**, 1915.
75. W. J. Albery, E. J. Calvo, *J. Chem. Soc., Faraday Trans. 1*, 1983, **79**, 2583.
76. W. J. Albery, S. Bruckenstein, *Trans. Faraday Soc.*, 1966, **62**, 1920.
77. W. J. Albery, S. Bruckenstein, *Trans. Faraday Soc.*, 1966, **62**, 1946.
78. W. J. Albery, S. Bruckenstein, D. C. Johnson, *Trans. Faraday Soc.*, 1966, **62**, 1938.
79. W. J. Albery, L. R. Svanberg, P. Wood, *J. Electroanal. Chem.*, 1984, **162**, 29.
80. W. J. Albery, L. R. Svanberg, P. Wood, *J. Electroanal. Chem.*, 1984, **162**, 45.
81. W. J. Albery, P. N Bartlett, A. E. G. Cass, D. H. Craston, B. G. D. Haggett, *J. Chem. Soc., Faraday Trans. 1*, 1986, **82**, 1033.
82. J. L. Lingane, *Electroananlytical Chemistry*, 2nd edn., Interscience Publishers, Inc., Easton, 1958, p. 546.
83. B. J. Seddon, C. F. Wang, W. Peng, X. Zhang, *J. Chem. Soc., Faraday Trans. 1*, 1994, **90**, 605.
84. J. E. Baur, H. M. Miller, M. A. Robinson, *Anal. Chim. Acta*, 1999, **397**, 123.
85. C. E. Chidsey, B. J. Feldman, C. Lundgren, R. W. Murray, *Anal. Chem.*, 1986, **58**, 601.
86. A. J. Bard, J. A. Crayston, G. P. Kittlesen, T. Varco Shea, M. S. Wightman, *Anal. Chem.*, 1986, **58**, 2321.
87. B. J. Seddon, H. H. Girault, M. J. Eddowes, *J. Electroanal. Chem.*, 1989, **266**, 227.
88. O. Niwa, M. Morita, H. Tabei, *Anal. Chem.*, 1990, **62**, 447.
89. M. S. Harrington, L. B. Anderson, *Anal. Chem.*, 1990, **62**, 546.
90. A. Aoki, T. Matsue, I. Uchida, *Anal. Chem.*, 1990, **62**, 2206.
91. O. Niwa, H. Tabei, *Anal. Chem.*, 1994, **66**, 285.
92. M. Paeschke, U. Wollenberger, C. Köhler, T. Lisec, U. Schnakenberg, R. Hintsche, *Anal. Chim. Acta*, 1995, **305**, 126.
93. T. A. Postlethwaite, J. E. Hutchison, R. Murray, B. Fosset, C. Amatore, *Anal. Chem.*, 1996, **68**, 2951.
94. Y-S. Fung, S-Y. Mo, *Anal. Chem.*, 1995, **67**, 1121.
95. H. Rajantie, D. E. Williams, *Analyst*, 2001, **126**, 86
96. Y. Xie, S. Dong, *J. Electroanal. Chem.*, 1990, **291**, 1.
97. J.T. Stock, *Amperometric Titrations*, 1st edn., Interscience Publishers, New York, 1965, pp. 3-14, 620-626.
98. E. Hakoila, in P. Kivalo (Ed.), *Sähkökemiallinen analyysi*, Teknillisten tieteiden akatemia ry, Vammala, 1978, pp. 135-226.

99. H. Rajantie, J. Strutwolf, D.E. Williams, *J. Electroanal. Chem.*, 2001, **500**, 108.
100. E. Raitanen, in P. Kivalo (Ed.), *Sähkökemiallinen analyysi*, Teknillisten tieteiden akatemia ry, Vammala, 1978, pp. 42-134.
101. H. Rajantie, D. E. Williams, *Analyst*, 2001, **126**, 1882.
102. L. B. Anderson, C. N. Reilley, *J. Electroanal. Chem.*, 1965, **10**, 295.
103. W. J. Albery, S. Bruckenstein, D. T. Napp, *Trans. Faraday Soc.*, 1966, **62**, 1932.
104. M. D. Greenberg, *Advanced Engineering Mathematics*, 1st edn., Prentice Hall, Inc., New Jersey, 1988, pp. 648, 698.
105. G. Arfken, *Mathematical Methods for Physicists*, 3rd edn., Academic Press, Inc., San Diego, 1985, pp. 454-463, 573-636, 831-838.
106. K. Aoki, K. Tokuda, H. Matsuda, *J. Electroanal. Chem.*, 1987, **230**, 61.
107. K. Aoki, K. Tokuda, H. Matsuda, *J. Electroanal. Chem.*, 1987, **225**, 19.
108. B. Fosset, C. Amatore, J. Bartelt, R. M. Wightman, *Anal. Chem.*, 1991, **63**, 1403.
109. C. G. Phillips, H. A. Stone, *J. Electroanal. Chem.*, 1997, **437**, 157.
110. Naglibrary, www.nag.co.uk, The Numerical Algorithms Group Ltd.
111. D. J. Gavaghan, *J. Electroanal. Chem.*, 1997, **420**, 147.
112. J. Strutwolf, W. W. Schoeller, *Electroanalysis*, 1997, **9**, 1403.
113. J. Strutwolf, D. E. Williams, *Electroanalysis*, 1999, **11**, 487.
114. R. J. Fessenden, J. S. Fessenden, *Organic Chemistry*, 5th edn., Brooks/Cole Publishing Company, Belmont, 1993, p. 260.
115. E. N. Frankel, *Food Chem.*, 1996, **57**, 51.
116. E. Kishida, Y. Nishimoto, S. Kojo, *Anal. Chem.*, 1992, **64**, 1505.
117. C. W. Bradberry, R. N. Adams, *Anal. Chem.*, 1983, **55**, 2439.
118. S. M. Sultan, *Talanta*, 1993, **40**, 593.
119. H. Zhang, A. Galal, J. F. Rubinson, I. Marawi, T. H. Ridgway, S. K. Lunsford, H. Zimmer, H. B. Mark Jr, *Electrochim. Acta*, 1998, **43**, 3511.
120. M. Cheregi, A.F. Danet, *Analytical Letters*, 1997, **30**, 2625.
121. A. M. Farrington, N. Jagota, J. M. Slater, *Analyst*, 1994, **119**, 233.
122. M. E. G. Lyons, W. Breen, J. Cassidy, *J. Chem. Soc. Faraday Trans.*, 1991, **87**, 115.
123. S. Dong, G. Che., *J. Electroanal. Chem.*, 1991, **315**, 191.
124. Z. Gao, A. Ivaska, T. Zha, G. Wang, P. Li, Z. Zhao, *Talanta*, 1993, **40**, 399.
125. Z. Gao, B. Chen, M. Zi, *J. Electroanal. Chem*, 1994, **365**, 197.
126. I.-F. Hu, T. Kuwana, *Anal. Chem.*, 1986, **58**, 3235.
127. F. Prieto, B. A. Coles, R. G. Compton, *J. Phys. Chem. B*, 1998, **102**, 7442.

128. N. Rukmini, V. S. N. P. Kavitha, K. D. Vijaya, *Talanta*, 1981, **28**, 332.

129. W. Wanzhi, X. Qingji, Y. Shouzhuo, *Electrochim. Acta*, 1995, **40**, 1057.

130. T. Vilarino, P. Alonso, X. L. Armesto, P. Rodriguez, M. E. S. de Vicente, *J. Chem. Research (S)*, 1998, 558.

131. N. Winograd, H.N. Blount, T. Kuwana, *J. Phys. Chem.*, 1969, **73**, 3456.

132. C. J. Miller, M. Majda, *Anal. Chem.*, 1988, **60**, 1168.

133. R. C. Weast (Ed.), *Handbook of Chemistry and Physics*, 57th edn., CRC Press, Cleveland, OH, 1976, Sect. D-141.

134. N. Ekkad, C. O. Huber, *Anal. Chim. Acta*, 1996, **332**, 155.

135. A. I. Vogel, *A Text-book of Quantitative Inorganic Analysis*, 3rd edn., Longmans, 1961, pp. 352-353.

136. W. M. Scheper, D. W. Margerum, *Inorg. Chem.* 1992, **31**, 5466.

137. I. M. Kolthoff, E. B. Sandell, E.H. Meehan, S. Bruckenstein, *Quantitative Chemical Analysis*, 4th edn., The Macmillan Company, Toronto, 1969, pp. 741-742, 816-860.

138. K. Brodersen, U. Werner, Y. A., Gawargious, S. Huang, *Talanta*, 1991, **38**, 785.

139. B. Walton, *Analyst*, 1992, **117**, 1757.

140. H. Egan, R. S. Kirk, R. Sawyer, *Pearson's Chemical Analysis of Foods*, 8th edn., Longman Scientific and Technical, Avon, 1981, pp. 60-66.

141. F. Clowes, J. B. Coleman, revised by D. Stockdale and J. Dexter, *Quantitative Chemical Analysis*, 13th edn. J. & A. Churchill, London, 1931, pp. 186-187.

142. S. S. Zumdahl, *Chemistry*, 3rd edn., Heath and Company, 1993, p. 911.

143. P. G. Desideri, L. Lepri, D. Heimler, in A. J. Bard (Ed.), *Encyclopedia of Electrochemistry of the Elements*, Vol. I, Marcel Dekker, Inc, 1973, pp. 91-153.

144. S. Y. Boudin, D. W. Margerum, *Inorg. Chem.* 1990, **29**, 1559.

145. F. P. Treadwell, revised by W. T. Hall, *Analytical Chemistry, Volume I, Qualitative Analysis*, 7th edn., John Wiley & Sons, Boston, 1932, pp. 322-333.

146. P. H. Qi, J. B. Hiskey, *Hydrometallurgy* 1993, **32**, 161.

147. X. Gao, M. J. Weaver, *J. Am. Chem. Soc.* 1992, **114**, 8544.

148. W. Zhang, H. Zha, B. Yao, C. Zhang, X. Zhou, S. Zhong, *Talanta* 1998, **46**, 711.

149. P. H. Qi, J. B. Hiskey, *Hydrometallurgy* 1991, **27**, 47.

150. A. Davis, T. Tran, D. R. Young, *Hydrometallurgy* 1993, **32**, 143.

151. T. N. Angelidis, K. A. Kydros, K.A. Matis, *Hydrometallurgy* 1992, **34**, 49.

152. D. Midgley, K. Torrance, *Potentiometric Water Analysis*, 1st edn., The Guesham Press, Old Woking, 1978, pp. 82-85.

153. Y.-C. Kim, K.-H. Lee, S. Sasaki, K. Hashimoto, K. Ikebukuro, I. Karube, *Anal. Chem.*, 2000, **72**, 3379.

154. C. C. Liang, in A. J Bard (Ed.), *Encyclopedia of Electrochemistry of the Elements*, Vol. I, Marcel Dekker, Inc, 1973, pp. 349-403.

155. J. R. Sutter, K. B. Park, *J. Phys. Chem.*, 1984, **88**, 770.

156. Z.-H. Mo, L.-H. Nie, S-Z. Yao, *Anal. Chim. Acta*, 1991, **246**, 421.

157. A. A. Ramirez, C. J. Linares, *Talanta*, 1992, **39**, 1121.

158. Y. Ni, A. Wu, *Anal. Chim. Acta*, 1999, **390**, 117.

159. G. Gran, A. Johansson, S. Johansson, *Analyst*, 1981, **106**, 1109.

160. J. F. Magallanes, A. F. Caridi, *Anal. Chim. Acta*, 1981, **133**, 203.

161. D. T. Burns, B. K. Maitin, G. Svehla, *Analyst*, 1983, **108**, 457.

162. E. Forizs, Cs. Muzsnay, *Talanta*, 1996, **43**, 1639.

163. N. B. H. Anh, M. Sharp, *Anal. Chim. Acta*, 2000, **405**, 145.

164. H. E. L. Madsen, H.H. Christensen, C. Gottlieb-Petersen, *Acta Chem. Scand. A*, 1978, **32**, 79.

165. R. L. Glass, *J. Agric. Food Chem.*, 1984, **32**, 1249.

166. V. Subramaniam, P. E. Hoggard, *J. Agric. Food Chem.*, 1988, **36**, 1326.

167. A. Piccolo, G. Celano, G. Pietramellarana, *Sci. Tot. Environ.*, 1992, **123/124**, 77.

168. J. Kobylecka, B. Ptaszynski, A. Zwolinska, *Monatsh. Chem.*, 2000, **131**,1.

169. D. S. Sagatys, C. Dahlgren, G. Smith, R. C. Bott, A. C. Willis, *Aust. J. Chem.*, 2000, **53**, 77.

170. P. Sprankle, W. F. Meggitt, D. Penner, *Weed Sci.*, 1975, **23**, 229.

171. R. J. Motekaikis, A. E. Martell, *J. Coord. Chem.* 1985, **14**, 139.

172. M. P. Abdullah, J. Daud, K. S. Hong, C. H. Yew, *J. Chromatogr. A*, 1995, **367**, 363.

173. C. D. Stalikas, G. A. Pilidis, *J. Chromatogr. A*, 2000, **872**, 215.

174. E. Börjesson, L. Torstensson, *J. Chromatogr. A*, 2000, **886**, 207.

175. P. G. Daniele, C. De Stefano, E. Prenesti, S. Sammartano, *Talanta*, 1997, **45**, 425.

176. M. G. Cikalo, D. M. Goodhall, W. Mattheys, *J. Chromatogr. A*, 1996, **745**, 189.

177. L. Abate, C. De Stefano, C. Foti, S. Sammartano, *Environ.Toxicol. Chem.*,

1999, **18**, 2133.

178. F. C. Ku, *Regulat. Toxicol. Pharmacol.*, 1995, **21**, 352.
179. C. Bolognesi, *Food Chem. Toxicol.*, 1997, **35**, 856.
180. H.-Q. Wu, G.-H. Xiao, X.-D. Lei, R. A. Prough, *Toxic. Letters*, 1998, **95**, 102.
181. T. Fujii, N. Inazu, C. Hase, *Toxic. Letters*, 1998, **95**, 216.
182. D. Heineke, S. J. Franklin, K. N. Raymond, *Inorg. Chem.*, 1994, **33**, 2413.
183. T. Undabeytia, M. V. Cheshire, D. McPhail, *Chemosphere*, 1996, **32**, 1245.
184. J. D. Nalewaja, R. Matusiak, *Weed Sci.*, 1991, **39**, 622.
185. K. D. Thelen, E. P. Jackson, D. Penner, *Weed Sci.*, 1995, **43**, 566.
186. S. H. Liu, A. I. Hsiao, W. A. Quick, *Crop Protect.*, 1992, **11**, 335.
187. M. McBride, K.-H. Kung, *Soil Sci. Soc. Am. J.*, 1989, **53**, 1668.
188. E. T. Clarke, P. R. Rudolf, A. E. Martell, A. Clearfield, *Inorg. Chim. Acta*, 1989, **164**, 59.
189. E. Prenesti, M. Gulmini, *Annali Di Chim.*, 1998, **88**, 591.
190. M. A. Dhansay, P. W. Linder, *J. Coord. Chem.*, 1993, **28**, 133.
191. B. Zhang, D. M. Poojary, A. Clearfield, *Chem. Mater.*, 1996, **8**, 1333.
192. D. C. Crans, F. Jiang, O. P. Anderson, S. M. Miller, *Inorg. Chem.*, 1998, **37**, 6645.
193. T. Glowiak, W. Sawka-Dobrowolska, B. Jezowska-Trzebiatowska, *Inorg. Chim. Acta*, 1980, **45**, L105.
194. M. I. Kabachnik, T. Ya. Medved, N. M. Dyatlova, M. V. Rudomino, *Russian Chem. Rev.*, 1974, **43**, 733.
195. A. Shaban, E. Kalman, I. Biczo, *Corr. Sci.*, 1993, **35**, 1463.
196. P. Sprankle, W. F. Meggitt, D. Penner, *Weed Sci.*, 1975, **23**, 235.
197. J. Vaari, *Fysiikan laboratoriotyöt*, 1st edn., Suomen Fyysikkoseuran julkaisuja 4, Gummerus Kirjapaino Oy, Jyväskylä, 1993, pp. 2-8.
198. F. P. Treadwell, revised by W. T. Hall, *Analytical Chemistry, Volume I, Qualitative Analysis*, 7th edn., John Wiley & Sons, Boston, 1932, pp. 322-333.
199. R. E. Hamm, C. M. Shull, D. M. Grant, *J. Am. Chem. Soc.*, 1954, **76**, 211.
200. A. E. Martell, R. M. Smith (Eds.), *Critical Stability Constants*, Vol. 3, Plenum Press, New York, 1977, pp. 3-7, 161-164.
201. M. Avramov-Ivic, V. Jovanovic, G. Vlajnic, J. Popic, *J. Electroanal. Chem.*, 1997, **423**, 119.
202. G. Treiliosi, E. R. Gonzalez, A. J. Motheo, E. M. Belgsir, J.-M. Leger, C. Lamy, *J. Electroanal. Chem.*, 1998, **444**, 31.
203. A. I. Hsiao, S. H. Liu, W. A. Quick, *J. Plant Growth Reg.*, 1996, **15**, 115.

204. W. A. Pline, K. K. Hatzios, E. S. Hagood, *Weed Techn.*, 2000, **14**, 667.

205. D. S. Sagatys, C. Dahlgren, G. Smith, R. C. Bott, J. M. White, *J. Chem. Soc., Dalton Trans.*, 2000, 3404.

206. M. Abramowitz, I. A. Stegun (Eds.), *Handbook of Mathematical Functions*, 1st edn., 2nd printing, National Bureau of Standards, Washington D. C., 1964, pp. 1019-1030.